A TRANSACTIVE ENERGY APPROACH FOR DESIGN AND OPERATIONS OF BATTERY SWAP AND SUPERCHARGING INFRASTRUCTURE

by

Moumita Saha, B.S.

A thesis submitted to the Graduate Council of
Texas State University in partial fulfillment
of the requirements for the degree of
Master of Science
with a Major in Engineering
May 2021

Committee Members:

Tongdan Jin, Chair

Sasha Dong

Rosario Rosas-Vega

FAIR USE AND AUTHOR'S PERMISSION STATEMENT

ACKNOWLEDGEMENTS

I am extremely grateful to my thesis advisor, Dr. Tongdan Jin in the Ingram School of Engineering at Texas State University for all his endless support and time for guiding me through my thesis research. The completion of my master's thesis would not have been possible without his support and guidelines. Dr. Jin always encourages me and has provided me with valuable life advice which will be helpful in my future career.

I am also grateful to Dr. Clara Novoa in the Ingram School of Engineering at Texas State University. During the weekly group meeting, I have greatly benefited from the insightful comments and suggestions from Dr. Novoa in terms of problem setting, model formulation, and solution result analysis.

I would like to extend my sincere thanks to Dr. Sasha Dong in the Ingram School of Engineering at Texas State University to provide me insightful help and support.

I am also grateful to Dr. Rosario Rosas-Vega in the Ingram School of Engineering at Texas State University for encouraging me and providing me valuable insight about my master's thesis.

I would also like to thank all the faculty and staff of the Ingram School of Engineering at Texas State University in extending their guidance throughout my school years. My appreciation is extended to NSF CBET ME-GREEN project (award # 1704933) through the weekly participation and discussion with the research team.

TABLE OF CONTENTS

LIST OF TABLES

Table **Page**

LIST OF FIGURES

Figure **Page**

LIST OF ABBREVIATIONS

Abbreviation	**Description**
AMPL	A Mathematical Programming Language
BCS	Battery Charging Station
BSS	Battery Swap Station
BASS	Bass Diffusion Model
CF	Capacity Factor
ESS	Energy Storage System
EV	Electric Vehicle
EVB	Electric Vehicle Battery
G2V	Grid to Vehicle
JBSS	Joint Battery Swap and Supercharging Station
LCC	Life Cycle Cost
MILP	Mixed Integer Linear Programming
PEV	Plug in Electric Vehicle
PHEV	Plug-in Hybrid Electric Vehicle
PSO	Particle Swarm Optimization
PV	Solar Photovoltaics
PASTA	Poisson Arrivals See Time Averages
RL	Residential Load
SCMG	Smart Community Microgrid

SOC	State of Charge
V2G	Vehicle to Grid
VPP	Virtual Power Plant
WT	Wind Turbine

ABSTRACT

Transactive energy refers to the planning and control of the two-way energy flow between distributed generation and main grid in regards to the realization of economic benefits. This study addresses two research questions related to transactive energy operations: first, how to allocate renewable microgrid system to energize the battery swap and supercharging stations under demand and supply uncertainty? Second, is it economically feasible for wind turbines (WT), solar photovoltaics (PV), and energy storage system (ESS) to participate in day-ahead transactive energy market as virtual power plants? An optimization framework for sizing and siting WT, PV and ESS in a battery swap and supercharging network considering both island and grid-tied operations is proposed. Mixed integer linear programming models are formulated to minimize the annualized battery service infrastructure cost considering facility setup, spare batteries, and supercharger installs. For island microgrid, reducing the cost of ESS does not significantly stimulate its adoption because renewable generation largely depends on capacity factor of PV and WT is shown. In grid-tied microgrid operation, reducing the PV cost by 50% makes the system to install more panels in both sunny cities and windy cities is shown. For network model, the work shows that by reducing the PV capacity cost by 75% from the benchmark cost makes the system choose more PV for Texas cities and reduces the annual network cost by 29%. The system opts to behave as “prosumer” who fulfills the charging demand of vehicle fleet as well as enhancing grid reliability and security by participating in transactive energy market.

1. INTRODUCTION

1.1 Research Motivation

Prosumers are different from conventional consumers. Prosumers are the producer and consumer at the same time. In the energy sector prosumer refers to as an energy user who generates renewable energy in his/her domestic environment and sells the surplus energy to the main grid or his/her neighboring systems after fulfilling own demand (Espe et al. 2018). Energy demand in the world is rising alarmingly. The US Energy Information Agency (EIA) projects that the world energy demand in all sectors will increase nearly 50% by 2050 led by the growth in Asia. EIA also projects that the energy consumption in transportation sector will increase by nearly 40% between 2018 and 2050. Hence, it is imperative to find alternative energy sources which are clean, abundant, and economical in nature, such as wind and solar power, and ocean and wave energy. Considering all these facts, allocating renewable microgrid in battery swap and supercharging station making the system prosumer (namely, being a consumer and producer at the same time) is becoming a new industry trend in smart grid era. North Carolina Clean Energy Technology Center has been working on a funded research project by SunShot and found that by adopting solar panels in 42 of America's 50 largest cities is less expensive than solely depending on a utility company for electricity (Trabish 2015).

Transportation is an important sector for energy consumption. According to US EIA, the transportation sector in USA consumes approximately 28% of energy used in USA. The International Energy Outlook (IEO 2017) projects a 28% increase in world energy consumption between 2015 and 2040. USA consumes 96% of transportation sector energy in the form of petroleum, 2.6% energy in natural gas and only less than 1%

energy in biomass, electricity, or other form of energy. For this reason, developments in electric transportation will provide clean energy for future. Additionally, it will provide alternative energy source for other industry sectors too. Electric transportation is a cost-effective approach for reducing the dependency on fossil fuel energy resources. Currently, electric vehicles (EV) consist just 3% of global new car sales and the number will increase by another 4% by 2023. It is projected that EV will comprise 58% of new vehicle sales globally by 2040 (Edelstein 2020).

Dependency and exploitation of finite energy resources has led to increased air pollution (Espe et al. 2018). The consequences of air pollution have been climate change through green-house gas emissions, and damage to human health. Hence reduction of air pollution by using alternative wind and solar energy resources is needed with the goal of ensuring zero carbon emissions in the environment. Walmart announced that suppliers have reported reducing more than 20 million metric tons of greenhouse gas emissions in the global value chain as a part of company's Project Gigaton initiative (Froese 2018). Walmart also announced that they are planning to reduce greenhouse gas emissions up to one billion metric ton by 2030 in the global value chain. Air pollution can be reduced by significant amounts by adopting electrical vehicles. EV produces 1/3 of greenhouse gas emission compared to a gas vehicle (Minnesota Pollution Control Agency 2020). The Next Generation Energy Act 2007 of Minnesota will act as a turning point for reducing greenhouse gas emission by 30% in 2025.

Based on the prosumer concept, reliance on fossil fuel can be reduced for energy generation and consumption. The adoption of prosumer concept motivates large industrial and commercial consumers to be self-reliance on their own energy generation as well as to reduce air pollution via the adaption of electrical transportation.

1.2 Literature Review

The literature review focuses on three areas of the state-of-the-art research. They are battery swap, supercharging station and joint battery swap and supercharging station.

1.2.1 Battery Swap Station

Zheng et al. (2012) proposed an operation model of battery swap station for a fleet of electric buses in public transportation. By analyzing the characteristics of the battery lease mode and electric city buses, an optimal solution was obtained to maximize the annual profit of battery swap station and to minimize the charging impact on the grid.

Pashajavid and Golkar (2013) proposed a scenario-based optimization algorithm for allocating charging station for a plug-in electric vehicles (PEV) fleet within a commercial area. The objective was to increase the penetration level of photovoltaic (PV) panels as well as to decrease side effects of vehicular loads. Based on the notion of copula, a multivariate stochastic modeling methodology was provided for developing a probabilistic model of the load demand due to PEV. Particle swarm optimization (PSO) algorithm was utilized to minimize energy loss as well as voltage deviation in the distribution system. The model was also tested by simulation.

Yang et al. (2014) proposed a dynamic operation model of Battery Swap Station (BSS) in electricity market. The new mathematical programming model seek the optimal short-term battery policy, and 24-hour simulation results showing the confirmation of the feasibility and practicability of the model.

Tan et al. (2014) formulated a model by using a mixed queueing network with an open queue of electric vehicles (EVs) and a closed queue of batteries. In the first research stream, queueing network models were proposed as a framework for modeling and designing battery swap stations with a local charging mode. They conducted the experimentation based on one battery swap station and used simulation techniques to reveal rich insights for the infrastructure planning of practical battery swapping services.

Yan et al. (2019) presented a real-time energy management strategy for a BSS based smart community microgrid (SCMG), using variable renewable energy to charge the EV batteries (EVB) and conventional residential loads (RL). A novel Lyapunov optimization framework based on queueing theory was designed to solve the proposed model. The proposed method simplifies the complex energy scheduling and transform it into a single optimization problem, making it suitable for real-time applications. Simulation results found that BSS used for the dual-purpose could improve the whole system economics and also facilitate the integration of renewable energy compared to isolated operations.

Mahoor et al. (2019) focused on developing a mathematical model for uncertainty constrained in battery swapping station (BSS) for optimal operation which covered both the random customer demand of fully charged batteries and leveraged the available batteries for reducing the operation cost through demand shifting and energy sellback. The authors used mixed integer linear programming for solving the BSS scheduling problem for one station and modeled the battery degradation by providing a practical solution. Simulation techniques were also used to demonstrate the effectiveness of the proposed model and analyzed the viability in achieving minimum operation cost.

1.2.2 Supercharging Stations

Yang et al. (2014) reviewed the state-of-the-art optimization methods on scheduling strategies for the grid integration with electric vehicles. The paper started with a concise introduction to analytical charging strategies, followed by a review of a number of classical numerical optimization methods, including linear, non-linear, dynamic programming as well as some other means such as queuing theory. Metaheuristic techniques were then discussed to deal with the complex, high-dimensional and multi-objective scheduling problem associated with stochastic charging and discharging of electric vehicles. Finally, future research directions were suggested.

Lu and Hua (2015) mainly focused on designing a supercharging station network by extending the flow refueling mode. Particularly, they combined with queueing theory and re-formulated a new location sizing model with a given largest waiting time that EV could accept. The location sizing model optimally allocated the charging spots without exceeding the given waiting time while maximizing the total charging service. The authors also pointed out several directions of the future development of the electric car.

Yao et al. (2017) aimed at addressing these difficulties by deploying an energy storage system (ESS) in parking stations and exploiting the charging and discharging scheduling of EV to achieve better utilization of intermittent PV for EV charging. A real-time charging optimization scheme was formulated by using mixed-integer linear programming (MILP). Extensive simulation techniques at the same time proposed the approach of maximizing the satisfaction of EV owners and minimizing the overall operational cost of the parking station. These supercharging station models usually did not incorporate or provide battery swap services.

Yang et al. (2017) aimed at presenting a data-driven optimization model for allocating charging stations and chargers for taxi in a city located in China. The objective function of this proposed approach was to minimize the overall investment considering vehicles' dwell pattern as input and the probability of BEVs being charged during their dwell time as constraints. Using regression and logarithmic transformation, the authors transformed the optimization model as an ILP problem and solved it using Gurobi solver. The notable findings from this research were the dwell pattern of the taxi fleet which determined the siting of charging stations. It also provided information regarding waiting spots. In addition to charging spots, the utilization of chargers increased and the number of required chargers at each site decreased. The research also provided information regarding the tradeoff between installing more chargers versus providing more waiting spaces which could be quantified by the cost ratio of chargers and parking spots.

Gusrialdi et al. (2017) proposed a strategy for coordinating the EV queues among charging stations getting information about the traffic flows around the areas charging stations were located. In this work, a distributed algorithm was proposed for scheduling the EV flows in the charging stations. Additionally, a distributed policy was also proposed for controlling the EV flows near the charging stations based on EVs own battery constraints. A real-life scenario of the highways in the United States, namely the Florida Turnpike was used for showing the performance improvement of the proposed strategy.

1.2.3 Joint Battery Swap and Supercharging Station

Short and Denholm (2006) modeled the effect of large-scale adoption of Plug-in Hybrid Electric Vehicle (PHEV) on the integration of wind energy into the US electricity mix. Installed wind capacity increased by 243 GW, or 6% of total generation, when the vehicle fleet was converted to 50% PHEV under a smart charging plan.

Turton and Moura (2008) used a global energy model that forecast the integration and impacts of EV and V2G. The authors found that the installed renewable energy capacity increased by 30 to 75% with V2G capable EV due to their ability to store intermittent energy and discharged it back to the grid when required.

Borba et al. (2012) took an interesting approach for modeling EVs and wind energy. The Brazilian power sector was modeled from 2010 to 2030, with an assumed 16-fold increase in wind generating capacity in the northeast. The authors then calculated the size of PHEV fleet that could be charged using the excess wind energy production. Since the excess production varied seasonally, occurring primarily between January and June, the authors assumed that the vehicles could drive on locally produced ethanol for the remainder of the year. Over 1.6 million vehicles could be powered in this manner by 2030.

Richardson (2013) reviewed the current literature on EV, the electric grid, and renewable energy integration. Key methods and assumptions of the literature were discussed. The economic, environmental and grid impacts of EVs were reviewed. Numerous studies assessing the ability of EVs to integrate renewable energy sources were assessed; the literature indicated that EV could significantly reduce the amount of excess renewable energy produced in an electric system. Studies on wind–EV interaction were much more detailed than those on solar PV and EV. The paper concluded with recommendations for future research.

Zheng et al. (2014) presented a framework for optimal design of battery charging/swap stations in distribution systems based on life cycle cost (LCC) minimization. The results showed that battery swap station was more suitable for public transportation in distribution systems.

Mwasilu et al. (2014) presented a comprehensive review and assessment of the latest research and advancement of electric vehicles (EVs) interaction with smart grid portraying the future electric power system model. The conceptual goal of the smart grid along with the future deployment of the EV put forward various challenges in terms of electric grid infrastructure, communication, and control. Following an intensive review on advanced smart metering and communication infrastructures, the strategy for integrating the EV into the electric grid was presented. Various EV smart charging technologies were also extensively examined with the perspective of their potential, impacts and limitations under the vehicle-to-grid (V2G) phenomenon. Moreover, the high penetration of renewable energy sources (wind and photovoltaic solar) was soaring up into the power system. However, their intermittent power output posed different challenges on the planning, operation and control of the power system networks. On the other hand, the deployment of EVs in the energy market could compensate for the fluctuations of the electric grid. In this context, a literature review on the integration of the renewable energy and the latest feasible solution using EV with the insight of the promising research gap to be covered up were investigated. Furthermore, the feasibility of the smart V2G system was thoroughly discussed. In this paper, the EVs interactions with the smart grid as the future energy system model were extensively discussed and research gap was revealed for the possible solutions.

Xu et al. (2015) focused on the mechanism of smart battery charging and swapping operation service network for EV including its overall architecture and operational mode. Two different types of demonstration projects were presented which expound on the condition of EV’s infrastructure construction. Lastly, performance analysis of the charging behaviors of electric taxis in fast charging station based on the queuing theory was proposed. The simulation results showed that the service time and the number of generators had an influence on the average waiting time and the length of queue.

Zhang and Wang (2016) studied a battery schedule framework to dispatch batteries between battery charging stations (BCS) and battery swap stations (BSS) efficiently. A two-direction battery dispatch model to reduce the transportation cost was established and solved by particle swarm optimization (PSO) method. Moreover, considering the serving ability limitations, the K-means clustering was utilized to pre-partition the BCS and BSS to make the battery dispatch more efficient and effective. The proposed methods were finally verified by an urban battery logistics case.

Zhang et al. (2016) proposed a new construction model by combining battery replacement and concentrated charging and presented a location optimization model. This location optimization model could be applied to determine appropriate places for establishing the power station and queueing theory to determine the optimal number of power equipment for achieving minimum costs.

Wu et al. (2017) proposed an optimal charging strategy to improve the self-consumption of PV-generated power and service availability while considering forecast errors. First, they introduced the typical structure and operation model of PV-based BSS. Second, three indexes were presented to evaluate operational performance. Then, PSO algorithm was developed to calculate the optimal charging power and to minimize the charging cost for each time slot. The proposed charging strategy helped decrease the impact of forecast uncertainties on the availability of the battery swapping service. Finally, a day-ahead operation schedule, a real-time decision-making strategy, and the proposed PSO charging strategy for PV-based BSS were simulated in a case study. The simulation results showed that the proposed strategy could effectively improve the self-consumption of PV-generated power and reduced charging cost.

Liu et al. (2018) achieved the optimal operation of BSCS, a closed-loop supply chain-based BSCS model was proposed to realize the combined operation of battery charging stations and battery swap stations (BSS) while the quality of battery swapping service at BSS was ensured with a network calculus-based service model. Simulation results verified the feasibility of the proposed model and the heuristic solution with small optimality losses and less computation time.

Ma and Zhang (2018) proposed a Bass diffusion model (BASS) model to predict the total number of electric vehicles and calculated the size of charging stations in the coming years. They considered that centralized charging stations were attached to substation construction which was considered as a fixed number. They also assumed that the less the battery changing stations in the city, the greater the total distance from the battery changing station to the charging station. A queuing model was formulated to optimize the location of charging stations and the model was solved to minimize the cost as the objective function by using the exhaustion method. The model was also tested using the data collected from China.

Sun et al. (2018) proposed an objective function for finding the optimal policy of charging in way the overall cost of charging was minimized by ensuring quality of service along with EV blocking probability did not exceed a certain value. The problem was formulated using constrained Markov decision process and the problem was solved using Lagrangian method and dynamic programming. In this paper, the problem was created considering one batter swapping and charging station.

Table 1.1 Summary of Literature Review

	Author	Journal Name	Year of Publish	Paper Id	Battery Swap/Supercharger/Both	Car/Truck/Ship	One station/ Network Design(Multi-Station)	Queueing Model/ Simulation/Statistics/Random Process Model	Type of optimization model	Single/Multi-objective	Min Cost/ Max Profit	Distributed Generation
1	Zhang,Dingli Qi,Wei Jiang,Shuang Lei	Promet-Traffic&Transportation	2016	Optimal allocation of changing station for electric vehicle based on queueing theory	Both	EV not stated clearly	Multi-station	Queueing Model	Linear Programming (Location Allocation)	Single objective	Min cost	N/A
2	Fang Lu, Guowei Hua	IEEE	2015	A location-sizing model for electric vehicle charging station deployment based on queuing theory	super charge	EV not stated clearly	Network (Multi Station)	Queueing Model	Linear Programming (Location Allocation)	Single objective	Max flow refilled with p facilities	N/A
3	Jian Ma, Liyan Zhang	Energy	2018	A deploying method for predicting the size and optimizing the location of an electric vehicle charging	Both	EV not stated clearly	Multi-station	Queueing Model	Linear Programming (Location Allocation)	Single objective	Min cost	N/A
4	JieYan, Mohan Menghwar, Ehtisham Asghar	Energy	2019	Real-time energy management forasmart-community microgrid with battery swapping and	Battery Swap	EV not stated clearly	Multi-station+ house-hold	Queueing Model	Linear Programming model+simulation	Single objective	Max use of renewable energy	Renewable energy
5	Shengjie Yang, Jiangang Yoa etc.	Energy	2014	Dynamic operation model of the battery swapping station for EV (electric vehicle) in electricity	Battery Swap	EV not stated clearly	One-station	Dynamic operation model	Dynamic operation model	Single objective	N/A	N/A
6	Mohsen Mahoor, Zohreh S. Hosseini, Amin	Energy	2019	Least-cost operation of a battery swapping station with random customer requests	Battery Swap	EV not stated clearly	One-station	-	Mixed Integer Linear Programming	Single objective	Min Operation Cost	N/A
7	Xiaoqi Tan, Bo Sun and Danny H.K. Tsang	IEEE	2014	Queueing Network Models for Electric Vehicle Charging Station with Battery Swapping	Battery Swap	EV not stated clearly	One-station	Queueing Network Model	Steady state distribution	Multi objective	N/A	N/A
8	E. Pashajavid, and M. A. Golkar	Journal of Renewable and Sustainable	2013	Optimal placement and sizing of plug in electric vehicles charging stations within distribution networks with high penetration of	Battery Swap Station	EV not stated clearly	Multi Station	Probabilistic Model	Metaheuristic	Multi objective	Min Energy loss + Voltage deviation	PV
9	Xiaohui Xu, Liangzhong Yao, Pingliang Zeng, Yujun Liu and,	Springer	2015	Architecture and performance analysis of a smart battery charging and swapping operation service network for electric vehicles in	Both	Electric Taxi	Multi Station	Queueing Network Model	Simulation	N/A	N/A	N/A
10	Leehter Yao, Zolboo Damiran and Wei Hong Lim	Energy	2017	Optimal Charging and Discharging Scheduling for Electric Vehicles in a Parking Station with Photovoltaic System and Energy Storage System	Super Charge	EV not stated clearly	One-station	Simulation	Mixed Integer Linear Programming	Multi objective	Max satisfaction of EV owner+Min	PV
11	Yang Dong, Yan Xu, Ke Meng, JunHua Zhao and Jing Qiu	IEEE	2014	Electric Vehicle Battery Charging/Swap Stations in Distribution Systems: Comparison Study and Optimal Planning	Both	Bus	Multi Station	Cost benefit analysis	Mixed Integer Linear Programming	Single objective	Max Net Present Value	N/A
12	Zhile Yang, Kang Li, Aoife Foley, Cheng Zhang	Proceedings of the 19th World Congress The International Federation of Automatic Control Cape Town, South Africa	2014	Optimal Scheduling Methods to Integrate Plug-in Electric Vehicles with the Power System: A Review	Super Charge	EV not stated clearly	N/A	Meta Heuristic Algorithm	LP, NLP, Dynamic programming	N/A	N/A	N/A
13	Xian Zhang, Guibin Wang	IEEE	2016	Vehicle Batteries between Battery Swapping Stations and Charging Stations	Both	EV not stated clearly	One-station	K means clusturing	Metaheuristic	Single objective	Min transportation cost	N/A
14	Tianyang Zhao, Shuhan Yao,	IEEE	2019	of Battery Swapping-Charging Systems	Both	Trucks	(Multi Station)	Time space network technique	Programming, Heuristic and Simulation	Multi objective	Max revenue	N/A
15	Qingshan Xu, Qun Li, Xiaodong Yuan, and Bing	International Journal of Photoenergy	2017	PV-Based Battery Swapping Stations in a DC Distribution System	Both	EV not stated clearly	One-station	Simulation	Metaheuristic	Single objective	charging cost for each time slot	PV
16	Zheng, D., Wen, F., & Huang, J.	IEEE	2012	Optimal Planning of Battery Swap Station	Battery Swapping	Electric bus	-	Simulation	Simulation	Single objective	maximize the annual profit of battery swap station and minimize the	N/A

1.3 Research Questions and Contributions

This research addresses following two questions related to allocation of renewable microgrid in battery swap and supercharging stations for electric vehicles:

- First, is it economically viable to integrate wind- and solar-based microgrid along with energy storage system (ESS) to power the battery swap and supercharging facilities in island operations?
- Second, is it economically viable to integrate wind- and solar-based microgrid along with main grid to power the battery swap and supercharging facilities in interconnected operation mode?

For answering those above questions and after reviewing all the state-of-the-art research conducted on this topic, the contribution of the thesis work is:

- First, the modeling of the optimization model of battery swap and supercharging stations consists of integrating renewable and distributed generating units such as WT and PV under power uncertainty.
- Second, the design of the optimization model of battery swap and supercharging stations not only consist of integrating renewable microgrid power, but also taking into account demand response and grid-tied operation with 2-way energy flow. That design and modeling framework makes the EV battery service stations to behave as “energy prosumer”.
- Third, the thesis also presents the design of a network optimization model of EV supercharging stations of Tesla located in Texas for showing the application of the research in real world.

1.4 Thesis Overview

The thesis consists of six chapters. Chapter 1 provides the research motivation, literature review, and research contributions.

Chapter 2 discusses the Erlang queueing models for battery services. The modeling of battery swap service using Erlang B, supercharging service using Erlang C, and Erlang A is for situations with battery service withdrawal are discussed in detail.

Chapter 3 proposes an optimization framework for allocating renewable microgrid in single battery swap station with island and grid-tied microgrid, respectively. A microgrid is comprised of wind turbine (WT), photovoltaics (PV) and energy storage systems (ESS). The optimization model has tested using ten different cities located in USA capacity factor data of WT and PV for renewable microgrid along with varying different other parameters in the models.

Chapter 4 proposes an optimization framework for allocating renewable microgrid in single joint battery swap and supercharging station with grid-tied-microgrid. The optimization model has tested using ten different cities located in USA capacity factor data of WT and PV for renewable microgrid along with varying different other parameters in the model.

Chapter 5 presents a network optimization framework of Tesla supercharging stations located in Texas. The network optimization model has solved using two approaches. In the first approach, the network optimization model has solved for each specific zone separately. In the second approach, the network optimization model has solved consisting of all zones together. This model has solved using seven cities located in Texas capacity factor data of WT and PV for renewable microgrid along with varying different other parameters in the model.

Chapter 6 concludes the work and discusses the future research directions.

2. ERLANG QUEUEING MODELS FOR BATTERY SERVICES

2.1 Erlang B Model for Battery Swap

Let k=0, 1, …, s be the number of batteries under recharging in the charge bay in a station. The battery swap process with EV blocked is modeled as M/G/s/s Erlang B queue, and its transition diagram is shown in Figure 2.1 below.

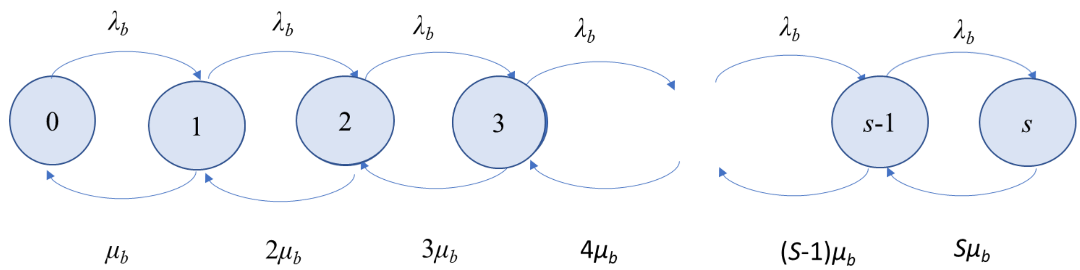

Figure 2.1 The M/G/s/s Queue (Erlang B)

In this case, λ_b is the EV arrival rate (e.g. cars/hour) of a station and μ_b is the battery recharge rate in the charge bay. Namely, to charge a depleted battery to the desired State of Charge (SOC) level, the average charging duration is $1/\mu_b$. To facilitate the model presentation, parameters and variables of Erlang B model are listed in Table 2.1.

Table 2.1 Notation

Symbol	Explanation
i	Index of customer zone for i=1, 2, …, I
j	Index of candidate station location, for j=1,2, …, J
λ_b	EV arrival rate of a station
λ_d	EV arrival rate of a supercharging service
μ_b	Battery recharge rate in the charge bay
μ_d	Supercharging rate
θ	Expected EV arrivals during a battery recharge cycle in the charge bay
φ	Expected EV arrivals during a supercharging cycle
$B(s)$	Probability of spare battery stockout
$C(m, s)$	Probability that an EV waits for a supercharger
N_b	The number of batteries in the charge bay under recharging
N_q	The number of EV waiting for superchargers
N_c	The number of EV under supercharging
N_d	Total number of EV in supercharging queue, and $N_d = N_q + N_c$
τ_b	Time duration for swapping a battery
P_b	Power for charging a battery in charge bay
P_d	Power for charging a battery using supercharger
P_s	Total power demand of a station
P_j	Power capacity or limit of station j
F_j	Setup cost for station j
F_b	Unit cost of spare battery
F_d	Unit cost of supercharger
x_j	Whether a station opens in location j, binary decision variable
s	The base stock level of spare batteries in a station, integer decision variable
m	The number of superchargers in a JBSS, integer decision variable

Let X be the random variable representing the number of vehicles arriving at a Joint Battery Swap and Supercharging (JBSS) station during $1/\mu_b$. Given the spare battery stock level is s, the chance that an EV is blocked in the swap queue (i.e. stockout probability) can be estimated as follows (Winston 2004).

Step 1: Solving for B_k for k=1, 2, …, s

$$B_k = \frac{\lambda_0}{\mu_1} = \frac{\lambda_b}{\mu_b} = \theta \tag{2.1}$$

$$\theta = \frac{\lambda_b}{\mu_b} \tag{2.2}$$

$$B_2 = \frac{\lambda_b^2}{\mu_b \quad 2\mu_b} = \frac{1}{2!}\theta^2 \tag{2.3}$$

$$B_k = \frac{1}{k!}\theta^k \;\; for\ k = 1, 2, \ldots s \tag{2.4}$$

Step 2: Compute π_0.

$$\pi_0 = \frac{1}{1+\sum_{k=1}^{s} B_k} = \frac{1}{1+\theta+\frac{1}{2!}\theta^2+\ldots+\frac{1}{k!}\theta^k} = \frac{1}{\sum_{k=0}^{s}\frac{\theta^k}{k!}} \tag{2.5}$$

Step 3: Compute all other π_k for k= 1, 2, 3, …, s.

$$\pi_1 = B_1\pi_0 = \frac{\theta}{\sum_{k=0}^{s}\frac{\theta^k}{k!}} \tag{2.6}$$

$$\pi_2 = B_2\pi_0 = \frac{\frac{\theta^2}{2!}}{\sum_{k=0}^{s}\frac{\theta^k}{k!}} \tag{2.7}$$

$$\pi_k = B_k\pi_0 = \frac{\frac{\theta^k}{k!}}{\sum_{k=0}^{s}\frac{\theta^k}{k!}} \quad k = 3, 4, \ldots s-1 \tag{2.8}$$

$$B(s) = \pi_s = B_s\pi_0 = \frac{\frac{\theta^s}{s!}}{\sum_{k=0}^{s}\frac{\theta^k}{k!}} \tag{2.9}$$

Where $B(s)$ is the probability of being blocked.

Step 4: Compute L, L_s, L_q, W, W_s, W_q.

$$W = W_s = \frac{1}{\mu_b} \tag{2.10}$$

$$L = L_s = \sum_{k=0}^{s} k\pi_k = \sum_{k=1}^{s} k\pi_k = \sum_{k=1}^{s} k\frac{\frac{\theta^k}{k!}}{\frac{\theta^k}{k!}} = \sum_{k=1}^{s}\left[\frac{\frac{\theta^k}{(k-1)!}}{\sum_{k=0}^{s}\frac{\theta^k}{k!}}\right] = \theta\sum_{k=1}^{s}\left[\frac{\frac{\theta^{k-1}}{(k-1)!}}{\sum_{k=0}^{s}\frac{\theta^k}{k!}}\right]$$

$$= \rho\sum_{k=0}^{s-1}\left[\frac{\frac{\theta^k}{k!}}{\sum_{k=0}^{s}\frac{\theta^k}{k!}}\right] = \left[\frac{\frac{\theta^0}{0!}}{\sum_{k=0}^{s}\frac{\theta^k}{k!}} + \frac{\frac{\theta^1}{1!}}{\sum_{k=0}^{s}\frac{\theta^k}{k!}} + \frac{\frac{\theta^2}{2!}}{\sum_{k=0}^{s}\frac{\theta^k}{k!}} + \ldots + \frac{\frac{\theta^{s-1}}{(s-1)!}}{\sum_{k=0}^{s}\frac{\theta^k}{k!}}\right] = \frac{\lambda_b}{\mu_b}(1-\pi_s) \qquad (2.11)$$

Where W is the total swap time in the queue system, W_s is the swap time, and W_q is the waiting time. For Erlang B, W_q=0. Similarly, L is the total number of EV in the queue system. L_s is the number of EV in swapping, and L_q is the number of EV waiting which is always zero for Erlang B model.

2.2 Erlang C Model for Supercharging

An arriving EV is directed to the supercharging queue if the stockroom has no spare battery. A supercharger represents the Level-3 DC fast charge technology with an output power up to 80kW based on SAEJ1772 standards (SAE 2010). Tesla EV service network maintains its own charging standard in which the power of a supercharger is between 72 kW to 150 kW. Let λ_d be the EV arrival rate of the supercharging queue, then

$$\lambda_d = \lambda_b B(s) \qquad (2.12)$$

The above result is due to the fact that an EV blocked in the swap queue moves to the superchargers. Since $0<B(s)\leq 1$, but here $\lambda_d \leq \lambda_b$. Let, m be the number of superchargers in a JBSS. Then the supercharging queuing process can be modeled as an M/M/m/∞ Erlang C queue. The state in the transition diagram below represents the number of EV for

supercharging service.

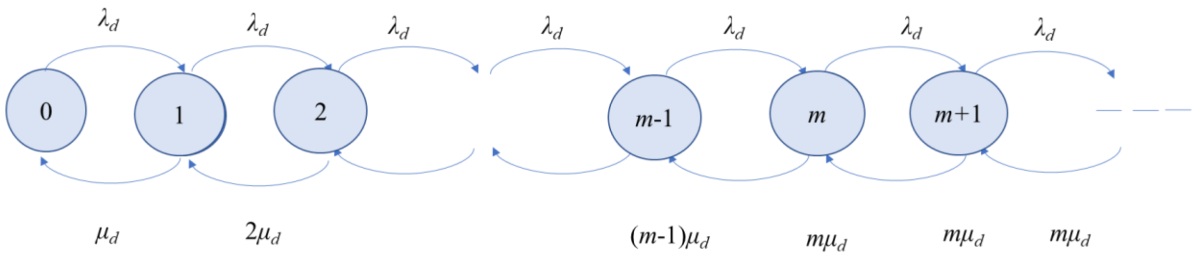

Figure 2.2 The M/M/m/∞ Queue (Erlang C)

Note that μ_d is the service rate per supercharger (e.g. cars/hour), or $1/\mu_d$ is the average time duration given the supercharger is available. The M/M/m/∞ system is also referred to as the Erlang C delayed model because it accommodates a waiting line when all superchargers are busy. This differs from Erlang B which does not accommodate the waiting. Let Y be the number of EV under supercharging service during a period of $1/\mu_d$. The probability that an EV has to wait in the supercharging queue is given as (Winston 2004):

For k=0, 1, 2, …., m.

$$\mu_d C_1 = \lambda_d C_0 \tag{2.13}$$

$$\lambda_d C_{k-1} + (k+1)\mu_d C_{k+1} = (\lambda_d + K\mu_d)C_{k,} \qquad 1 \le k \le m-1 \tag{2.14}$$

$$\lambda_d C_{k-1} + m\mu_d C_{k+1} = (\lambda_d + m\mu_d)C_k, \qquad k \ge m \tag{2.15}$$

$$k\mu_d C_k = \lambda_d C_{k-1}, \qquad 1 \le k \le m \tag{2.16}$$

$$k\mu_d C_k = \lambda_d C_{k-1}, \qquad k \ge m \tag{2.17}$$

$$C_k = \frac{\lambda_d C_{k-1}}{k\mu_d} = \frac{\lambda_d^2 C_{k-2}}{k(k-1)\mu_d^2} = \ldots = \frac{1}{k!}\frac{\lambda_d^k}{\mu_d}C_0, \qquad 1 \le k \le m \tag{2.18}$$

$$C_k = \left(\frac{\lambda_d}{m\mu_d}\right)^2 C_{k-2} = \ldots\ldots = \left(\frac{\lambda_d}{m\mu_d}\right)^{k-m} C_m = \frac{\left(\frac{\lambda_d}{\mu_d}\right)^k}{m!m^{k-m}} C_0, \qquad k \ge m \tag{2.19}$$

$$\varphi = \frac{\lambda_d}{\mu_d} \tag{2.20}$$

$$\sum_{k=0}^{\infty} C_k = 1 \tag{2.21}$$

$$\frac{\varphi}{m} \langle 1, \quad \frac{1}{C_0} = \sum_{k=0}^{m-1} \frac{\varphi^k}{k!} + \frac{m^m}{m!} \sum_{k=m}^{\infty} \left(\frac{\varphi}{m}\right)^k = \sum_{k=0}^{m-1} \frac{\varphi^k}{k!} + \frac{\varphi^m}{(m-1)!(m-\varphi)} \tag{2.22}$$

The probability distribution, for the number of EV in the Erlang C queue system,

$$C_k = C_0 \frac{\varphi^k}{k!}, \qquad 0 \le k \le m \tag{2.23}$$

$$C_k = C_0 \frac{m^m}{m!} \left(\frac{\varphi}{m}\right)^{k-m}, \qquad k \ge m \tag{2.24}$$

An EV that has arrived at the supercharging area needs to wait if all superchargers are busy and occupied by earlier arrived cars. Owing to the PASTA property (PASTA stands for Poisson Arrivals See Time Averages), the wait probability is given by,

$$C(m,s) = C(w\rangle 0) = \sum_{k=m}^{\infty} C_k = C_m \sum_{k=m}^{\infty} \left(\frac{\varphi}{m}\right)^{k-m} = \frac{C_m m}{m-\varphi} = \frac{C_o \varphi^m}{(m-1)!(m-\varphi)}$$

$$= \frac{\frac{\varphi_m}{(m-1)!(m-\varphi)}}{\sum_{k=0}^{m-1} \frac{\varphi^k}{k!} + \frac{\varphi^m}{(m-1)!(m-\varphi)}} = \frac{\frac{\varphi^m}{m!(1-\frac{\varphi}{m})}}{\sum_{k=0}^{m-1} \frac{\varphi^k}{k!} + \frac{\varphi^m}{m!(1-\frac{\varphi}{m})}} = \frac{\frac{(m\rho_d)^m}{m!(1-\rho_d)}}{\sum_{k=0}^{m-1} \frac{(m\rho_d)^k}{k!} + \frac{(m\rho_d)^m}{m!(1-\rho_d)}} \tag{2.25}$$

$$\varphi = \frac{\lambda_d}{\mu_d} = \mathit{offered\ rate} \tag{2.26}$$

$$\rho_d = \frac{\lambda_d}{m\mu_d} = traffic\ \text{int}ensity\ rate \tag{2.27}$$

$$\lambda_d = \lambda_b B(s) \tag{2.28}$$

$$\rho_d = \frac{\lambda_b B(s)}{m\mu_d} \tag{2.29}$$

It is worth mentioning that the PASTA property refers to the expected state of a queueing system as seen by an arrival from a Poison process. An arrival from a Poisson process observes the system as if it were arriving at a random moment in time. Therefore, the expected value of any parameter of the queue at the instant of a Poisson arrival is simply the long-run average value of that parameter (Ibe, 2013). By substituting equation (2.25), we have

$$C(m,s) = \frac{\dfrac{\left(\dfrac{B(s)\lambda_b}{\mu_d}\right)^m}{m!\left(\dfrac{1-B(s)\lambda_b}{m\mu_d}\right)}}{\displaystyle\sum_{k=0}^{m-1}\frac{\left(\dfrac{B(s)\lambda_b}{\mu_d}\right)^k}{k!} + \frac{\left(\dfrac{B(s)\lambda_b}{\mu_d}\right)^m}{m!\left(\dfrac{1-B(s)\lambda_b}{m\mu_d}\right)}} \tag{2.30}$$

2.3 Erlang A Model for Customer Withdrawal

In the Erlang A model customers arrive to the queueing system according to a poison process with rate λ. Customers are equipped with patience times τ that are exp(θ) independent and identically across customers. The service times are also independent and identically distributed with rate μ. Finally, the processes of arrivals, patience and service are mutually independent. For a given customer, the patience time τ results in an abandonment if the waiting time is prolonged.

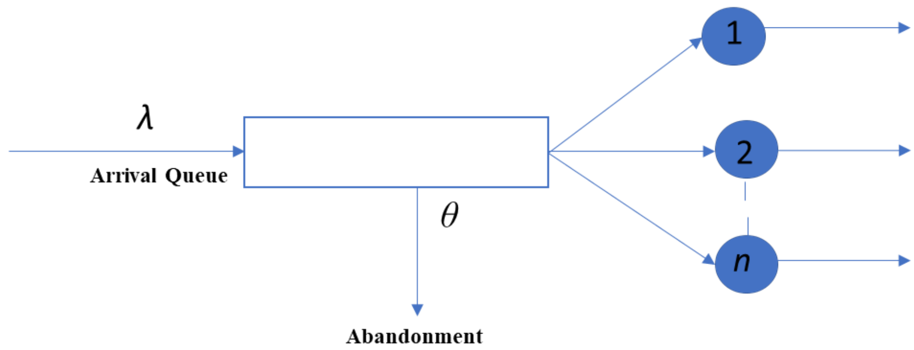

Figure 2.3 Erlang A Queue with Customer Abandonment

Let v be the offered waiting time i.e., the time a customer equipped with infinite patience must wait in order to get service. The actual waiting/queueing time then equals

$$W=\min\{v,\ \tau\}. \tag{2.31}$$

$L(t)$ =The total number of customers in system at time t (served plus queued).

$L=\{L(t),\ t\geq 0\}$ is for Markov birth-death process with the following transition-rate diagram.

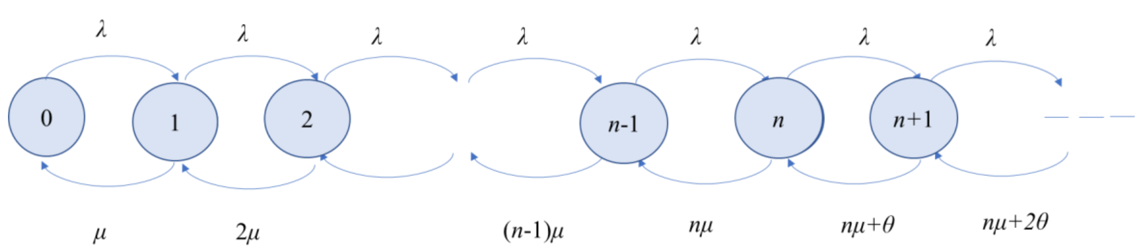

Figure 2.4 The M/M/N+M (G) Queue (Erlang A)

Let, d_j stands for the death-rate in state j, for $0\leq j\leq\infty$, Then

$$j.\min(\mu,\theta)\leq d_j\leq j.\max(\mu,\theta) \tag{2.32}$$

The bounds on the left-hand and right-hand sides of (2.32) correspond to death-rates of an M/M/∞ queue with service rates min (μ, θ) and max (μ, θ). In some sense, which can be made precise via stochastic orders between distributions, these two M/M/∞ queues provide lower and upper (stochastic) bounds for Erlang-A system. The lower bound will be used later to prove that Erlang-A always reaches the steady-state. In the special case of equal service and abandonment rate (μ=θ), the Erlang-A and M/M/∞ in fact coincide. As customary, define the limiting distribution of L by,

$$\pi_j = \lim_{t\to\infty} P\{L(t) = j\}, \qquad j \geq 0 \tag{2.33}$$

When existing, the limit distribution is also a steady-state (or stationary) distribution, which is calculated via the following version of the steady-state equations:

$$\lambda\pi_j = (j+1).\mu\pi_{j+1}, \qquad 0 \leq j \leq n-1 \tag{2.34}$$

$$\lambda\pi_j = (n\mu + (j+1-n)\theta)\pi_{j+1}, \qquad j \geq n \tag{2.35}$$

It is straightforward to derive the "recipe" solution:

$$\begin{aligned} \pi_j &= \frac{\left(\frac{\lambda}{\mu}\right)}{j}\pi_0, \qquad 0 \leq j \leq n \\ \pi_j &= \prod_{k=n+1}^{j}\left(\frac{\lambda}{n\mu+(k-n)\theta}\right)\frac{\left(\frac{\lambda}{\mu}\right)}{n!}\pi_0, \qquad j \geq n+1 \end{aligned} \tag{2.36}$$

Where,

$$\pi_0 = \left[\sum_{j=0}^{n}\frac{\left(\frac{\lambda}{\mu}\right)^j}{j!} + \sum_{j=n+1}^{\infty}\prod_{k=n+1}^{j}\left(\frac{\lambda}{n\mu+(k-n)\theta}\right)\frac{\left(\frac{\lambda}{\mu}\right)^n}{n!}\right]^{-1} \tag{2.37}$$

The solution makes sense-equivalently the Markov Process L is ergodic, if the infinite sum in (2.37) converges, which is a consequence of the lower bound in (2.32),

$$\sum_{j=0}^{n}\frac{\left(\frac{\lambda}{j}\right)^{j}}{j!}+\sum_{j=n+1}^{\infty}\prod_{k=n+1}^{j}\left(\frac{\lambda}{n\mu+(k-n)\theta}\right)\frac{\left(\frac{\lambda}{\mu}\right)^{n}}{n!}\leq\sum_{j=0}^{\infty}\frac{\left(\frac{\lambda}{\min(\mu,\theta)}\right)^{j}}{j!}=e^{-\frac{\lambda}{\min(\mu,\theta)}} \tag{2.38}$$

The Gamma function is defined by

$$\Gamma(x)=\int_{0}^{\infty}t^{x-1}e^{-t}dt, \qquad x>0 \tag{2.39}$$

The incomplete Gamma function is defined as

$$\Upsilon(x,y)=\int_{0}^{\infty}t^{x-1}e^{-t}dt, \qquad x>0, y\geq 0 \tag{2.40}$$

Let

$$A(x,y)=\frac{xe^{y}}{y^{x}}.\Upsilon(x,y)=1+\sum_{j=1}^{\infty}\frac{y^{j}}{\prod_{k=1}^{j}(x+k)} \qquad x>0, y\geq 0 \tag{2.41}$$

Let, $B_{1,n}$ denote the blocking probability in M/M/n/n system (Erlang B) and recall the Erlang-B formula,

$$B_{1,n}=\frac{\frac{\left(\frac{\lambda}{\mu}\right)^{n}}{n!}}{\sum_{j=0}^{n}\frac{\left(\frac{\lambda}{\mu}\right)^{j}}{j!}} \tag{2.42}$$

A simple way for calculating $B_{1,n}$ is the recursion,

$$B_{1,0}=0; \qquad B_{1,n}=\frac{\rho B_{1,n-1}}{1+\rho B_{1,n-1}} \qquad n\geq 1 \tag{2.43}$$

$$\rho\triangleq\frac{\lambda}{n\mu}$$

Where ρ is called offered load per server.

Using equations (2.37), (2.41) and (2.42), one obtains.

$$\pi_0^{-1} = \sum_{j=0}^{n} \frac{\left(\frac{\lambda}{\mu}\right)^j}{j!} + \frac{\left(\frac{\lambda}{\mu}\right)^n}{n!} . \sum_{j=n+1}^{\infty} \prod_{k=n+1}^{j} \left(\frac{\lambda}{n\mu + (k-n)\theta} \right) = \frac{\left(\frac{\lambda}{\mu}\right)^n}{n!} \left[\frac{1}{B_{1,n}} + \sum_{j=1}^{\infty} \frac{\left(\frac{\lambda}{\theta}\right)^j}{\prod_{k=1}^{j} \left(\frac{n\mu}{\theta}, \frac{\lambda}{\theta} \right)^{-1}} \right]$$

$$= \frac{\left(\frac{\lambda}{\mu}\right)^n}{n!} \left[\frac{1}{B_{1,n}} + A\left(\frac{n\mu}{\theta}, \frac{\lambda}{\theta} \right)^{-1} \right] \tag{2.44}$$

$$\pi_0 = \frac{B_{1,n}}{1 + \left[A\left(\frac{n\mu}{\theta}, \frac{\lambda}{\theta} \right) - 1 \right] . B_{1,n}} . \frac{n!}{\left(\frac{\lambda}{\mu}\right)^n} \tag{2.45}$$

$For, \qquad 1 \le j \le n$

$$\pi_j = \pi_0 . \frac{\left(\frac{\lambda}{\mu}\right)^j}{j!} = \frac{B_{1,n}}{1 + \left[A\left(\frac{n\mu}{\theta}, \frac{\lambda}{\theta} \right) - 1 \right] . B_{1,n}} . \frac{n!}{j! \left(\frac{\lambda}{\mu}\right)^{n-j}} \tag{2.46}$$

$$\pi_n = \frac{B_{1,n}}{1 + \left[A\left(\frac{n\mu}{\theta}, \frac{\lambda}{\theta} \right) - 1 \right] . B_{1,n}} \tag{2.47}$$

2.4 Modeling Battery Swap Services Using Erlang B

For example, EV arrival rate of a station, λ_b = 1.5 EV/hour, battery recharge rate in the charge bay, μ_b =0.5 EV/hour and the number of batteries under recharging in the charge bay k=3. The probability of spare battery stockout is given,

$$B(s) = \pi_s = B_s \pi_0 = \frac{\frac{\theta^s}{s!}}{\sum_{k=0}^{s} \frac{\theta^k}{k!}} \tag{2.48}$$

Putting the values in the above equation, the probability of spare battery stockout $B(s)$= 0.213. For this particular system, L_q=0, L_s=L, W_q=0, W_s=W. Since, cars receive immediate service once entering the system. We can compute L and L_s by using these formulas stated below,

$$L = L_s = \frac{\lambda_b}{\mu_b}(1-\pi_s) \tag{2.49}$$

$$W = W_s = \frac{1}{\mu_b} \tag{2.50}$$

By using the previous data, the value of L=L_s = 2.36 and the value of W=W_s = 2. EV arrival rate of a station, λ_b = 1.5 EV/hour and battery recharging rate in the charge bay, μ_b =0.5 EV/hour. The expected EV arrivals during a battery recharge cycle in the charge bay,

$$\theta = \frac{\lambda_b}{\mu_b} = \frac{1.5}{0.5} = 3$$

The computation of π_s, L, L_q, L_s, W, W_q, W_s for the values of k from 0 to 10 are listed in Table 2.2.

Table 2.2 Values of π_s, L, L_q, L_s, W, W_q, W_s

k	π_s	L	L_q	L_s	W	W_q	W_s
0	0.047	2.86	0	2.86	2	0	2
1	0.142	2.58	0	2.58	2	0	2
2	0.213	2.36	0	2.36	2	0	2
3	0.213	2.36	0	2.36	2	0	2
4	0.160	2.52	0	2.52	2	0	2
5	0.096	2.72	0	2.72	2	0	2
6	0.048	2.86	0	2.86	2	0	2
7	0.021	2.94	0	2.94	2	0	2
8	0.008	2.98	0	2.98	2	0	2
9	0.003	2.99	0	2.99	2	0	2
10	0.001	2.99	0	2.99	2	0	2

The Erlang B queueing model by using MATLAB programming is given below,

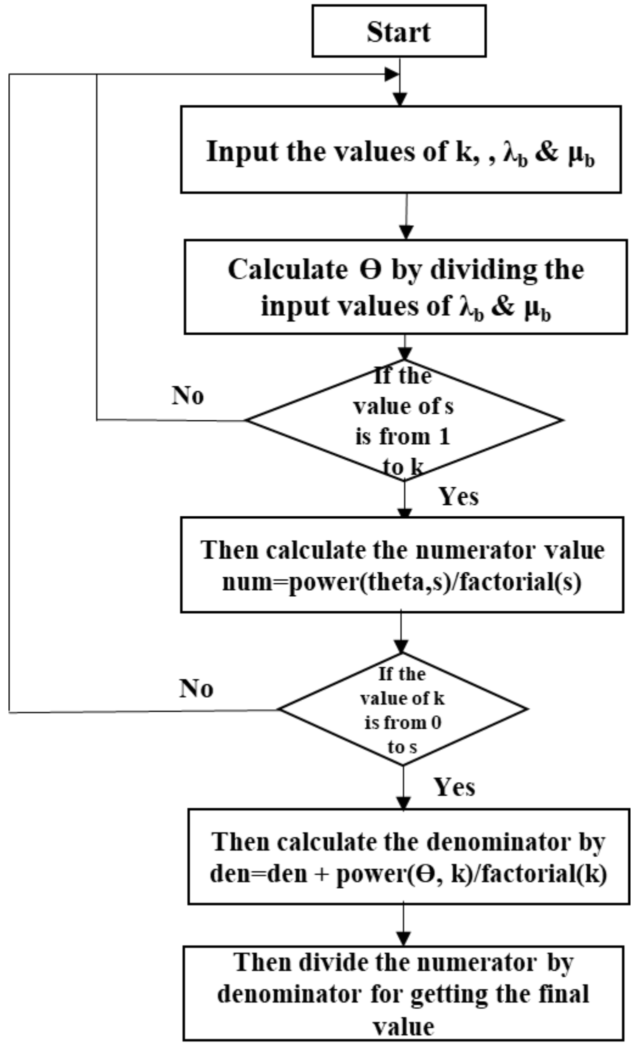

Figure 2.5 Flow Chart of Erlang B Model in MATLAB Code

The computation of Erlang B can be easily implemented in Matlab programming environment. At the start of the Erlang B model in Matlab first input the values of k, λ_b and μ_b. Then the model will calculate the θ value by diving λ_b and μ_b. If the value of s is from 1 to k, the model will go to the next step of the flowchart, otherwise the model will start from the beginning. If the model goes to the next step by following the conditions, it will start calculating the numerator value by using power (theta, s)/factorial(s). After that if the value of k is from 0 to s then the model will go to the next step and calculate the denominator value by using den + power (θ, k)/factorial(k). If the condition is not fulfilled, the model will start from the beginning. Now, the final result can be obtained by diving the numerator from the denominator.

After running the model for the value of k=9, λ_b =1.5 and μ_b = 0.5, the obtained value of π_s from the MATLAB is 0.003. From the excel model of Erlang B the π_s value for k=9, λ_b =1.5 and μ_b = 0.5 is 0.0026. Both results are almost identical (Please refer Appendix 1).

2.5 Modeling Supercharging Service Using Erlang C

For example, EV arrival rate of a station, λ_b = 1.5 EV/hour and battery recharge rate in the charge bay, μ_b =0.5 EV/hour. The Erlang C model,

$$\frac{\lambda_d}{m\mu_d} \langle 1 \qquad (2.51)$$

Putting the values in the above equation, the number of superchargers in a JBSS station which is m≥4 can be obtained.

To calculate the probability that an EV needs to wait for a supercharger, the equation below can be used

$$C(m,s) = \frac{\frac{(m\rho_d)^m}{m!(1-\rho_d)}}{\sum_{k=0}^{m-1}\frac{(m\rho_d)^k}{k!} + \frac{(m\rho_d)^m}{m!(1-\rho_d)}} \qquad (2.52)$$

$$\rho_d = \frac{\lambda_b B(s)}{m\mu_d} \qquad (2.53)$$

The value of $B(s)$ is obtained from Erlang B model. By putting the value of m=4, λ_b = 1.5, μ_b =0.5, $B(s)$=0.213 and k=3 in the above equations, $C(m, s)$= 0.119 is obtained. The values of L, L_s, L_q, W, W_s, W_q can be calculated by using the equations below,

$$L = L_q + \frac{\lambda_b}{\mu_d} \tag{2.54}$$

$$L_q = \frac{C(m,s)\rho_d}{1-\rho_d} \tag{2.55}$$

$$L_s = L - L_q \tag{2.56}$$

$$W_q = \frac{C(m,s)}{m\mu_d - \lambda_b} \tag{2.57}$$

$$W_s = \frac{1}{\mu_d} \tag{2.58}$$

$$W = W_q + W \tag{2.59}$$

After putting the above stated values in the equations, the obtained results are L_q = 0.023, L= 3.03, L_s=3, W_s=2, W_q= 0.24 and W= 2.24.

The computation of $C(m, s)$, L, L_q, L_s, W, W_q, W_s for the values of k from 0 to 10 are listed below,

Table 2.3 Values of $C(m, s)$, L, L_q, L_s, W, W_q, W_s

k	$B(s)$	ρ_d	$C(m, s)$	L	L_q	L_s	W	W_q	W_s
0	0.047	0.036	1.65E-05	3.000	6.07E-07	3	2.0000	3.29E-05	2
1	0.142	0.107	0.0029	3.003	0.00035	3	2.0058	0.0058	2
2	0.213	0.160	0.0279	3.005	0.00532	3	2.0558	0.0558	2
3	0.213	0.160	0.1185	3.023	0.02258	3	2.2370	0.2370	2
4	0.160	0.120	0.4681	3.064	0.06386	3	2.9361	0.9361	2
5	0.096	0.072	0.9415	3.073	0.07308	3	3.8831	1.8831	2
6	0.048	0.036	0.9993	3.038	0.03733	3	3.9986	1.9986	2
7	0.021	0.015	0.9999	3.016	0.01568	3	3.9999	1.9999	2
8	0.008	0.006	1	3.006	0.00582	3	4	2	2
9	0.003	0.002	1	3.002	0.00193	3	4	2	2
10	0.001	0.001	1	3.001	0.00058	3	4	2	2

The Erlang C model by using MATLAB program is given below,

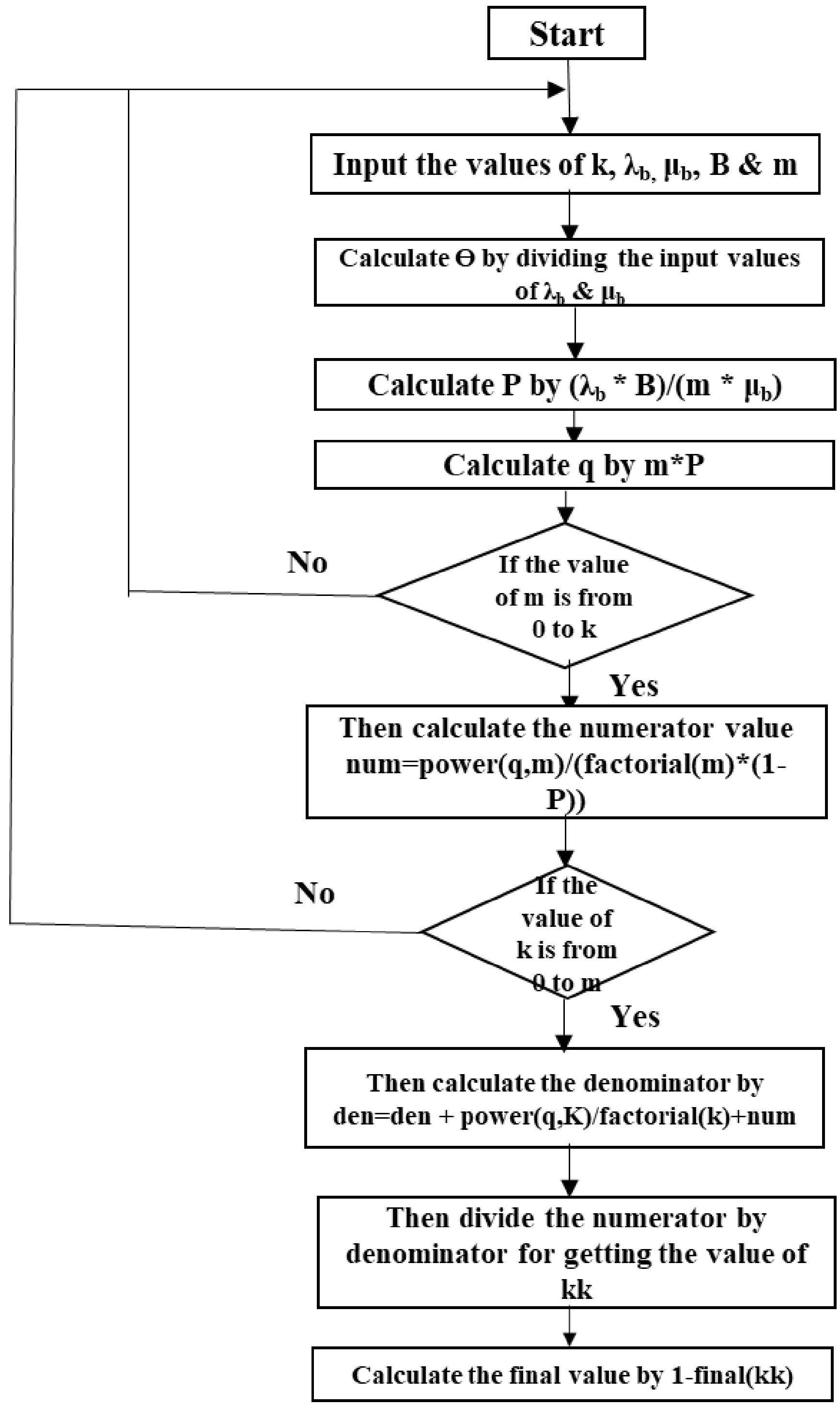

Figure 2.6 Flow Chart of Erlang C Model in MATLAB Code

At the start of the Erlang C model in MATLAB, the first input values are k, λ_b, μ_b, B and m. Then the model will calculate the θ value by diving the λ_b and μ_b. Then the model calculates the P value by using this formula ($\lambda_b B$) / ($m\mu_b$). At the next step, the model will calculate the q value by multiplying m and P values. If the value of m is from 0 to k then the model will go to the next step of the flowchart, otherwise the model will start from the beginning. If the model goes to the next step by following the conditions then it will start calculating the numerator value by using num=power (q, m)/factorial(m) × (1-P). After that if the value of k is from 0 to m then the model will go to the next step and calculate the denominator value by using den + power (q, k)/factorial(k) + num. If the condition is not fulfilled, then the model will start from the beginning. Now, the model can calculate the value of kk by diving the numerator value and denominator value. At the last step of the model, the final value can be obtained by using this formula 1-final(kk). After running the model for the value of k=9, λ_b =1.5, μ_b = 0.5, B=0.0026, m=4 then the model can calculate the value of $C(m,s)$ from the MATLAB which is 1. From the excel model of Erlang C the value $C(m,s)$ for k=9, λ_b =1.5, μ_b = 0.5, B=0.0026, m=4 is 1 which are similar values (Please refer Appendix 2).

3. MICROGRID SIZING FOR A SINGLE BATTERY SERVICE STATION

3.1 Minimizing Cost of Battery Swap Station with Island Microgrid

3.1.1 System Configuration

An EV battery swap station in island microgrid operation is designed to meet the battery service demand under the environmental requirement. Island microgrid operation is an electrical power supply mode with a small number of distributed generating units and consumers. It has the capability to connect with main grid system. Island microgrid operation is chosen based on different factors like geographical area, cost, and climate condition. The EV battery swap station with an island microgrid consists of wind turbine (WT), solar photovoltaic (PV), energy storage system (ESS), and the EV battery swap station acts as the load. Here, WT and PV are primary power units and the ESS stores the surplus energy which is not consumed by the battery swap station and saved for later use when the output of WT and PV become low.

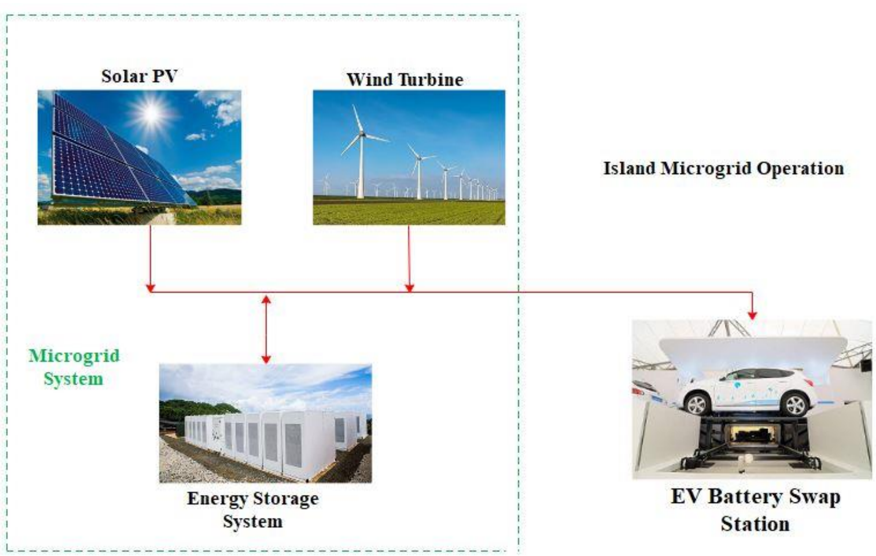

Figure 3.1 An EV Battery Swap Station in Island Microgrid Operation

3.1.2 Operating Principle of a Battery Swap Station

Firstly, some basic terminologies are introduced below.

Vehicle Arrival: Two assumptions are made regarding the EV arrival process. First, EV arrivals at a battery swap station occur randomly and independently. Second, the arrival rate is assumed to be constant value. In essence, these two assumptions allow to model the arrival process as a Poisson process, which also has been used in the literature, for example Tan et al. (2014), Mak et al. (2013), and Avci et al. (2015).

Battery Charging Duration: The charging duration of a depleted battery is assumed to follow a general distribution. In this thesis model, the charging duration is defined as charging a battery from a low state-of-charge (SOC) level to the desired SOC level. Some studies use specific distributions to model the charging duration (Chen 2007). The actual duration may vary significantly because the energy residuals of batteries unloaded from EV differ from each other. As a result, a general distribution is more appropriate to represent the charging duration. In addition, given two identical batteries with the same energy residuals, the charging duration also differs depending on the level of the charging power used in the charge bay (Voelcker 2018).

Battery Inventory: The spare battery inventory is a decision variable and plays a critical role in achieving the service level requirement. In our model, an incoming EV receives the swap service only if the stockroom possesses a spare battery with the required SOC level; otherwise, the EV needs to wait for the next available spare battery.

Service Time: Service time refers to the time duration from when the EV arrives in the station to when the battery is swapped for leaving. If a spare battery is available, it takes couple of minutes to complete the exchange. However, the service time is prolonged if an on-hand spare battery is not available upon the EV arrival. Figure 3.2 depicts the operational procedure of the EV battery swap station. Using Erlang-C queueing model for battery swap, the goal of the model here is to determine the base stock level of battery, the capacity of WT, PV, and ESS such that during the course of a year, the station achieves the zero-energy performance at the minimum cost.

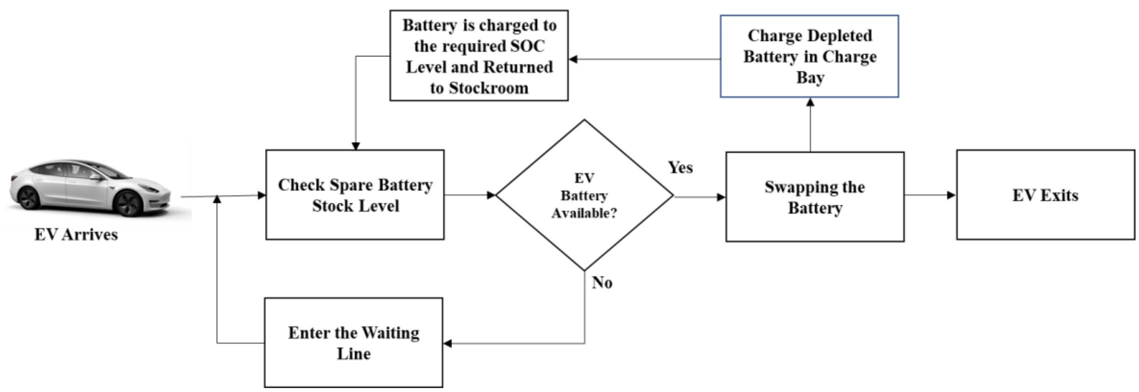

Figure 3.2 The Process of Battery Swap Service with Waiting (Zhang et al. 2021)

3.1.3 Description of Optimization Model

The following model is defined in the context of island microgrid operation condition. The objective function consists of cost of investing spare batteries, station facility, and the microgrid system. The latter consist of WT, PV, and ESS units. Note that both ESS and EV battery can store electric energy, the former is use as energy buffer for absorbing surplus renewable energy from WT or PV.

Table 3.1 Notation of Modeling Battery Swap Station

Notation	Explanation
s	number of spare EV batteries in the station
a_B	unit cost of an EV battery
a_{WT}	unit cost of WT system (unit: \$/MW)
a_{PV}	unit cost of PV system (unit: \$/MW)
a_{ESS}	unit cost of ESS system (unit: \$/MWh)
ϕ_B	capital recovery factor of an EV battery unit
ϕ_{WT}	capital recovery factor of WT system
ϕ_{PV}	capital recovery factor of PV system
ϕ_{ESS}	capital recovery factor of ESS system
τ_{WT}	operating hours of WT per period (unit: hour)
τ_{PV}	operating hours of PV per period (unit: hour)
T	number of periods
t	index of period and t=1, 2, …, T
$\lambda_{WT,t}$	capacity factor of WT at time t
$\lambda_{PV,t}$	capacity factor of PV at time t
b_{WT}	operation and maintenance cost of WT per MWh (unit: \$/MWh)
b_{PV}	operating and maintenance cost of PV per MWh (unit: \$/MWh)
b_{ESS}	operating and maintenance cost of ESS per MWh (unit: \$/MWh)
c_{WT}	carbon credits or incentive of WT per MWh (unit: \$/MWh)
c_{PV}	carbon credits or incentive of PV per MWh (unit: \$/MWh)
c_{ESS}	carbon credits or incentive of ESS per MWh (unit: \$/MWh)
$\lambda_{EV,t}$	EV arrival rate at time t
τ	time step size or duration of a period (unit: hour)
P_{EV}	power for charging a depleted battery (MW)

Table 3.2 Explanation of Decision Variables

Notation	Explanation
$P^c{}_{WT}$	installed capacity of WT (unit: MW)
$P^c{}_{PV}$	installed capacity of PV (unit: MW)
$B^c{}_{ESS}$	installed capacity of ESS (unit MWh)
$B_{ESS,t}$	the amount of energy stored in ESS at time t (unit: MWh)

The following cost model is formulated to capture the annualized cost of a battery swap station:

$$f(P_{PV}^c, P_{WT}^c, P_{ESS}^c) = \phi_B a_B s + \phi_{WT} a_{WT} P_{WT}^c + \phi_{PV} a_{PV} P_{PV}^c + \phi_{ESS} a_{ESS} B_{ESS}^c + \sum_{t=1}^{T} \tau_{WT}(b_{WT} - c_{WT}) \lambda_{WT,t} P_{WT}^c + \sum_{t=1}^{T} \tau_{PV}(b_{PV} - c_{PV}) \lambda_{PV,t} P_{PV}^c + \sum_{t=1}^{T} (b_{ESS} - c_{ESS}) B_{ESS,t} \tag{3.1}$$

The objective function is the minimization of the annualized cost of a battery swap station. There are two major constraints associated with this model:

a) Energy balance in each period

$$\lambda_{EV,t} \tau P_{EV} + B_{ESS,t} - B_{ESS,t-1} \le \lambda_{WT,t} P_{WT}^c \tau_{WT} + \lambda_{PV,t} P_{PV}^c \tau_{PV}, \qquad \text{for } t=1, 2, ..., T. \tag{3.2}$$

b) ESS State at time *t*

$$0 \le B_{ESS,t} \le B_{ESS}^c, \text{ for } t=1, 2, ..., T. \tag{3.3}$$

c) Initial ESS energy state (assuming it is full)

$$B_{ESS,0} = B^c{}_{ESS} \tag{3.4}$$

d) End time ESS energy

$$B_{ESS,T} = B^c{}_{ESS} \tag{3.5}$$

e) Non-Negativity of Decision Variables

$$P_{WT}^c, P_{PV}^c, B_{ESS}^c \ge 0 \tag{3.6}$$

3.1.4 Parameters of Numerical Experiments

Parameters are the values assumed to be known and serve as the input data of the optimization model. The parameters for our optimization model are given below:

Table 3.3 Parameters of WT, PV and ESS

Notation	Value	Unit
a_B	1200 (for Nissan Leaf 2nd Generation)	\$/item
a_{WT}	1.5M	\$/MW
a_{PV}	2M	\$/MW
a_{ESS}	0.5M (Case1 as benchmark)	\$/MWh
	0.2M (Case2)	\$/MWh
ϕ_B	0.12	n/a
ϕ_{WT}	0.08024	n/a
ϕ_{PV}	0.08024	n/a
ϕ_{ESS}	0.12	n/a
τ_{WT}	1	hour
τ_{PV}	1	hour
τ	1	hour
T	8736	hour
t	index of period and t=1, 2, …, T	hour
$\lambda_{WT,t}$	Each city hourly WT capacity factor	n/a
$\lambda_{PV,t}$	Each city hourly PV capacity factor	n/a
$\lambda_{EV,t}$	2	cars/hour
P_{EV}	0.075	MW
b_{WT}	8	\$/MWh
b_{PV}	4	\$/MWh
b_{ESS}	2	\$/MWh
c_{WT}	0	\$/MWh
c_{PV}	10	\$/MWh
c_{ESS}	0	\$/MWh

3.1.5 Charactering Climate Profiles

For the optimization model of single battery swap station, the hourly capacity factor over the course of a year is used to implement the island microgrid model in ten different cities. That means 8736 capacity factor data of WT and PV, respectively, for each city is used. The cities are Reno, Yuma, Tucson, Las Vegas, Los Angeles, Salt Lake City, San Jose, Sacramento, San Francisco and Phoenix. These ten cities are chosen based on their diversity in weather condition. These ten cities have categorized based on two criteria. The first one is strong wind and strong sun, the second one is weak wind and strong sun. If the capacity factor (CF) of WT is less than 0.19 then the city has weak wind and if the CF of WT is higher than 0.19 then the city has strong wind. Additionally, if the capacity factor of PV is less than 0.2 then the city has weak sun and vice versa. These two criteria actually cover a diverse weather profile in the world.

Table 3.4 Weather Condition of Ten Cities

Wind	Sun	City
Strong	Strong	Las Vegas, Sacramento, Salt Lake City, San Francisco
Weak	Strong	Reno, Yuma, Tucson, Phoenix, San Jose, Los Angeles

For better understanding of the capacity factor of WT and PV of ten different cities, the maximum and minimum values are calculated, and the results are shown in Table 3.5.

Table 3.5 Capacity Factor of WT and PV at Each City

City and State	Minimum Capacity Factor WT	Maximum Capacity Factor WT	Avg. Capacity factor WT	Minimum Capacity Factor PV	Maximum Capacity Factor PV	Avg. Capacity factor PV
Reno, AZ	0	0.96	0.14	0.156	0.467	0.314
Yuma, AZ	0	1	0.19	0.194	0.51	0.349
Tucson, AZ	0	0.96	0.15	0.255	0.579	0.417
Las Vegas, NV	0	0.96	0.207	0.253	0.547	0.393
Los Angeles, CA	0	0.996	0.134	0.103	0.431	0.259
Salt Lake City, UT	0	0.96	0.219	0.057	0.358	0.201
San Jose, CA	0	0.88	0.118	0.13	0.46	0.285
Sacramento, CA	0	1	0.192	0.173	0.562	0.379
San Francisco, CA	0.087	0.73	0.387	0.052	0.364	0.215
Phoenix, AZ	0.007	0.21	0.097	0.134	0.396	0.289

The average capacity factor of WT and PV of ten different cities are also calculated. Those data will be helpful to provide additional information about the renewable power generation as well as giving general idea about the weather condition of these cities.

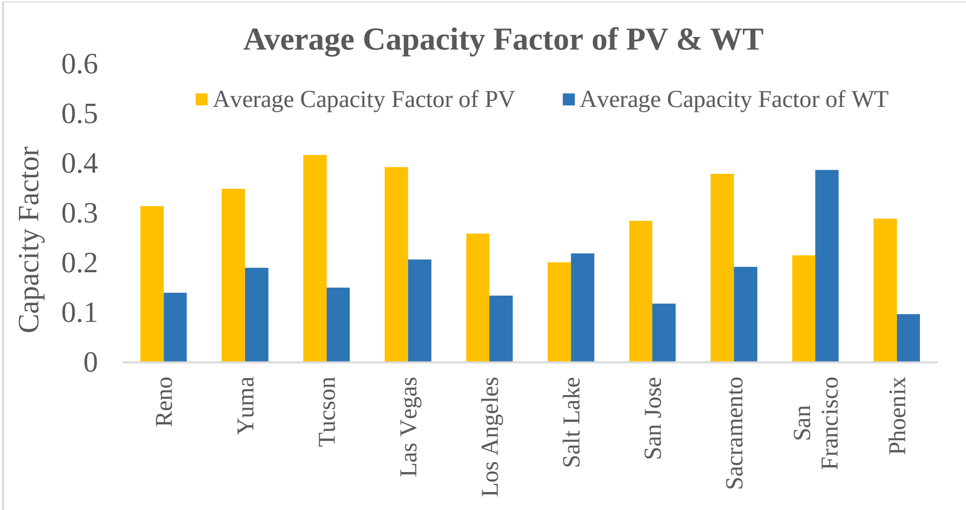

Figure 3.3 Average Capacity Factor of PV and WT for Each City

3.1.6 Computational Results and Discussion

Model 3.1 is executed in AMPL computational environment with the given parameters and hourly wind and solar capacity factors of ten cities. Case 1 serves as the benchmark, and the optimal sizing of WT, PV and ESS units along with the costs are summarized in Table 3.6. Note that the ESS capacity cost is assumed to be $0.5M/MWh.

Table 3.6 Installation Capacity of PV, WT and ESS and System Cost for Case 1

City	WT (MW)	PV (MW)	ESS (MWh)	Annual Cost ($)
Reno, AZ	0.008	0.85	0.034	155,780
Yuma, AZ	0	0.71	0.024	132,451
Tucson, AZ	0	0.56	0.011	107,115
Las Vegas, NV	0	0.55	0.032	108,303
Los Angeles, CA	0.012	1.19	0.068	209,787
Salt Lake, UT	0.001	1.91	0.354	337,370
San Jose, CA	0	0.990	0.077	178,442
Sacramento, CA	0	0.81	0.031	144,158
San Francisco, CA	1.01	0.25	0.079	220,999
Phoenix, AZ	0	0.99	0.038	175,819

For further study of the feasibility of the model with different parameter values, Model 3.1 is run by reducing ESS system cost from $0.5M/MWh to $0.2M/MWh. Table 3.7

presents the results for Case 2 based on the reduced ESS cost.

Table 3.7 Capacity of PV, WT and ESS for Case 2 (Unit Cost of ESS is $0.2M/MWh)

City	WT (MW)	PV (MW)	ESS (MWh)	Annual Cost ($)
Reno, AZ	0.025	0.83	0.12	154,251
Yuma, AZ	0	0.68	0.19	130,783
Tucson, AZ	0	0.56	0.028	106,607
Las Vegas, NV	0	0.55	0.044	107,122
Los Angeles, CA	0.023	1.14	0.196	204,328
Salt Lake, UT	0.01	1.84	0.611	320,414
San Jose, CA	0	0.996	0.078	175,634
Sacramento, CA	0	0.77	0.177	141,466
San Francisco, CA	1.02	0.24	0.117	217,678
Phoenix, AZ	0	0.94	0.267	171,446

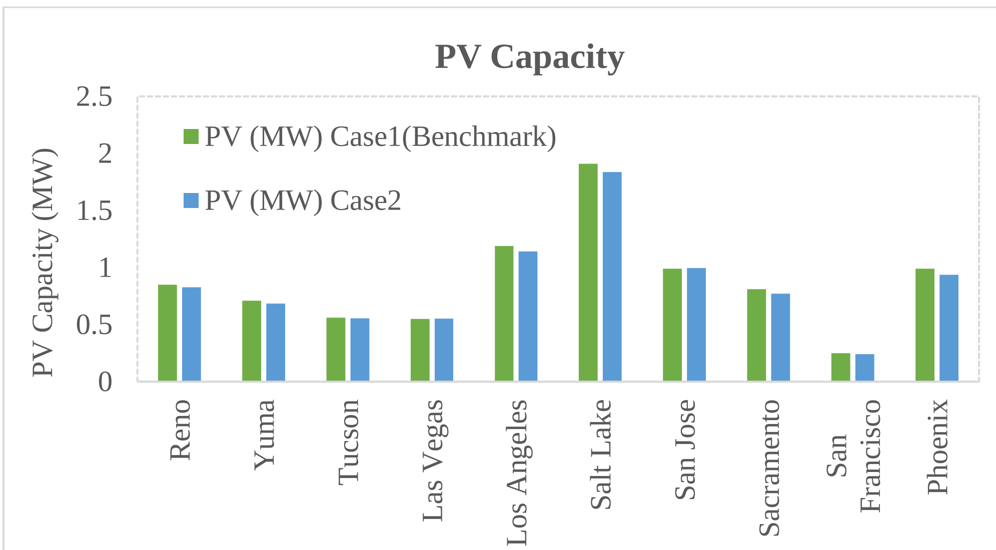

Figure 3.4 PV Capacity of Each City

The PV Capacity of Each City graph shows that Tucson, Las Vegas and San Jose, in these three cities the capacity of PV remains same despite the cost of ESS being 40% of $0.5M/MWh. The possible reason could be the energy generation from PV does not increase as the PV output depends on the capacity factor of PV of each city. The ESS does not actively contribute to power generation, rather its role is for regulating the uncertainty of power supply through storing and discharging energy. That is why in these three cities the capacity of PV remains almost same after reducing the price of ESS.

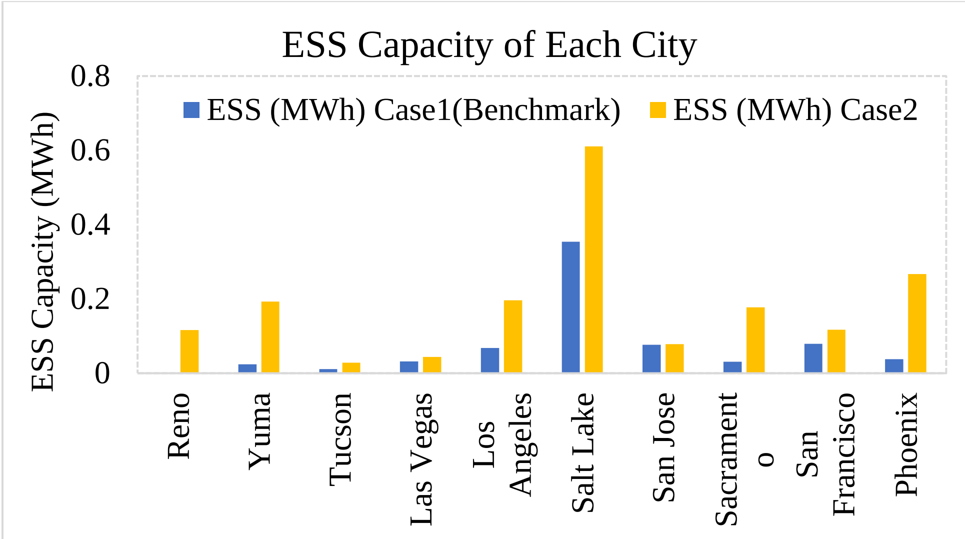

Figure 3.5 ESS Capacity of Each City

Fig 3.5 shows that the ESS capacity of Reno, Yuma, Los Angeles, Salt Lake City, Sacramento and Phoenix increases significantly. However, the graph also shows that the ESS capacity of San Jose remain the same even if the price of ESS is down from \$0.5M/MWh to \$0.2M/MWh. Reducing the ESS price do not increase the energy generation from PV and WT. Energy generation from WT and PV depend on the capacity factor of PV and WT of each city. So, reducing the price actually does not increase the capacity of ESS at San Jose because of this.

3.2 Minimizing Battery Swap Station Cost with Grid-tied Microgrid

3.2.1 System Configuration

In this setting, the microgrid is interconnected with the main grid through circuit breakers or common coupling point. As such the system is able to realize two-way power flow. The microgrid under study consists of WT, solar PV, energy storage system (ESS), and the EV battery swap station that acts as the load. A grid-tied microgrid system is investigated by considering two operational scenarios. In scenario one, if the wind blows hard or the sunshine is strong, the microgrid is able to fully energize the swap station with no reliance on the main grid. If surplus power is generated from WT and PV, it can be stored in the ESS or fed into the main grid. In scenario two, if the aggregate power output of WT and PV is less than the load, the ESS plays as complementary energy source to co-power the battery swap station. Situations may also occur when the main grid power must be imported if the energy of ESS is depleted.

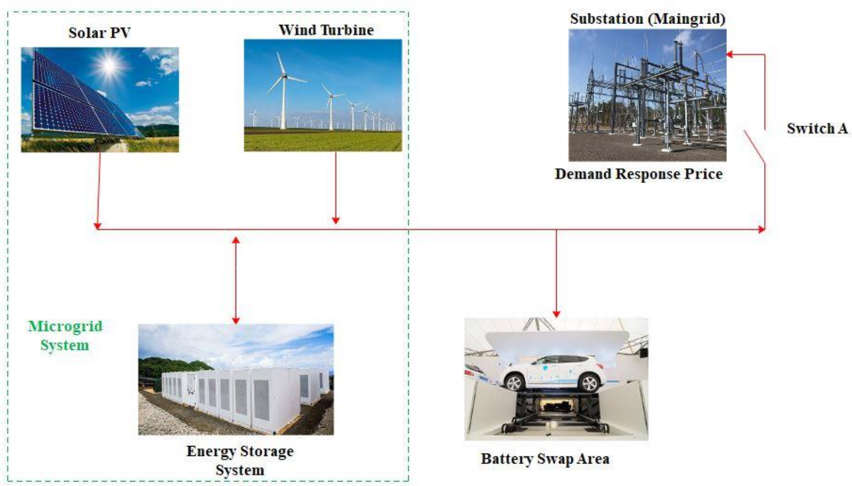

Figure 3.6 An EV Battery Swap Station with Grid-Tied Microgrid

3.2.2 Model Formulation

In this section, an integrated microgrid and battery swap station (BSS) planning model is presented with the goal of minimizing annual system cost. The goal is to size WT, PV and ESS units as well as to allocate the number of spare EV batteries. There are five major cost items involved: 1) annualized microgrid installation cost; 2) microgrid maintenance and operation cost; 3) carbon credits which is revenue to the station; 4) EV battery purchase and holding cost; and 5) the revenue of selling to or cost of purchasing electricity from the main grid.

Table 3.8 Notation for Modeling Battery Swap Station with Grid-Tied Microgrid

Notation	Explanation
T	number of planning periods (e.g., for one-year T=8,736 for hourly planning)
τ_g	operating time of generator g in a period
a_g	capacity cost of renewable generator g. (unit: \$/MW)
b_{ES}	ES operating cost (unit: \$/MWh)
d_{ES}	capacity cost of electric energy storage ES unit in station. (unit: \$/MWh)
$D_{VB,k}$	unit cost of EV battery pack type i in station. (unit: \$/item)
ϕ_g	capital recovery factor for renewable generator g.
ϕ_{ES}	capital recovery factor for electric energy storage unit in station.
ϕ_{VB}	capital recovery factor for EV battery packs in station.
$\rho_{IM,t}$	price of importing electricity to the main grid at time t (unit: \$/MWh)
$\rho_{EX,t}$	price of selling (or exporting) electricity to the main grid at time t (unit: \$/MWh).
$\lambda_{EV,k,t}$	arrival rate of EV with battery type k at time t. (unit: cars/hour)
$P_{EV,k}$	power for charging a unit of battery type k. (unit: MW/battery)
τ	time step of one planning period. (e.g. if T=8736 hours/year, then τ=1 hour)

Table 3.9 Explanation of Decision Variables

Notation	Explanation
P_g^c	power capacity of renewable generator g for g=1, 2, …, G.
B^c_{ES}	energy capacity of electrical storage unit in station.
s_k	number of spare EV battery type k in station for k=1, 2, …, K.
$B_{ES,t}$	amount of energy stored in ES unit at time t. (unit: MWh)
$E_{IM,t}$	the amount of energy imported from the main grid at time t
$E_{EX,t}$	the amount of energy exported to the main grid at time t

The following cost model is developed to capture these five cost items of a battery swap station:

$$\begin{aligned} f_2(\mathbf{P}_g{}^c, \mathbf{s}_k, B^c_{ES}) = \sum_{g=1}^{G}\phi_g a_g P_g^c + \sum_{t=1}^{T}\sum_{g=1}^{G}(b_g - c_g)\lambda_{gt}P_g^c\tau_g + \phi_{ES}d_{ES}B^c_{ES} + \sum_{t=1}^{T} b_{ES}B_{ES,t} \\ + \sum_{k=1}^{K}\phi_{VB}d_{VB,k}s_k + \sum_{t=1}^{T}(\rho_{IM,t}E_{IM,t} - \rho_{EX,t}E_{EX,t}) \end{aligned} \tag{3.7}$$

There are five major constraints associated with this planning model:

a) Energy balance in each period

$$\sum_{k=1}^{K}\lambda_{EV,k,t}\tau P_{EV,k} + B_{ES,t} - B_{ES,t-1} + E_{EX,t} - E_{IM,t} = \sum_{g=1}^{G}\lambda_{gt}P_g^c\tau_g \text{ for } t=1, 2, ..., T. \tag{3.8}$$

b) EV spare battery demand constraints

$$\lambda_{EV,k,t}\tau \le s_k \text{ , for } t=1, 2, ..., T, \text{ and for } k=1, 2, ..., K. \tag{3.9}$$

c) Energy Storage State at time *t*

$$0 \le B_{ES,t} \le B_{ES}^c \text{ , for } t=1, 2, ..., T. \tag{3.10}$$

d) Initial energy stored in ES at *t*=0

$$B_{ES,0} = B_{ES}^c \tag{3.11}$$

e) End time ES energy at *t*=*T*

$$B_{ES,T} = B_{ES}^c \tag{3.12}$$

f) Electricity import and export

$$E_{EX,t}, E_{IM,t} \ge 0 \text{ , for } t=1, 2, ..., T. \tag{3.13}$$

g) Non-Negativity of Decision Variables

$$P_g^c \ge 0 \text{ , for } g=1, 2, \ldots, G. \tag{3.14}$$

$$B_{ES}^c \ge 0 \text{ ,} \tag{3.15}$$

$$s_k \in \{0, 1, 2, \ldots\}, \text{ for } k=1, 2, \ldots, K. \tag{3.16}$$

3.2.3 Results and Discussion for Phoenix

Three cities are chosen to test the model: Phoenix, San Francisco, and Salt Lake City. These cities are the good representatives of the mix of wind and weather conditions. Model 3.2 is solved in AMPL computational environment with the given parameters and among ten different cities hourly capacity factors of WT and PV Phoenix is picked as the first city to run the optimization model. Case 1 is denoted as a benchmark, the optimal sizing of WT, PV and ESS units along with the number of battery packs and the annual cost are summarized in Table 3.12.

Table 3.10 Parameter Values with Unit for Model 3.2 (Case 1 for Benchmark)

Notation	**Value**	**Unit**
G	Since wind and PV are used, G=2	n/a
τ	1	hour
T	8736	hours
a_1	1.5M (g=1 is for WT)	\$/MW
a_2	2M (g=2 is for PV)	\$/MW
d_{ES}	0.4M (ES capacity cost)	\$/MWh
$d_{VB,1}$	7,000 (for Nissan Leaf 1st generation battery)	\$/item
$d_{VB,2}$	12,000 (for Nissan Leaf 2nd Generation)	\$/item
b_1	8 (WT operating cost)	\$/MWh
b_2	4 (PV operating cost)	\$/MWh
b_{ES}	2 (ES operating cost)	\$/MWh
c_1	0 (WT carbon credit)	\$/MWh
c_2	10 (PV carbon credits)	\$/MWh
ϕ_1	0.0944 (7% compound interest, 20 years)	n/a
ϕ_2	0.0944 (7% compound interest, 20 years)	n/a
ϕ_{ES}	0.1424 (7% compound interest, 10 years)	n/a
ϕ_{VB}	0.1424 (7% compound interest, 10 years)	n/a
$\lambda_{1,t}$	Hourly WT capacity factor for t=1, 2, …, T	n/a
$\lambda_{2,t}$	Hourly PV capacity factor for t=1, 2, …, T	cars/hour
$\lambda_{EV,k,t}$	5 for t=1, 2, …, T	n/a
$P_{EV,1}$	0.024 (power for charging 1st generation Leaf battery)	MW
$P_{EV,2}$	0.040 (power for charging 2nd generation Leaf battery)	MW
$\rho_{IM,t}$	70 (electricity price of importing from main grid)	\$/MWh
$\rho_{EX,t}$	35 (electricity sale price of exporting to main grid)	\$/MWh

Table 3.11 Parameter Values for Sensitivity Analysis for Model 3.2 (Cases 2 to 9)

Case	Notation	Value	Unit
2	a_2	1M (g=2 is for PV)	\$/MW
3	d_{ES}	0.1M (ES capacity cost)	\$/MWh
4	d_{ES}	0.05M (ES capacity cost)	\$/MWh
5	$d_{VB,1}$	3,500 (for Nissan Leaf 1st generation battery)	\$/item
	$d_{VB,2}$	6,000 (for Nissan Leaf 2nd Generation)	\$/item
6	c_2	0 (PV carbon credits)	\$/MWh
7	$\lambda_{EV,k,t}$	10 for t=1, 2, …, T, for k=1 and 2	car/hour
8	$P_{EV,1}$	0.048 (power for charging 1st generation Leaf battery)	MW
	$P_{EV,2}$	0.08 (power for charging 2nd generation Leaf battery)	MW
9	$\rho_{IM,t}$	150	\$/MWh

Table 3.12 Total Cost, Capacity of PV, WT and ESS for Cases 1 to 9 in Phoenix

Case	Annual cost ($)	WT (MW)	PV (MW)	Battery type 1	Battery type 2	ESS (MWh)	Prosumer behavior
1	206,616	0	0.85	5	5	0	Import, export
2	-71,131	0	20	5	5	0	export
3	206,616	0	0.85	5	5	0	Import, export
4	206,616	0	0.85	5	5	0	Import, export
5	199,852	0	0.85	5	5	0	Import, export
6	209,215	0	0	5	5	0	import
7	413,232	0	1.71	10	10	0	Import, export
8	399,704	0	1.71	5	5	0	Import, export
9	231,478	0	1.19	5	5	0	Import, export

After comparing Cases 1 with 2 and find out that reducing the PV capacity cost by half and down to $1M/MW makes the system increases PV capacity from 0.85MW to 20 MW. The negative cost indeed indicates that the system in Case 2 creates profit by selling surplus PV energy to the grid. Cases 3 and 4 are computed at the reduced cost of ESS unit. It is interesting to see that ESS is not competitive in Phoenix if even the cost is down to $0.1M/MWh as opposed to current cost of $0.4M/MWh. In other words, the system never chooses ESS even the cost is down to $0.1M/MWh, and the station opts to export the energy to the main grid instead of storing at the ESS. In case of power shortage, the station chooses to import the energy from the main grid. In Case 5, the EV battery cost is halved, the required spare parts remain the same as these of Case 1. This shows that the station will not keep more spare battery packs because of reduced cost.

Case 7 shows that by doubling the battery swap demand, the station needs to install twice of PV capacity to fulfill the demand. This result is reasonable because the station needs more PV power to charge more exchanged batteries given the same time. Case 8 assumes that the charge power for each battery type doubles as oppose to Case 1. Though the demand for spare battery remains the same, the installed PV capacity also doubles to meet the increased charged power.

Case 9 shows that by increasing the electricity purchase price from the main grid from \$70/MWh to \$150/MWh, the install capacity of PV is increased. The result is reasonable because it is better off to install more PV to fulfill the demand of the battery swapping station and the additional energy can be easily sold to the main grid which is profitable. The amount of energy export to the main grid is also increased in each hour.

Now, the objective function value of our optimization model is compared which is annual cost of the battery swap station with grid tied micro-grid among different cases of Phoenix. In comparison between Case1 (i.e. benchmark) with Case 5, Figure 3.7 shows that reducing the EV battery cost by a half from the benchmark case, the total annual cost of battery swap station drops by certain amounts, but not significant. Additionally, in comparison between Cases 1 with 2, Figure 3.7 also shows that reducing the PV capacity cost down to a half of the benchmark case makes the system profitable.

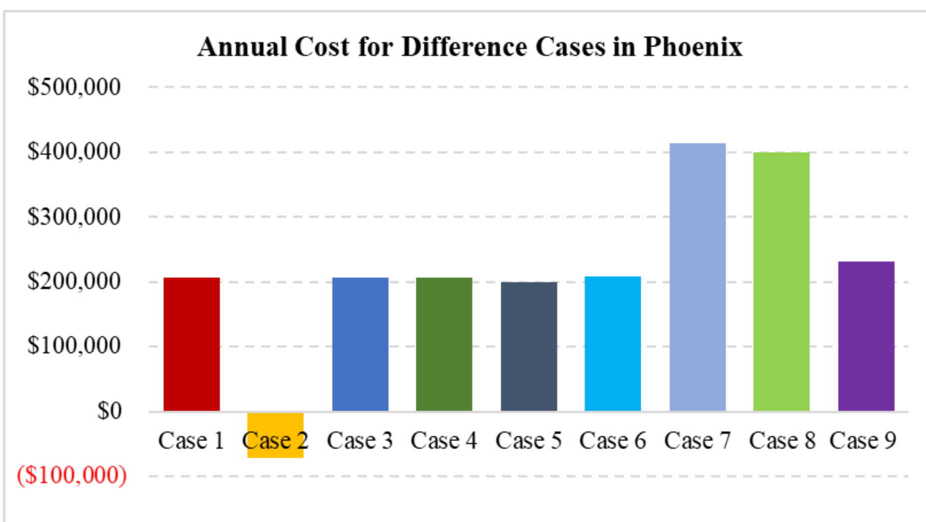

Figure 3.7 Annual Cost for Each Case for Phoenix

Comparison between the Cases 1 with 8 shows that the amount of energy imported from the main grid in December doubles in Case 8 because of doubling the power for the batteries compared to Case1. December is chosen because at this time the PV generation is the lowest in a year and this is a perfect period to compare the amount of energy purchased from the main grid.

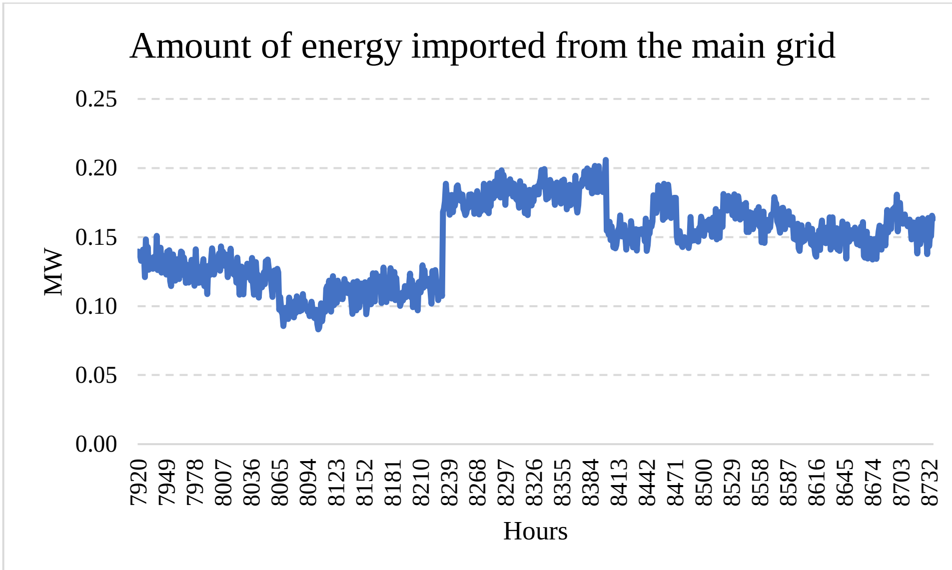

Figure 3.8 Energy Imported from Main Grid in December (Case 1)

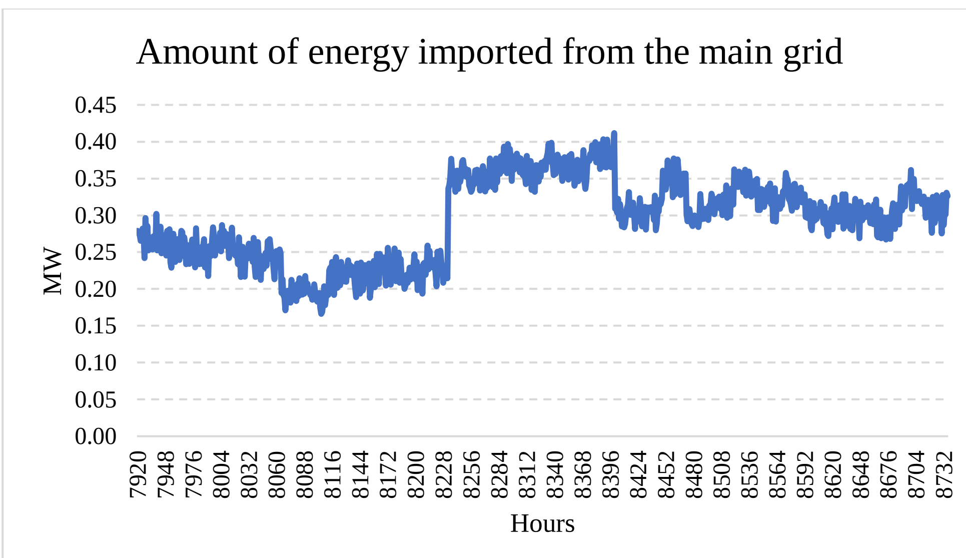

Figure 3.9 Energy Imported from Main Grid in December (Case 8)

Comparison between Cases 1 with 2 shows that the amount of energy exported to the main grid in May turns out to be quite high for Case 2 by reducing the capacity cost of

PV by $1M/MW from the Case1.

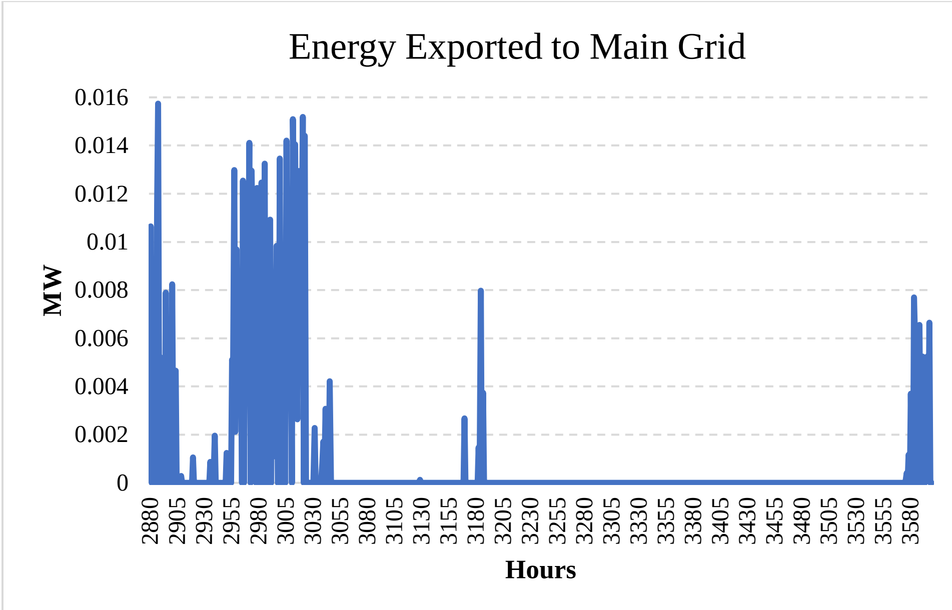

Figure 3.10 Energy Exported to the Main Grid in May (Case 1)

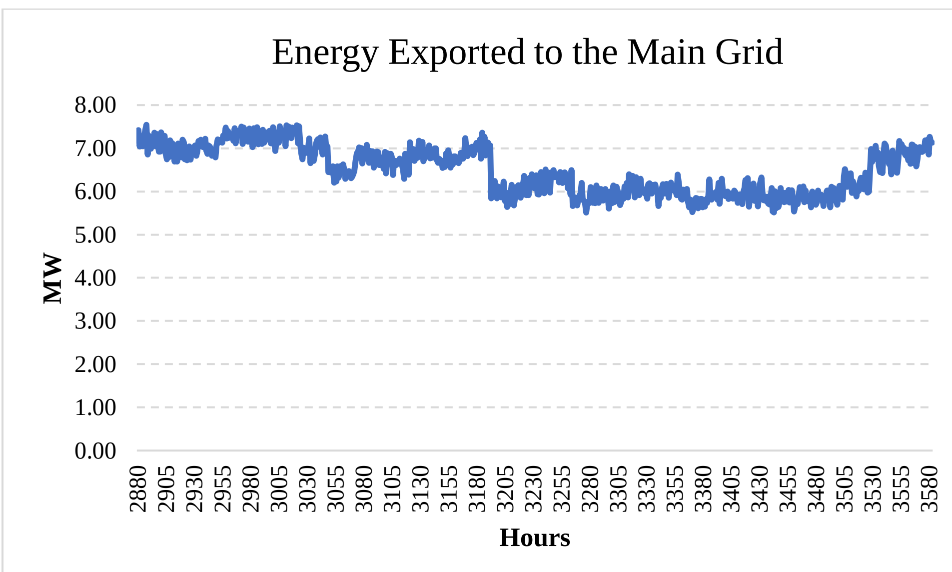

Figure 3.11 Energy Exported to the Main Grid in May (Case 2)

3.2.4 Results and Discussion for Las Vegas, Reno, Sacramento, San Jose, Tucson and Yuma

Model 3.2 is solved in AMPL computational environment with the given parameters and among ten different cities hourly capacity factors of WT and PV, Phoenix is picked as the first city to run our optimization model. Additionally, Model 3.2 has run in AMPL computational environment for other cities like Las Vegas, Reno, Sacramento, San Jose, Tucson and Yuma. Case 1 is denoted as a benchmark, the optimal sizing of WT, PV and ESS units along with the number of battery packs and the annual cost are summarized in Table 3.13, 3.14, 3.15, 3.16, 3.17 and 3.18. All these six cities are showing similar results like Phoenix due to having similar weather condition.

Table 3.13 Total Cost, Capacity of PV, WT and ESS for Cases 1 to 9 in Las Vegas

Case	Annual cost ($)	WT (MW)	PV (MW)	Battery type 1	Battery type 2	ESS(MWh)	Prosumer
1	156,445	0	0.83	5	5	0	import export
2	-817,982	0	20	5	5	0	export
3	156,445	0	0.83	5	5	0	import export
4	156,438	0	0.83	5	5	0.003	import export
5	149,681	0	0.83	5	5	0	import export
6	183,236	0	0.73	5	5	0	import export
7	312,890	0	1.66	10	10	0	import export
8	299,362	0	1.66	5	5	0	import export
9	162,885	0	0.96	5	5	0	import export

Table 3.14 Total Cost, Capacity of PV, WT and ESS for Cases 1 to 9 in Reno

Case	Annual cost ($)	WT (MW)	PV (MW)	Battery type 1	Battery type 2	ESS(MWh)	Prosumer
1	193,728	0	0.85	5	5	0	import export
2	-249,761	0	20	5	5	0	export
3	193,728	0	0.85	5	5	0	import export
4	193,727	0	0.85	5	5	0.0008	import export
5	186,964	0	0.85	5	5	0	import export
6	209,214	0	0	5	5	0	import
7	387,456	0	1.7	10	10	0	import export
8	373,928	0	1.7	5	5	0	import export
9	212,178	0	1.09	5	5	0	import export

Table 3.15 Total Cost, Capacity of PV, WT and ESS for Cases 1 to 9 in Sacramento

Case	Annual cost ($)	WT (MW)	PV (MW)	Battery type 1	Battery type 2	ESS (MWh)	Prosumer
1	164,961	0	0.83	5	5	0	import export
2	-717,466	0	20	5	5	0	export
3	164,961	0	0.83	5	5	0	import export
4	164,961	0	0.83	5	5	0	import export
5	158,197	0	0.83	5	5	0	import export
6	189,659	0	0.69	5	5	0	import export
7	329,922	0	1.66	10	10	0	import export
8	316,394	0	1.66	5	5	0	import export
9	175,661	0	1.06	5	5	0	Import export

Table 3.16 Total Cost, Capacity of PV, WT and ESS for Cases 1 to 9 in San Jose

Case	Annual cost ($)	WT (MW)	PV (MW)	Battery type 1	Battery type 2	ESS(MWh)	Prosumer
1	208,999	0	0.72	5	5	0	Import export
2	-40,944	0	20	5	5	0	export
3	208,999	0	0.72	5	5	0	import export
4	208,999	0	0.72	5	5	0	import export
5	202,235	0	0.72	5	5	0	import export
6	209,214	0	0	5	5	0	import
7	417,998	0	1.44	10	10	0	import export
8	404,470	0	1.44	5	5	0	import export
9	231,328	0	1.19	5	5	0	import export

Table 3.17 Total Cost, Capacity of PV, WT and ESS for Cases 1 to 9 in Tucson

Case	Annual cost ($)	WT (MW)	PV (MW)	Battery type 1	Battery type 2	ESS(MWh)	Prosumer
1	147,137	0	0.8	5	5	0	import export
2	-987,834	0	20	5	5	0	export
3	147,137	0	0.8	5	5	0	import export
4	147,133	0	0.8	5	5	0.002	import export
5	140,373	0	0.8	5	5	0	import export
6	174,997	0	0.73	5	5	0	import export
7	294,274	0	1.6	10	10	0	import export
8	280,746	0	1.6	5	5	0	import export
9	152,616	0	0.93	5	5	0	import export

Table 3.18 Total Cost, Capacity of PV, WT and ESS for Cases 1 to 9 in Yuma

Case	Annual cost ($)	WT (MW)	PV (MW)	Battery type 1	Battery type 2	ESS (MWh)	Prosumer
1	176,682	0	0.83	5	5	0	import export
2	-502,022	0	20	5	5	0	export
3	176,682	0	0.83	5	5	0	import export
4	176,682	0	0.83	5	5	0	import export
5	169,918	0	0.83	5	5	0	import export
6	200,493	0	0.73	5	5	0	import export
7	353,364	0	1.66	10	10	0	import export
8	339,836	0	1.66	5	5	0	import export
9	188,828	0	1.06	5	5	0	import export

3.2.5 Results and Discussion for San Francisco:

Model 3.2 is solved for the wind and weather condition of San Francisco. Case 1 is denoted as a benchmark, the optimal sizing of WT, PV and ESS units along with the number of battery packs and the annual cost are summarized in Table 3.19.

Table 3.19 Total Cost, Capacity of PV, WT and ESS for Cases 1 to 9 in San Francisco

Case	Annual cost ($)	WT (MW)	PV (MW)	Battery type 1	Battery type 2	ESS (MWh)	Prosumer
1	172,075	0.66	0	5	5	0	import export
2	148,707	0	1.73	5	5	0	import export
3	172,075	0.66	0	5	5	0	import export
4	172,075	0.66	0	5	5	0	import export
5	165,311	0.66	0	5	5	0	import export
6	172,075	0.66	0	5	5	0	import export
7	344,150	1.31	0	10	10	0	import export
8	330,622	1.31	0	5	5	0	import export
9	210,137	1.37	0	5	5	0	import export

Comparison between the Case 1 with Case 2 shows that reducing the PV capacity cost by half and down to $1M/MW makes the system chooses PV capacity of 1.73 MW instead of WT capacity of 0.66 MW. The annual cost of battery swapping station in Case 1 is reduced by 13.6% in Case 2 because of reducing the PV capacity cost by half and down to $1M/MW. Cases 3 and 4 are computed at the reduced cost of ESS unit. It is interesting to see that ESS is not competitive in San Francisco if even the cost is down to $0.1M/MWh as opposed to current cost of $0.4M/MWh. In other words, the system never chooses ESS even the cost is down to $0.05M/MWh, and the station opts to export the energy to the main grid instead of storing at the ESS. In Case 5, the EV battery cost is halved, the required spare parts remain the same as these of Case 1. This shows that the station will not store more spare battery packs because of reduced cost.

Case 7 shows that by doubling the battery swap demand, the station needs to install twice of WT capacity to fulfill the demand. This result is reasonable because the station needs more WT power to charge more exchanged batteries given the same time. Case 8 assumes that the charge power for each battery type doubles as oppose to Case 1. Though the demand for spare battery remains the same, the installed WT capacity also doubles to meet the increased charged power.

Case 9 shows that by increasing the electricity importing price from the main grid from $70/MWh to $150/MWh, the install capacity of WT is increased. The result is reasonable because it is better to install more WT to fulfill the demand of the battery swapping station and the additional energy can be easily sold to the main grid which is profitable. For this reason, the amount of exporting of energy to the main grid is also increased in each hour.

3.2.6 Results and Discussion for Salt Lake City:

Model 3.2 is solved for Salt Lake City and Case 1 is denoted as a benchmark. The optimal sizing of WT, PV and ESS units along with the number of battery packs and the annual cost are summarized in Table 3.20.

Table 3.20 Total Cost, Capacity of PV, WT and ESS for Cases 1 to 9 in Salt Lake City

Case	Annual cost ($)	WT (MW)	PV (MW)	Battery type 1	Battery type 2	ESS (MWh)	Prosumer
1	209,214	0	0	5	5	0	import
2	159,186	0	1.6	5	5	0	import export
3	209,214	0	0	5	5	0	import
4	209,214	0	0	5	5	0	import
5	202,450	0	0	5	5	0	import
6	209,214	0	0	5	5	0	import
7	418,429	0	0	10	10	0	import
8	404,901	0	0	5	5	0	import
9	328,993	0	1.16	5	5	0	import export

Comparison between the Cases 1 with 2 shows that reducing the PV capacity cost by half and down to $1M/MW makes the system to install 1.6 MW PV instead of 0 MW. The annual cost of battery swap station in Case 2 is reduced by 23.9% compared with Case 1 because of reducing the PV capacity cost by half.

Case 9 shows that by increasing the electricity import price from $70/MWh to $150/MWh, the system prefers to install more PV capacity. The result is reasonable because it is better to install more PV to fulfill the demand of the battery swap station instead of importing from the main grid and the surplus energy can be sold to the main grid for revenue generation. For this reason, the amount of energy exported to the main grid also increases in each hour.

4. MICROGRID SIZING FOR A JOINT BATTERY SWAP AND SUPERCHARGING STATION

4.1 Microgrid Sizing for a Joint Battery Swap and Supercharging Station

4.1.1 System Setting

In this setting, the station offers two types of services: battery swapping and on-board supercharging. When an EV arrives in the station, the depleted battery is exchanged if a spare battery is available in the stock. Upon exchange, the EV exists the station and the depleted battery is moved to the charge bay for recharging. If the battery stock has no spare pack, the EV approaches an onsite supercharger to recharge the on-board battery with no need of exchange.

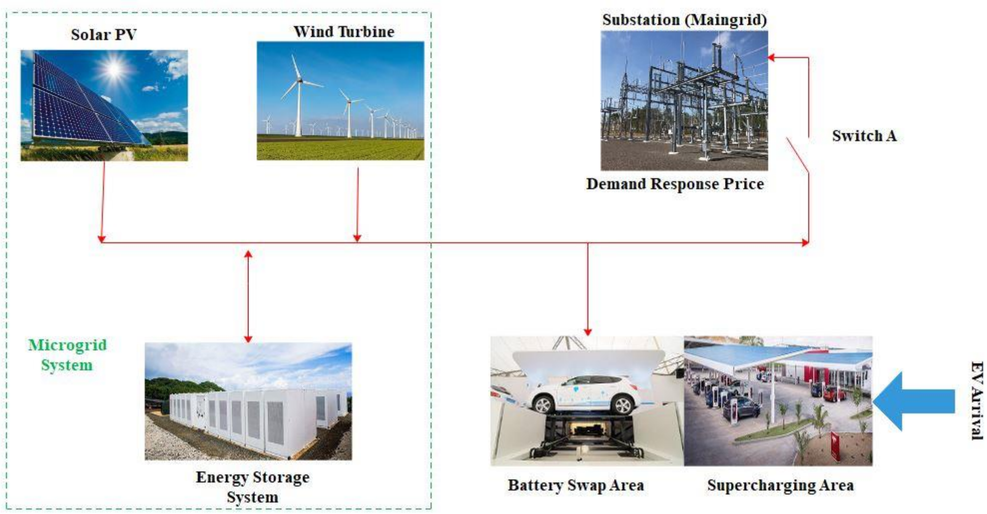

Figure 4.1 A Battery Swap and Supercharging Station with Grid-Tied Microgrid

A station capable of performing battery swap and supercharging is depicted in Figure 4.1. The electricity of the joint battery swap and supercharging (JBSS) station is co-powered by the microgrid and the main grid. The microgrid consists of WT, PV and energy storage (ES) system. Since the microgrid is interconnected with the main grid, the operating principle is the same as the pure battery swap station in Chapter 3.

4.1.2 Model Formulation

In this section, the microgrid sizing model in Chapter 3 is extended to a JBSS station that offers both battery swap and on-board supercharging. Besides the battery inventory, the supercharging equipment is also part of the station's asset. By comparing with Model 3.2, the cost of the JBSS station now includes the installation of superchargers.

Table 4.1 Notation for Modeling Battery Swap and Supercharging Stations

Notation	Explanation
T	number of planning periods (e.g. for one-year T=8736 for hourly planning)
G	Since WT and PV are used, G=2
τ	time step or length of one planning period. (e.g. if T=8736 hours/year, then τ=1 hour)
τ_g	operating time of generator g in a period
τ_{swap}	the time to exchange a battery given a spare battery is available (unit: hour)
τ_{max}	the maxium acceptable service time of an EV for swap or supercharging (unit: hour)
a_g	capacity cost of renewable generator g. (unit: \$/MW)
d_{ES}	capacity cost of electric energy storage ES unit in station. (unit: \$/MWh)
$d_{VB,k}$	unit cost of EV battery pack type i in station. (unit: \$/item)
d_{SC}	installation cost of a supercharger
b_{ES}	ES operating cost (unit: \$/MWh)
b_g	operating cost of generator g for g= 1,2, …, G.
ϕ_g	capital recovery factor for renewable generator g
ϕ_{ES}	capital recovery factor for electrical energy storage unit in station
ϕ_{VB}	capital recovery factor for spare battery packs in station
ϕ_{SC}	capital recovery factor of superchargers (where 'SC' stands for supercharging)
$\rho_{IM,t}$	price of importing or buying electricity from the main grid at time t (unit: \$/MWh)
$\rho_{EX,t}$	price of exporting selling electricity to the main grid at time t (unit: \$/MWh).
$\lambda_{EV,k,t}$	arrival rate of EV with battery type k at time t. (unit: cars/hour)
$\lambda_{g,t}$	hourly capacity factor of WT and PV t=1, 2, …, T
c_g	carbon credits of renewable generator g.
$B^c_{VB,k}$	capacity of battery type k. (unit: MWh/battery)
π_k	probability that an EV uses a supercharger due to stockout of battery type k
α_k	service level criterion for using bettery swap
P_{SC}	power of a supercharger (unit: MW)
$P_{VB,k}$	power of recharging battery type k in charge bay (unit: MW)

Table 4.2 Explanation of Decision Variables

Notation	Explanation
P_g^c	power capacity of renewable generator *g* for *g*=1, 2, …, *G*. (unit: MW)
B^c_{ES}	energy capacity of electrical storage unit in station (unit: MWh)
$B_{ES,t}$	amount of energy stored in ES unit at time *t* (unit: MWh)
s_k	number of spare battery type *k* in station for *k*=1, 2, …, *K*
m	number of superchargers in a station
$E_{IM,t}$	the amount of energy imported from the main grid at time *t* (unit: \$/MWh)
$E_{EX,t}$	the amount of energy exported to the main grid at time *t* (unit: \$/MWh)

The annualized cost of the JBSS station is given as follows:

$$\begin{aligned} f_3(\mathbf{P}^c, \mathbf{s}, B_{es}^c) = \sum_{g=1}^{G}\phi_g a_g P_g^c + \sum_{t=1}^{T}\sum_{g=1}^{G}(b_g - c_g)\lambda_{gt} P_g^c \tau + \phi_{ES} d_{ES} B_{ES}^c + \sum_{t=1}^{T} b_{ES} B_{ES,t} \\ + \sum_{k=1}^{K}\phi_{VB} d_{VB,k} s_k + \phi_{SC} d_{SC} m + \sum_{t=1}^{T}\left(\rho_{IM,t} E_{IM,t} - \rho_{EX,t} E_{EX,t}\right) \end{aligned} \tag{4.1}$$

There are five major constraints associated with the hourly operation of a JBSS station.

These constraints are elaborated below.

a) Energy balance in each period

$$\sum_{k=1}^{K}(1-\pi_k)\lambda_{EV,k,t}\tau B_{VB,k}^c + \sum_{k=1}^{K}\pi_k \lambda_{EV,k,t}\tau B_{VB,k}^c + B_{ES,t} - B_{ES,t-1} + E_{EX,t} - E_{IM,t} = \sum_{g=1}^{G}\lambda_{gt}\tau P_g^c,$$

$$\text{for } t=1, 2, ..., T. \tag{4.2}$$

Or equivallently

$$\sum_{k=1}^{K}\lambda_{EV,k,t}\tau B_{VB,k}^c + B_{ES,t} - B_{ES,t-1} + E_{EX,t} - E_{IM,t} = \sum_{g=1}^{G}\lambda_{gt}\tau P_g^c \text{ , for } t=1, 2, ..., T. \tag{4.3}$$

Note that the value of π_k falls between 0 and 1. If π_k=0, it means all incoming EV receives battery swap services, and there is no use of superchargers. If π_k=1, it means all EV need to recharge their on-board battery using superchargers because the statiom has no spare packs. In reality 0<π_k<1 depending on the allocated safety stock level of the spare battery in a JBSS station.

b) Service level requirement (probability vs. time constraints)

$$(1-\pi_k)\tau_{swap} + \frac{\sum_{k=1}^{K}\pi_k \lambda_{EV,k,t}\tau B^c_{VB,k}}{\tau m P_{SC}} \le \tau_{\max} \text{ , for } t=1, 2, ..., T, \text{ and } k=1, 2, ..., K. \quad (4.4)$$

Equation (4.4) can be re-arranged as follows

$$(1-\pi_k)\tau_{swap} + \frac{1}{mP_{SC}}\sum_{k=1}^{K}\pi_k \lambda_{EV,k,t} B^c_{VB,k} \le \tau_{\max} \text{ , for } t=1, 2, ..., T, \text{ and } k=1, 2, ..., K. \quad (4.5)$$

Or equivalently

$$\tau_{\max} mP_{SC} - (1-\pi_k)\tau_{swap} mP_{SC} \ge \sum_{k=1}^{K}\pi_k \lambda_{EV,k,t} B^c_{VB,k} \text{ , for } t=1, 2, ..., T, \text{ and } k=1, 2, ..., K. \quad (4.6)$$

c) Spare battery demand constraints

An amount of spare battery units is allcoated in the JBSS station to meet the swap demand. This constraint is defined as follows

$$(1-\pi_k)\lambda_{EV,k,t}\tau \le \frac{P_{VB,k}\tau}{B^c_{VB,k}} s_k \text{ , for } t=1, 2, ..., T, \text{ and for } k=1, 2, ..., K. \quad (4.7)$$

Where the left hand side represents the minimum amount of batteries being exchanged for type k with probability 1-π_k. Here $B^c_{VB,k}$ is the capacity of battery type k, and $P_{VB,k}$ is the recharge power of battery type k in the charge bay. Note that τ is the time duration of a planning period. The right hand side represents the turn-around rate of the battery inventory. For instance, during period τ, if only one depleted battery can be recharged, the inventory must have s_k units to meet the swap demand with probability1-π_k. If the recharge turn-around time doubles, it implies that two empty batteries can be recharged to full or $P_{VB,k}/B^c_{VB,k}$=2. Then only 0.5s_k spare batteris are needed to meet the swap demand during τ. In an extreme case which though never happens: when the time to recharge a empty battery is zero, there is only one spare battery is needed, i.e., s_k=1, to meet the deamand. Equation (4.7) can also be rewritten as

$$s_k P_{VB,k} \geq \lambda_{EV,k,t} B^c_{VB,k} (1-\pi_k) \text{ , for } t=1, 2, ..., T, \text{ and for } k=1, 2, ..., K. \tag{4.8}$$

d) ES capacity limit at time *t*

$$0 \leq B_{ES,t} \leq B^c_{ES} \text{ , for } t=1, 2, ..., T. \tag{4.9}$$

e) Initial ES energy at *t*=0

$$B_{ES,0} = B^c_{ES} \tag{4.10}$$

f) ES energy at end time at *t*=*T*

$$B_{ES,T} = B^c_{ES} \tag{4.11}$$

g) Non-negativity of decision variables

$$P^c_g \geq 0 \text{ , for } g=1, 2, \ldots, G. \tag{4.12}$$

$$B^c_{ES} \geq 0 \text{ ,} \tag{4.13}$$

$$E_{IM,t} \geq 0 \text{ , for } t=1, 2, \ldots, T. \tag{4.14}$$

$$E_{EX,t} \geq 0 \text{ , for } t=1, 2, \ldots, T. \tag{4.15}$$

$$s_k \in \{0, 1, 2, \ldots\}, \text{ for } k=1, 2, \ldots, K. \tag{4.16}$$

$$m \in \{0, 1, 2, \ldots\} \tag{4.17}$$

4.2 Numerical Experiments

4.2.1 Values of Model Parameters

Parameters are the values (or data) which are known in the optimization model. The parameters for the optimization model are summarized in Table 4.3 below:

Table 4.3 Parameters with Unit for Model 4.1 (Case 1 for Benchmark)

Notation	Value	Unit
G	Since WT and PV are used, G=2	n/a
τ	1	hour
T	8736	hour
a_1	1.5M (g=1 is for WT)	$/MW
a_2	2M (g=2 is for PV)	$/MW
d_{ES}	0.4M (ES capacity cost)	$/MWh
$d_{VB,1}$	7,000 (for Nissan Leaf 1st generation battery)	$/item
$d_{VB,2}$	12,000 (for Nissan Leaf 2nd Generation)	$/item
b_1	8 (WT operating cost)	$/MWh
b_2	4 (PV operating cost)	$/MWh
b_{ES}	2 (ES operating cost)	$/MWh
c_1	0 (WT carbon credit)	$/MWh
c_2	10 (PV carbon credits)	$/MWh
ϕ_1	0.0944 (7% compound interest, 20 years)	n/a
ϕ_2	0.0944 (7% compound interest, 20 years)	n/a
ϕ_{ES}	0.1424 (7% compound interest, 10 years)	n/a
ϕ_{VB}	0.1424 (7% compound interest, 10 years)	n/a
$\lambda_{1,t}$	Each city hourly WT capacity factor for t=1, 2, …, T	n/a
$\lambda_{2,t}$	Each city hourly PV capacity factor for t=1, 2, …, T	car/hour
$\lambda_{EV,k,t}$	5 for t=1, 2, …, T	n/a
$P_{EV,1}$	0.024 (power for charging 1st generation Leaf battery)	MW
$P_{EV,2}$	0.040 (power for charging 2nd generation Leaf battery)	MW
$\rho_{IM,t}$	140 (electricity price of importing from main grid)	$/MWh
$\rho_{EX,t}$	35 (electricity sale price of exporting to main grid)	$/MWh
τ_{swap}	0.05(the time to swapping battery given a spare pack is available)	hours
τ_{max}	0.3 (the maxium acceptable service time of an EV for swap or supercharging)	hour
d_{SC}	150,000 (installation cost of a supercharger)	$/supercharger
ϕ_{SC}	0.0944 (7% compound interest, 20 years)	n/a
$B^c_{VB,k}$	0.024 and 0.04 (capacity of EV battery type k)	MWh/battery
π_k	0.1 (probability that an EV uses supercharger because battery type k is out of stock)	n/a
α_k	0.8 (service level criterion for using bettery swap)	n/a
P_{SC}	0.15 (power of a supercharger)	MW
$P_{VB,k}$	0.8 (the recharge power of battery type k in charge bay)	MW

4.2.2 Computational Results and Discussions

Model 4.1 is solved in AMPL computational environment with the given parameters in Table 4.3. The model is implemented in ten different cities based on the hourly capacity factors of WT and PV. The optimal sizing of WT, PV and ESS units, the number of spare batteries and superchargers (SC), and the associated annual cost are found which are summarized in Table 4.4.

Table 4.4 Results of Objective Function and Decision Variables in Each City

City	Annual cost ($)	WT (MW)	PV (MW)	Battery type 1	Battery type 2	ESS (MWh)	Num of SC	Prosumer
Phoenix	396,005	0	0.60	2	3	0	1	Import, export
San Francisco	179,265	1.55	0	2	3	0	1	Import, export
Salt Lake City	336,991	0.90	0	2	3	0	1	Import, export
Reno	377,934	0.35	0.50	2	3	0	1	Import, export
Yuma	346,499	0.56	0.41	2	3	0	1	Import, export
Tucson	345,510	0.34	0.51	2	3	0	1	Import, export
Las Vegas	334,129	0.42	0.47	2	3	0	1	Import, export
Los Angeles	355,876	0.74	0	2	3	0	1	Import, export
Sacramento	342,138	0.49	0.44	2	3	0	1	Import, export
San Jose	394,293	0.35	0.50	2	3	0	1	Import, export

Phoenix is a sunny city based on weather conditions. For this reason, after analyzing the values from the table, Phoenix chooses to install 0.6 MW of PV as microgrid generation. From Table 4.4, San Francisco installs 1.55 MW of WT as microgrid generation. This makes sense from Chapter 3 weather condition data (see Tables 3.4 and 3.5), that San Francisco is a city with strong wind.

According to Chapter 3 weather condition data, Salt Lake City is a strong wind and strong sun city but from Table 4.4, Salt Lake City only installs 0.9 MW of WT as power generating unit with not installing any PV is found. For Reno, Yuma and Tucson these three cities have strong sun and weak wind according to weather condition data in Tables 3.4 and 3.5 of Chapter 3. The results indicate that these three cities opt to install both WT and PV as microgrid generating units. Las Vegas and Sacramento both possess strong wind and strong sun. From Table 4.4, both of these cities choose WT and PV as onsite generating units based on their weather condition.

An interesting result for Los Angeles is found. Based on the weather data in Tables 3.4 and 3.5, Los Angeles is a city with weak wind and strong sun but from the above table, Los Angeles is installing WT as onsite generation and also importing and exporting energy to the main grid. These process makes the whole system act as prosumer. Since, San Jose has strong sun and weak wind. But from Table 4.4, San Jose is installing both WT and PV as distributed power generating units.

In summary, Table 4.4 shows that all these ten cities are importing energy from the main grid and also exporting energy to the main grid and serving as prosumer.

4.3 Sensitivity Analysis

4.3.1 Values of Model Parameter

The sensitivity analysis parameters are defined based on the consideration of technology change, government incentives, and energy market dynamics. With the advancement of technology, the capacity cost of PV and ES system and the cost of swapping battery may go down in near future. These scenarios have considered while choosing the sensitivity analysis value for Cases 2, 3, 4 and 5. The government currently gives carbon credits to PV installation. In future when the PV cost continues to decline, the government could terminate the carbon credits. In Case 6, this scenario has considered while setting zero carbon credits for PV. When EV becomes more accessible to people, the demand for EV battery swap and supercharging station are expected to go up. For this reason, the EV battery service demand has doubled in Case 7. With the advancement of technology, the battery power capacity and supercharger power could increase as well. These factors have considered in Cases 8 and 11. In real life, the electricity purchase price varies with time during a day. This scenario has captured by changing the electricity importing price based on TOU in Case 9. In future the demand for renewable energy could increase to mitigate the climate change. For this reason, the selling price of renewable energy could go up. This situation is captured in Case 10.

Table 4.5 Parameter for Sensitivity Analysis for Model 4.1 (Cases 2 to 11)

Case	Notation	Value	Unit	Comments
2	a_2	1M	\$/MW	g=2 is for PV
3	d_{ES}	0.1M	\$/MWh	ES capacity cost
4	d_{ES}	0.05M	\$/MWh	ES capacity cost
5	$d_{VB,1}$	3,500	\$/item	for Nissan Leaf 1st generation battery
	$d_{VB,2}$	6,000	\$/item	for Nissan Leaf 2nd Generation
6	c_2	0	\$/MWh	PV carbon credits
7	$\lambda_{EV,k,t}$	10	car/hour	for t=1, 2, …, T, for k=1 and 2
8	$P_{EV,1}$	0.048	MW	power for charging 1st generation Leaf battery
	$P_{EV,2}$	0.08	MW	power for charging 2nd generation Leaf battery
9	$\rho_{IM,t}$	140, 70	\$/MWh	TOU rate \$140/MWh from 9am to 9pm, and \$70/MWh from 10pm to 8am
10	$\rho_{EX,t}$	70	\$/MWh	standard utility rate
11	P_{SC}	0.3	MW	supercharger power

The ten cities have been categorized based on two criteria. The first one is strong wind and strong sun, the second one is weak wind and strong sun. If the capacity factor (CF) of WT is less than 0.19 then the city has weak wind and if the CF of WT is higher than 0.19 then the city has strong wind. Additionally, If the capacity factor of PV is less than 0.2 then the city has weak sun and vice versa. These two criteria actually cover a diverse weather profile in the world. Different cities have picked from each category to run the sensitivity analysis for covering a diverse weather profile.

Table 4.6 Weather Condition of Ten Cities

Wind	Sun	City
Strong	Strong	Las Vegas, Sacramento, Salt Lake City, San Francisco
Weak	Strong	Reno, Yuma, Tucson, Phoenix, San Jose, Los Angeles

4.3.2 Phoenix

Phoenix is picked as the first city to carry out the sensitivity analysis. Model 4.1 is solved in AMPL computational environment with the given parameters using the hourly capacity factors of WT and PV in Phoenix. The optimal sizing of WT, PV and ESS units along with the number of spare batteries and superchargers are summarized in Table 4.7. Note that Case 1 is a benchmark.

Table 4.7 Results of Objective Function and Decision Variables in Phoenix

Case	Annual cost ($)	WT (MW)	PV (MW)	Battery type 1	Battery type 2	ESS (MWh)	Num. of SC	Prosumer
1	396,005	0	0.60	2	3	0	1	Import, export
2	314,276	0	1.33	2	3	0	1	Import, export
3	395,851	0	0.62	2	3	0.061	1	Import, export
4	394,296	0	0.79	2	3	0.56	1	Import, export
5	392,445	0	0.60	2	3	0	1	Import, export
6	404,666	0	0.54	2	3	0	1	Import, export
7	789,305	0	1.21	3	5	0	2	Import, export
8	789,305	0	1.21	3	5	0	2	Import, export
9	311,327	0	0.57	2	3	0	1	Import, export
10	395,079	0	0.66	2	3	0	1	Import, export
11	396,005	0	0.60	2	3	0	1	Import, export

After comparing Cases 1 and 2, find out that reducing the PV capacity cost by half (i.e. down to $1M/MW) makes the system increases PV capacity from 0.60 MW to 1.33 MW. The annual cost of $314,276 is less than the benchmark cost of $396,005, indicating that the system in Case 2 creates profit by selling more surplus PV energy to the main grid. Cases 3 and 4 are computed at the reduced cost of ESS unit. It is interesting to see that ESS is became competitive in Phoenix when the cost is down to $0.05M/MWh as opposed to current cost of $0.4M/MWh in Case 4. In other words, the system chooses ESS to store energy when the cost is down to $0.1M/MWh and $0.05M/MWh. In Case 5, the EV battery cost is halved, the required spare parts remain the same as those of Case 1. This shows that the station will not store more battery packs because of reduced cost. Case 6 indicates that PV is still advantageous compared to wind even if the carbon credits are removed.

Case 7 shows that by doubling the battery swap demand, the station needs to install twice of PV capacity to fulfill the demand. This result is reasonable because the station needs more PV power to charge more exchanged batteries given the same time period. By doubling the battery swap demand, the station requires more spare battery packs and superchargers for fulfilling the increased demand of the station.

Case 8 assumes the charge power for each battery type doubles relative to Case 1. As a result, the installed PV capacity also doubles to meet the increased charging power. In addition, the station is storing more spare battery packs and superchargers for fulfilling the increased EV service demand of the station.

Case 9 shows that by reducing the electricity importing price from the main grid from $140/MWh to $70/MWh between 10pm and 8am, the annual cost of the battery swap and super charging station is reduced.

After comparing Case 10 with Case 1, find that by increasing the selling price of electricity to the main grid, the station opts to install more PV capacity to fulfill the demand of the battery swap and supercharging station and sells the surplus energy to main grid which is profitable.

Comparison between Case 11 with Case 1, find that by increasing the level of supercharging power from 0.15MW to 0.3MW there is no significant impact on the installation capacity of PV, ESS, and the number of spare batteries and superchargers.

4.3.3 Salt Lake City

Salt Lake City is chosen as the second city to run the optimization model for sensitivity analysis. Case 1 is denoted as a benchmark, the optimal sizing of WT, PV and ESS units, the number of battery packs and superchargers and the annual cost are summarized in Table 4.8.

Table 4.8 Results of Objective Function and Decision Variables in Salt Lake City

Case	Annual cost ($)	WT (MW)	PV (MW)	Battery type 1	Battery type 2	ESS (MWh)	Num. of SC	Prosumer
1	336,991	0.90	0	2	3	0	1	Import, export
2	323,853	0.67	0.71	2	3	0	1	Import, export
3	336,991	0.90	0	2	3	0	1	Import, export
4	336,990	0.90	0	2	3	0.003	1	Import, export
5	333,431	0.90	0	2	3	0	1	Import, export
6	336,991	0.90	0	2	3	0	1	Import, export
7	671,276	1.80	0	3	5	0	2	Import, export
8	671,276	1.80	0	3	5	0	2	Import, export
9	289,052	0.65	0	2	3	0	1	Import, export
10	240,153	9.29	0	2	3	0	1	Import, export
11	336,991	0.90	0	2	3	0	1	Import, export

After comparing Case 2 with Case 1, find that reducing the PV capacity cost by half makes the system to increase PV capacity from 0 to 0.71 MW. The annual cost of $323,853 indicates that the system in Case 2 creates profit by selling surplus PV energy to the main grid. Cases 3 and 4 are computed at the reduced cost of ESS unit. In Case 3, it is interesting to see that ESS is still not competitive in Salt Lake City when the cost is down from $0.4M/MWh to $0.1M/MWh. In other words, the station opts to export the surplus renewable energy to the main grid instead of storing in the ESS. In Case 4, by reducing the ESS cost to $0.05M/MWh, the station installs very small capacity of ESS which again shows that ESS is not even competitive in Salt Lake City. In Case 5, the EV battery cost is halved, the required spare parts remain the same as those of Case 1. This shows that the station will not store more spare battery packs because of reduced cost.

Case 6 indicates that PV is not advantageous compared to wind for Salt Lake City with and without carbon credits of PV.

Case 7 shows that by doubling the battery swap demand, the station needs to install twice of WT capacity to fulfill the demand. This result is reasonable because the station needs more WT power to charge more swapped batteries given the same time. By doubling the battery swap demand, the station requires more spare battery packs and superchargers for fulfilling the EV service demand.

Case 8 assumes the charging power for each battery type doubles as oppose to Case 1. The installed WT capacity also doubles to meet the increased charging power. In addition, the station is keeping more spare battery packs and installing more superchargers for fulfilling the increased demand of the station.

Case 9 shows that by reducing the electricity importing price from the main grid from $140/MWh to $70/MWh between 10pm and 8am, the annual cost of the battery swap and supercharging station is reduced.

After comparing Case 10 with Case 1, find that by increasing the exporting cost of electricity from the main grid, the station opts to install more WT capacity which is 9.29MW, more than ten times of 0.9MW in Case 1. It is profitable to sell surplus energy to the main grid due to increasing exporting price of electricity. It also helps to fulfill the demand of the battery swap and supercharging station.

After comparing Case 11 with Case 1, find that increasing the level of supercharging power from 0.15MW to 0.3MW does not have any impact on the installation capacity of PV and ESS, and the number of spare batteries and superchargers.

4.3.4 San Francisco

Model 4.1 is solved in AMPL computational environment with the given parameters for sensitivity analysis and the hourly capacity factors of WT and PV in San Francisco are used to run the optimization model. Case 1 is denoted as a benchmark, the optimal sizing of WT, PV and ESS units along with the number of battery packs and superchargers and the annual cost are summarized in Table 4.9.

Table 4.9 Results of Objective Function and Decision Variables in San Francisco

Case	Annual cost ($)	WT (MW)	PV (MW)	Battery type 1	Battery type 2	ESS (MWh)	Num. of SC	Prosumer
1	179,265	1.55	0	2	3	0	1	Import, export
2	179,265	1.55	0	2	3	0	1	Import, export
3	179,265	1.55	0	2	3	0	1	Import, export
4	179,258	1.56	0	2	3	0.01	1	Import, export
5	175,705	1.55	0	2	3	0	1	Import, export
6	179,265	1.55	0	2	3	0	1	Import, export
7	355,825	3.09	0	3	5	0	2	Import, export
8	355,825	3.09	0	3	5	0	2	Import, export
9	174,395	1.24	0	2	3	0	1	Import, export
10	112,093	3	0	2	3	0	1	Import, export
11	179,265	1.55	0	2	3	0	1	Import, export

After comparing the Case 2 with Case 1, find out that reducing the PV capacity cost by half and down to $1M/MW does not make the system chooses any PV capacity for San Francisco. Cases 3 and 4 are computed at the reduced cost of ESS unit. In Case 3, it is interesting to see that ESS is not even competitive in San Francisco when the cost is down to $0.1M/MWh as opposed to current cost of $0.4M/MWh. In other words, the system does not choose ESS to store energy when the cost is down to $0.1M/MWh, hence the station opts to export energy to the main grid instead of storing at the ESS. In Case 4, by reducing the ESS cost to $0.05M/MWh, the station installs very small capacity of ESS which again shows that ESS is not even competitive in San Francisco. In Case 5, the EV battery cost is halved, the required spare parts remain the same as these of

Case 1. This shows that the station will not store more spare battery packs because of reduced cost. Case 6 indicates that PV is not advantageous compared to wind for San Francisco with and without carbon credits of PV.

Case 7 shows that by doubling the battery swap and supercharging station demand, the station needs to install twice of WT capacity to fulfill the demand. This result is reasonable because the station needs more WT power to charge more exchanged batteries given the same time. By doubling the battery swap demand, the station is installing more spare battery packs and superchargers for fulfilling the demand of the station.

Case 8 assumes that the charging power for each battery type doubles as oppose to Case 1. As a result, the installed WT capacity also doubles to meet the increased charged power. Not only that but also the station is installing more spare battery packs and superchargers for fulfilling the increased demand of the station.

Case 9 shows that by reducing the electricity importing price from the main grid from 10 pm to 8am from \$140/MWh to \$70/MWh, the annual cost of the battery swap and supercharging station is reduced.

After comparing Case 10 with Case 1, find out that by increasing the exporting cost of electricity from the main grid, the station opts to install more WT capacity which is 3MW from 1.55MW to fulfill the demand of the battery swap and supercharging station. The negative cost indicates that the battery swap and supercharging station sells the surplus energy to main grid which is profitable due to increasing exporting cost of electricity.

After comparing Case 11 with Case 1, find out that by increasing the super chargers power from 0.15MW to 0.3MW does not has any impact on the installation capacity of PV, ESS, number of spare batteries and number of super chargers.

4.3.5 Los Angeles

Model 4.1 is solved in AMPL computational environment with the given parameters for sensitivity analysis and among ten different cities hourly capacity factors of WT and PV Los Angeles is picked as the fourth city to run the optimization model. Case 1 is denoted as a benchmark, the optimal sizing of WT, PV and ESS units along with the number of battery packs and superchargers and the annual cost are summarized in Table 4.10.

Table 4.10 Results of Objective Function and Decision Variables in Los Angeles

Case	Annual cost ($)	WT (MW)	PV (MW)	Battery type 1	Battery type 2	ESS (MWh)	Num. of SC	Prosumer
1	355,876	0.74	0	2	3	0	1	Import, export
2	309,986	0.38	1.01	2	3	0	1	Import, export
3	355,876	0.74	0	2	3	0	1	Import, export
4	355,876	0.74	0	2	3	0.001	1	Import, export
5	352,316	0.74	0	2	3	0	1	Import, export
6	355,876	0.74	0	2	3	0	1	Import, export
7	709,046	1.49	0	3	5	0	2	Import, export
8	709,046	1.49	0	3	5	0	2	Import, export
9	298,227	0.43	0	2	3	0	1	Import, export
10	301,674	3.90	0	2	3	0	1	Import, export
11	355,876	0.74	0	2	3	0	1	Import, export

After comparing Case 2 with Case 1, find out that reducing the PV capacity cost by half and down to $1M/MW makes the system chooses PV capacity of 1.01 MW from 0 MW for Los Angeles. Cases 3 and 4 are computed at the reduced cost of ESS unit. In Case 3, it is interesting to see that ESS is not even competitive in Los Angeles when the cost is down to $0.1M/MWh as opposed to current cost of $0.4M/MWh. In other words, the system does not choose ESS to store energy when the cost is down to $0.1M/MWh hence the station opts to export energy to the main grid instead of storing at the ESS. In

Case 4, by reducing the ESS cost to $0.05M/MWh, the station installs very small capacity of ESS which again shows that ESS is not even competitive in Los Angeles. In Case 5, the EV battery cost is halved, the required spare parts remain the same as these of Case 1. This shows that the station will not store more spare battery packs because of reduced cost. Case 6 indicates that PV is not advantageous compared to wind for Los Angeles with and without carbon credits of PV.

Case 7 shows that by doubling the battery swap and supercharging station demand, the station needs to install twice of WT capacity to fulfill the demand. This result is reasonable because the station needs more WT power to charge more exchanged batteries given the same time. By doubling the battery swap demand, the station is installing more spare battery packs and superchargers for fulfilling the demand of the station.

Case 8 assumes the charge power for each battery type doubles as oppose to Case 1. So, the installed WT capacity also doubles to meet the increased charged power. Not only that but also the station is installing more spare battery packs and superchargers for fulfilling the increased demand of the station.

Case 9 shows that by reducing the electricity importing price from the main grid from 10 pm to 8am from $140/MWh to $70/MWh, the annual cost of the battery swap and supercharging station is reduced.

After comparing Case 10 with Case 1, find out that by increasing the exporting cost of electricity from the main grid, the station opts to install more WT capacity which is 3.9 MW from 0.74 MW to fulfill the demand of the battery swap and supercharging station. The annual cost indicates that the battery swap and supercharging station sells the surplus energy to main grid which is profitable due to increasing exporting cost of electricity.

After comparing Case 11 with Case 1, find out that by increasing the super charger’s power from 0.15MW to 0.3MW does not has any impact on the installation capacity of PV, ESS, the number of spare batteries and super chargers.

5. VIRTUAL POWER PLANT PLANNING FOR EV SERVICE NETWORK

5.1 Virtual Power Plant (VPP)

5.1.1 The Concept of VPP

A virtual power plant works remotely to combine a number of independent energy resources from disparate locations into a network that provides reliable power in 24 hours a day. Relatively new on the energy landscape, the plants employ software-based technology that relies on the smart grid infrastructure and communication protocols. They utilize planning, scheduling, and bidding of distributed energy resources (DER) to create the energy network that provides reliable electric power. (Cohn 2018)

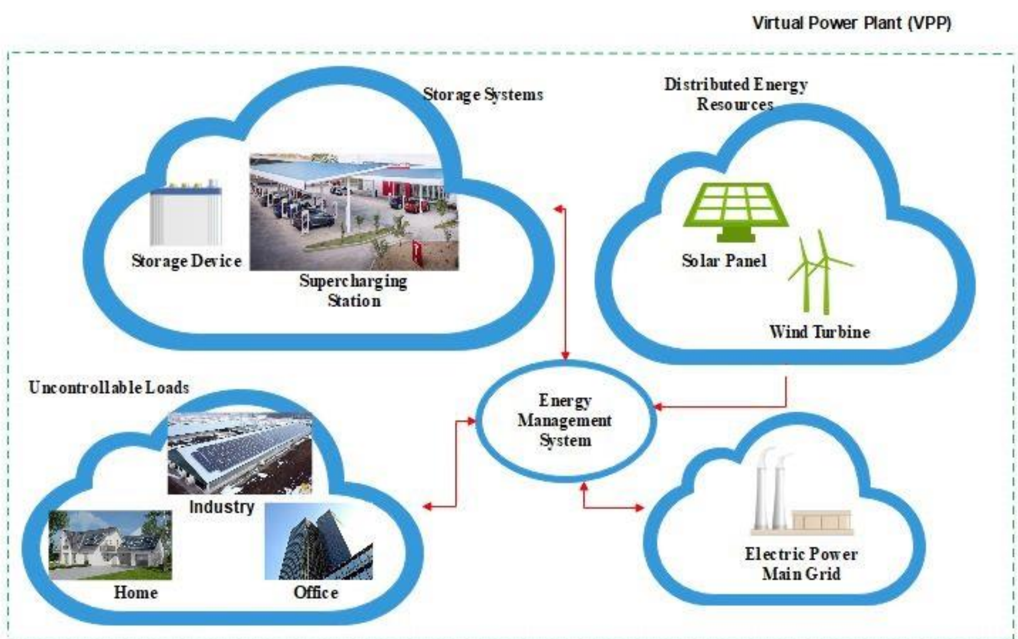

Figure 5.1 Structure of Virtual Power Plants (VPP)

5.1.2 Advantage and Disadvantages of VPP

VPP can provide ancillary services to respond to the imbalances created by renewable energy and other intermittent resources, or failures of large power plants. The following advantages and disadvantages of VPP are elaborated (Cohn 2018).

Advantages:

1) lower cost,
2) more flexibility,
3) reduction in harmful emissions, and
4) lower energy loss

Disadvantages:

1) vulnerable to cyber-attacks,
2) high levels of distributed energy resources can affect local voltage, unless a voltage control scheme is in place, and
3) regulatory obstacle: incentives are needed to help VPP operators bring their benefits to the system.

5.1.3 The Current Deployment of VPP in the World

Below the details of the current deployment of VPP in USA, Europe and Japan are discussed.

USA:

California: Due to wildfire, Californian residents face power outage frequently. A German energy storage company named Sonnen is planning to spread across seven large apartment complex in California combining solar panels and energy storage systems in a form of VPP to power them. By applying these measure, residents of those apartment complex will not have to reply on the utility companies and the power outage rate will be reduced (Calma 2020). In Los Angeles, California Sunrun Inc. is planning to incorporate virtual solar plant with batteries in 75,000 apartment buildings which will provide enough power to replace one of retiring plants in LA (Cowan 2019).

Colorado: Holy Cross Energy has developed a VPP consisting of four homes with PV, energy storage system, EV chargers and heat pumps to power those homes (Howland 2020).

New York: The utility company Con Edison announced that they are planning to offer 300 homes in Queens and Brooklyn with solar panels combining with battery so that it can create virtual power plant for New York's grid (Coren 2016). The state of New York is reforming their energy vision with VPP and they are planning to apply VPP in cinema hall in NY (Cohn 2018).

Texas: According to Jack Daly, assistant to city manager of David Morgan, Georgetown Texas is planning to apply VPP technology to compensate their high rising power demand (Howland 2020). AutoGrid company is teaming up Japanese energy service company to create battery storage system for exiting solar panels at house in Austin, Texas (Marcus 2020).

Europe:

Denmark: Centrica has got the contract to develop a VPP for 87,000 homes and businesses in Denmark (Nhede 2018). One of the Danish island named Bornholm, will be the one of the world's smartest grids using VPP under the EcoGrid Project (Kumegai 2012).

Germany: Statkraft has the largest VPP in Germany which consists of 1300 wind farms, 100 solar panels, 12 biomass power plant and 8 hydro power plants (statkraft.com). Sonnen a German company claims that they can offer up to 90% more cost efficiency by using VPP (Enkhardt 2020).

UK: Centrica along with Sonnen have installed a network consisting of 100 domestic batteries forming the UK's most advanced VPP (centrica.com). Tesla has launched UK based VPP project which will encourage EV owners in UK to install domestic PV and batteries for creating flexible energy services to the grid (edie newsroom 2020).

Japan: ENERES a Japan based company is developing a VPP consisting of 10,000 assets. ENERES will use software from California's AutoGrid company (Driscoll 2019).

5.1.4. VPP Application in Transportation Electrification

Goa et al. (2014) present the analysis of characteristics of the EV and also summarize the possibility of accessing EV as grid. The paper represents a detailed introduction of VPP concept and its participation mechanism. In addition, the paper aims to propose an accessing mode based on the VPP concept along with the advantages of the mode. Hassan et al. (2013) models an energy system of the Great Britain (GB) energy at the national level for a range of wind power penetration and three different transport scenarios: vehicles with internal combustion engines (IC), electric vehicles (EV) without vehicle-to-grid (V2G) capability, and EV with V2G capability. The paper presents that adding V2G capability in EV can provide a flexible energy storage mechanism that reduces the necessary electricity imports, and increases the autonomy of such systems, even at low wind power penetration levels. Sousa et al. (2011) present a simulated annealing approach for addressing energy management from the point of view of a VPP operating in a smart grid. Distributed generation, demand response, and grid enable vehicles are intelligently managed on a multi period basis according to V2G users' profiles and requirements.

5.2 Tesla Supercharging Network

In this section the overview of the Tesla supercharging network was presented in three different regions of the world: North America, Europe, and East Asia.

5.2.1 Overview of Tesla Supercharging Network World-Wide

Tesla Inc. is an American electric vehicle manufacturing and clean energy company (tesla.com). Tesla so far build Model S, Model 3, Model X and Model Y electric vehicles. Tesla also has manufactured solar roof tile and energy storage system (i.e. battery) (tesla.com, Raz (2017)). Tesla has started building their supercharging network around the world in 2012 and the supercharging station network consists of 480-volt fast chargers known as superchargers (Lambert 2019). Tesla build three types of super chargers so far. The first one super charger V1, the second one is super charger V2 and the latest one is super charger V3. Tesla improved its supercharging technology from supercharger V1 to V2 (and currently V3) to make higher power charging possible, hence reducing the amount of time it takes to recharge Tesla EV battery using Tesla supercharger (P.E. 2019). Tesla supercharger V1 and V2 could charge up to 150 kW power distributed between two cars at the maximum speed of 150 kW per car depending on model version of EV (Field 2020, Lambert 2019). Tesla supercharger V3 could deliver up to 250 kW power (Field 2020). Depending on the model of cars and how many people are using supercharging facility to charge their cars on the supercharging stations can decide the supercharging time of the SOC level of battery. According to Tesla website, until July 2020, Tesla owns 1971 supercharging stations globally which contains 17467 super-chargers (tesla.com). Particularly, Tesla deploys supercharging stations in North America, Europe and Asia Pacific. In the USA, Tesla has so far 1004 supercharging stations all over the states (www.tesla.com).

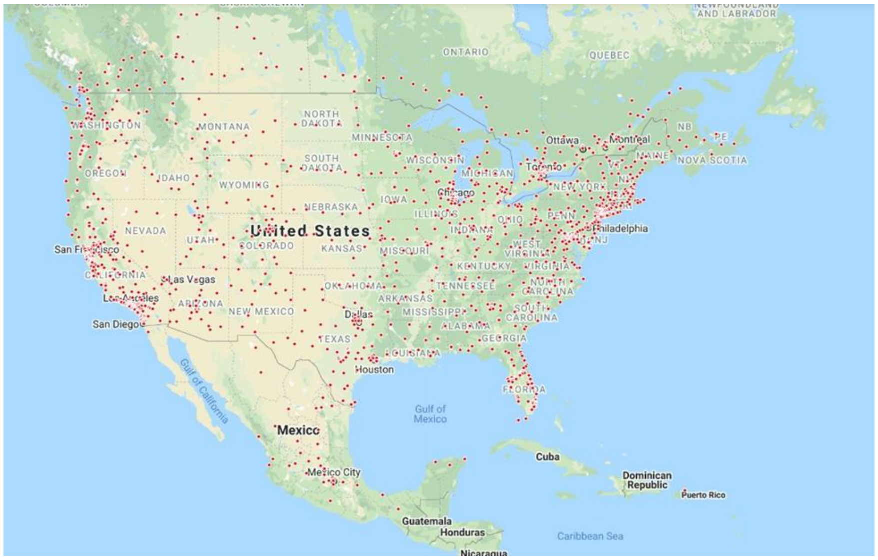

Figure 5.2 Tesla Supercharging Network in North America (Source: Tesla Website, Year: 2020)

Table 5.1 List of Supercharging Stations in USA (Source: Tesla Website)

State Name	Total # of SC	State Name	Total # of SC
Alabama	7	North Carolina	19
Arkansas	2	North Dakota	6
Arizona	25	Nebraska	5
California	199	New Hampshire	7
Colorado	23	New Jersey	39
Connecticut	24	New Mexico	9
District of Columbia	2	Nevada	20
Delaware	4	New York	51
Florida	55	Ohio	18
Georgia	18	Oklahoma	5
Iowa	11	Oregon	18
Idaho	6	Pennsylvania	27
Illinois	27	Puerto Rico	1
Indiana	16	Rhode Island	1
Kansas	9	South Carolina	6
Kentucky	7	South Dakota	8
Louisiana	7	Tennessee	11
Massachusetts	27	Texas	65
Maryland	25	Utah	12
Maine	11	Virginia	30
Michigan	25	Vermont	4
Minnesota	15	Washington	30
Missouri	14	Wisconsin	13
Mississippi	6	West Virginia	8
Montana	15	Wyoming	11

In Europe, Tesla has so far 586 supercharging stations in different European countries.

The map and list of the number of supercharging stations in Europe are given below.

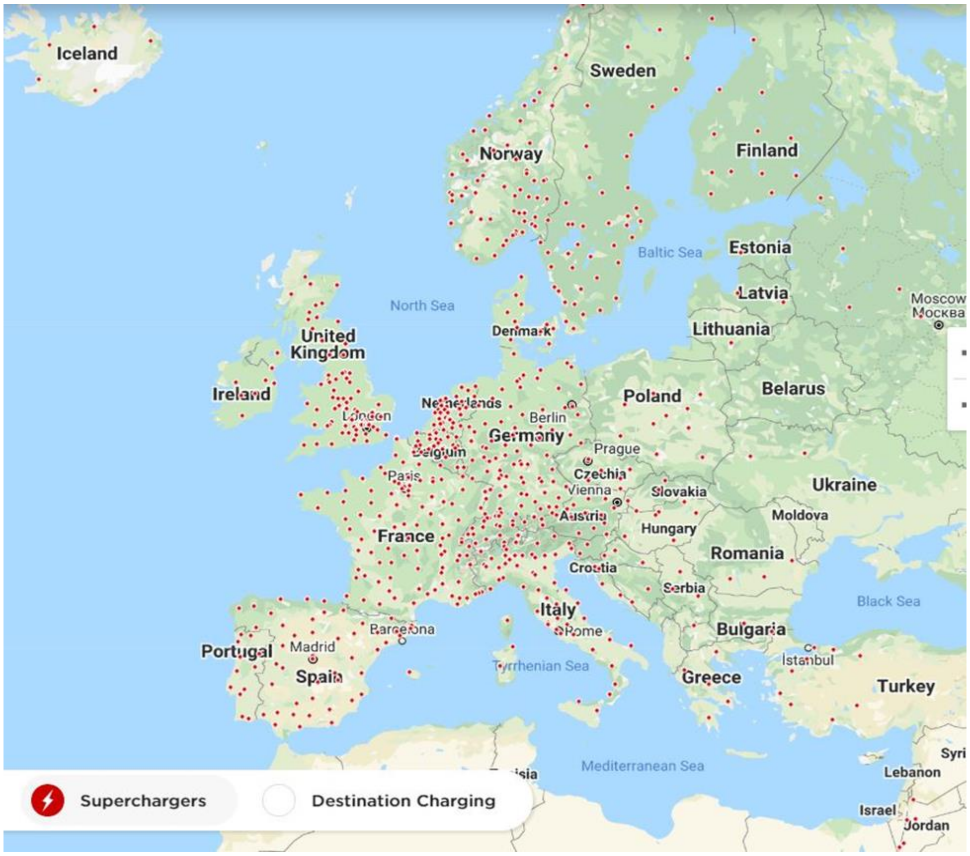

Figure 5.3 Tesla Supercharging Network in Europe (Source: Tesla Website, Year: 2020)

Table 5.2 List of Supercharging Stations in Europe (Source: Tesla Website)

State Name	Total # of SC	State Name	Total # of SC
Austria	22	Luxembourg	1
Belgium	15	Netherlands	31
Bulgaria	1	Norway	69
Croatia	8	Poland	9
Czech Republic	4	Portugal	8
Denmark	13	Russia	1
Finland	9	Serbia	2
France	83	Slovakia	3
Germany	81	Slovenia	3
Hungary	7	Spain	34
Iceland	3	Sweden	43
Ireland	5	Switzerland	19
Italy	37	United Kingdom	75

Figure 5.4 Tesla Supercharging Network in Asia (Source: Tesla Website, Year: 2020)

Table 5.3 List of Supercharging Stations in Asia Pacific (Source: Tesla Website)

Country Name	**Total # of SC**
China	281
Japan	25
South Korea	32
Taiwan	20
UAE	3
Australia	41
Jordan	4
Kazakhstan	2
New Zealand	10

5.2.2 Tesla Supercharging Network in Texas

Tesla has built 46 supercharging stations in the state of Texas actively giving its service to the EV owners which is indicated by the red sign in the map of Figure 5.5. The gray sign in the map indicates that Tesla is working on the construction of the new supercharging stations in those places. The number of supercharging stations in Texas are under-construction is 19. According to Tesla, those supercharging stations will open for service at the end of year 2020. There are total 395 super charging point installed in all the opened stations which means 395 EV can be recharged at the same time. The average number of supercharging points or installs in each station is 8.6 in Texas. The standard deviation of the supercharging point is 2.6. The maximum number of supercharging points in a station is 18 and the minimum number of supercharging points in a station is 2. In Texas there are 45 supercharging stations install 150 kW of supercharger and only 3 supercharging stations install 72 kW of supercharger. All these supercharging stations in combination create demand for energy about 57.04 MW. (Source: tesla.com)

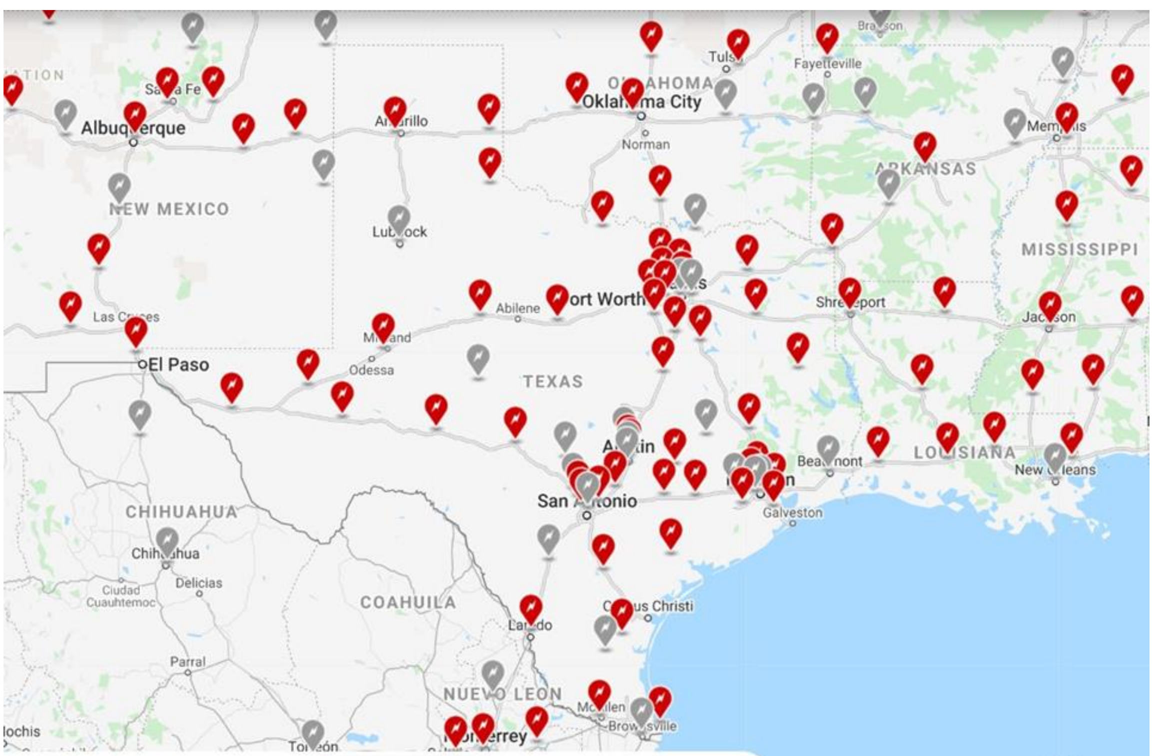

Figure 5.5 Tesla Supercharging Network in Texas (Source: Tesla Website, Year: 2020)

Table 5.4 List of Supercharging Stations in Texas (Source: Tesla Website, Year: 2020)

Station No.	**Address**	**City**	**# of SC**	**Zone**	**WT/PV CF**
1	San Marcos Premium Outlets 3939 Interstate 35	San Marcos, TX 78666	12	Austin	Same WT and PV CF
2	6406 N. Interstate 35 Frontage Road	Austin, TX 78752-0000	8	Austin	
3	Gateway Shopping Center 9607 Research Boulevard	Austin, TX 78759	18*	Austin	
4	CEFCO Convenience Store 3025 East Austin Street	Giddings, TX 78942	8	Austin	
5	Amigos Country Corner and Travel Center 1415 FM 609	Flatonia, TX 78941	8	Austin	
6	La Quinta Inn and Suites 3107 S Laurent St.	Victoria, TX 77901	6	Corpus Christi	Same WT and PV CF
7	Embassy Suites by Hilton 110 Calle Del Norte Drive	Laredo, TX 78041-9143	8	Corpus Christi	
8	Holiday Inn Express & Suites Kingsville 2400 South US Hwy 77	Kingsville, TX 78363-2844	8	Corpus Christi	
9	Schlitterbahn Resort South Padre Island 100 Padre Blvd	South Padre Island, TX 78597	2*	Corpus Christi	
10	16851 IH 20	Cisco, TX 76437	8	Dallas	Same WT and PV CF
11	2616 Whitmore Street	Fort Worth, TX 76107	16*	Dallas	
12	1200 Ballpark Way	Arlington, TX 76011-5110	10	Dallas	
13	261 North Carroll Avenue	Southlake, TX 76092	10	Dallas	
14	9740 North Central Expressway	Dallas 75231-4302	11	Dallas	
15	7161 Bishop Road	Plano, TX 75024	12	Dallas	
16	2700 West University Drive	Denton, TX 76201	6	Dallas	
17	237 Frontage Road	Henrietta, TX 76365	12	Dallas	
18	1300 Ave F NW Childress, Texas	Childress, TX 79201	8	Dallas	
19	8231 West Amarillo Blvd.	Amarillo, TX 79124	8	Dallas	
20	107 East 12th Street	Shamrock, TX 79079	6	Dallas	
21	Collin Street Bakery 701 Interstate 35	Bellmead, TX 76705	10	Dallas	
22	Love's Travel Stop 1021 Dale Evans Drive	Italy, TX 76651	10	Dallas	

Table 5.4 List of Supercharging Stations in Texas Continued

23	Collin Street Bakery 2035 Interstate 45 Frontage Rd	Corsicana, TX 75109	10	Dallas	Same WT and PV CF
24	City of Sulphur Springs Police Department 300 W Tomlinson Street	Sulphur Springs, TX 75482	8	Dallas	
25	Collin Street Bakery 17044 I-20	Lindale, TX 75771	8	Dallas	
26	Olive Garden 3101 Mall Drive	Texarkana, TX 75503-2434	8	Dallas	
27	6401 South Desert Boulevard	El Paso, TX 79932-8515	8	El Paso	Same WT and PV CF
28	1921 Frontage Rd	Van Horn, TX 79855	8	El Paso	
29	25675 Nelson Way	Katy, TX 77494	12	Houston	Same WT and PV CF
30	Gateway Travel Plaza 2615 NW Stallings Dr	Nacogdoches, TX 75964-2629	8	Houston	
31	Holiday Inn Express & Suites 148 Interstate 45	Huntsville, TX 77340	6	Houston	
32	Atrium Inn & Suites 2535 Texas 71	Columbus, TX 78934	6	Houston	
33	20500 Southwest Freeway	Richmond, TX 77469	8	Houston	
34	Holiday Inn - Houston East 16311 East Fwy	Channelview, TX 777530	8	Houston	
35	Rudy's Country Store and BBQ 14620 Northwest Freeway	Houston, TX 77040	8	Houston	
36	14820 North Fwy	Houston, TX 77090	6	Houston	
37	100 East Pinehurst Street	Pecos, TX 79772	8	Midland	Same WT and PV CF
38	3001 Antelope Trail	Midland, TX 79706-3525	8	Midland	
39	300 SE Georgia Ave.	Sweetwater, TX 79556	8	Midland	
40	2571 North Front Street	Fort Stockton, TX 79735	8	Midland	
41	2415 N Main Street	Junction, TX 76849	8	San Antonio	Same WT and PV CF
42	1307 Ave. A	Ozona, TX 76943	6	San Antonio	
43	24165 I-10 #300	San Antonio, TX 78357	10	San Antonio	
44	Huebner Oaks Shopping Center 11745 I-10	San Antonio, TX 78230	10	San Antonio	
45	Schertz H-E-B Plus! 17460 IH 35N	Schertz, TX 78154	8	San Antonio	
46	Love's Travel Center 2645 S. Hwy 37	Three Rivers, TX 78071	8	San Antonio	

The sign (*) in the top left indicates 72kW per SC and all others are 150kW per SC.

5.3 Wind and Solar Data in Texas

5.3.1 Wind Speed Data of Texas Cities

Weibull distribution is widely used to model the wind speed profile. Weibull distribution has two parameters: the scale parameter c and shape parameters k. The scale parameter describes the height of the distribution curve while the shape parameter describes the slope of the curve. Weibull wind distribution curve is calculated either annually or monthly. (oneenergy.com) Figure 5.6 below shows the probability density distribution of wind speed in cities of Texas. The distribution of wind speed is skewed (i.e. it is not symmetrical) on the right side for Corpus Christi, San Antonio, El Paso and Austin. The distribution of wind speed is skewed on the left side for Midland. The distribution of wind speed is symmetrical for Dallas and Houston.

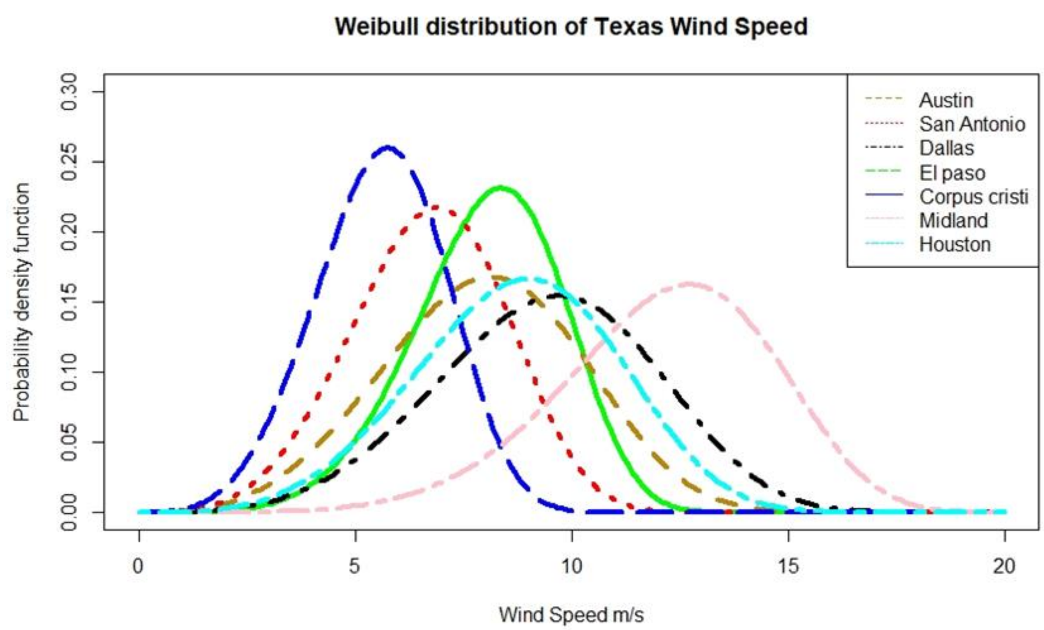

Figure 5.6 Weibull Distribution of Texas Wind Speed (one year)

The below graph represents the monthly average wind speed of seven Texas cities. From the graph, in January Corpus Christi has the highest average wind speed which is 5.11

m/s. In February Midland has the highest average wind speed which is 5.30 m/s. In March, April and May, Corpus Christi has the highest average wind speed which are 5.75, 6.07 and 6.48 m/s. In June, Midland has highest average wind speed which is 5.29 m/s. In July, Corpus Christi and Midland have highest average wind speed which is 4.65 m/s. In August, Corpus Christi and Midland have again highest average wind speed which is 4.73 m/s. In September, Midland has highest average wind speed which is 4.93 m/s. In October and December, Midland and Corpus Christi have highest average wind speed which are 5.07 and 4.12 m/s. In November, Corpus Christi has highest average wind speed which is 4.78 m/s.

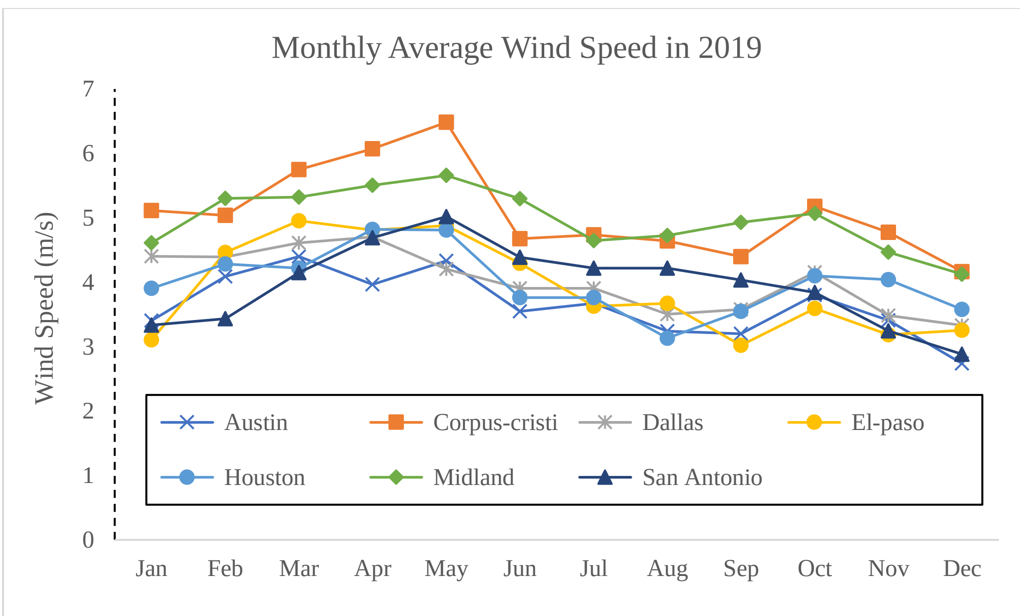

Figure 5.7 Monthly Average Wind Speed of Texas Cities in 2019

Figure 5.8 gives more statistical characteristics of seven Texas cities and offers more insights about the wind speed data. The graph informs us about the maximum, the minimum, the median and the average wind speed of seven Texas cities.

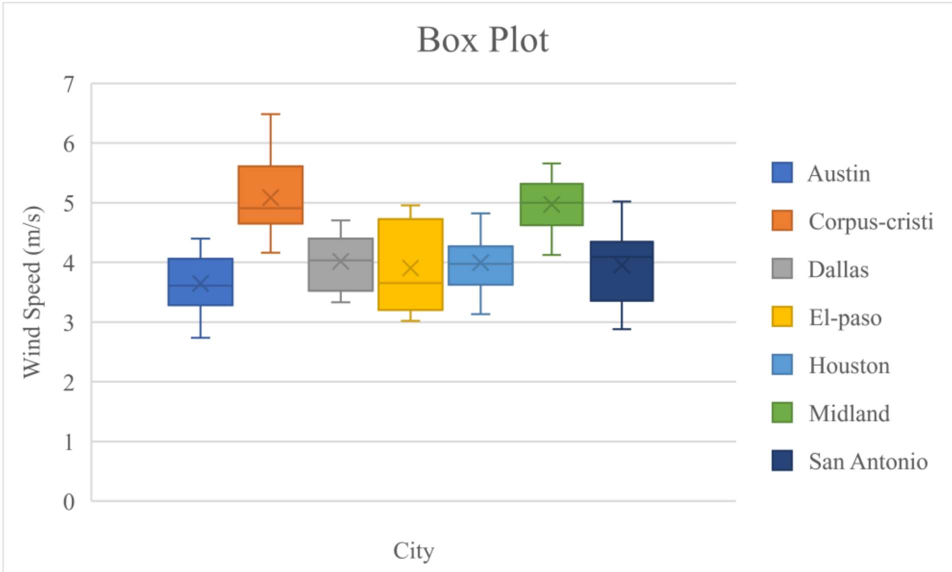

Figure 5.8 Box Plot of Average Wind Speed in 2019

5.3.2 Estimating Capacity Factor of Wind Turbine

Wind Speed data shown at the previous section are collected from web portal of Weather Underground (wunderground.com). The website usually records their data by using the Automated Surface Observing Systems (ASOS) at the local airport (Pham 2019). The ASOS wind sensors are installed 8-10 m above the ground. According to Heier (2005), the wind speed at reference height (measured in meters) can be measured using the following equation:

$$v_h = v_g \left(\frac{h}{h_g}\right)^{\kappa};\ for\ h \geq h_g \tag{5.1}$$

Let v_g (m/s) be the wind speed measured near the ground at height h_g. The parameter k is the Hellman exponent that depends on the coastal location and the shape of the terrain on the ground, and the stability of the air. Table 5.5 provides example values of the Hellmann exponent. This research uses the unstable air above human inhabited areas k= 0.27.

Table 5.5 Hellmann Exponent (Kaltschmitt, M. et al. 2007)

Location	κ
Unstable air above open water surface	0.06
Neutral air above open water surface	0.1
Unstable air above flat open coast	0.11
Neutral air above flat open coast	0.16
Stable air above open water surface	0.27
Unstable air above human inhabited areas	0.27
Neutral air above human inhabited areas	0.34
Stable air above flat open coast	0.4
Stable air above human inhabited areas	0.6

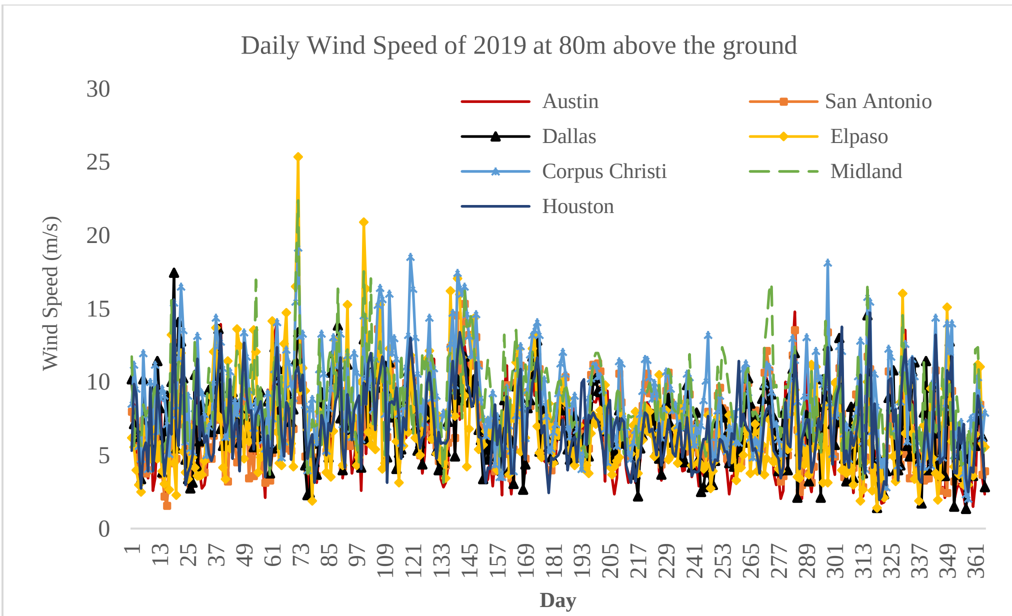

Figure 5.9 Daily Wind Speed of 2019 at 80m Above the Ground

A wind turbine (WT) system possesses four operating phases depending on the wind speed. Let $P_w(v)$ be the instantaneous output of wind turbine at wind speed v. Then the cubic power curve is given as (Thiringer and Linders, 1993).

$$p_w(v) = \begin{cases} 0 & v < v_{c,}\ v > v_s \\ p_m(\frac{v}{v_r})^3 & v_c \le v \le v_r \\ p_m & v_r \le v \le v_s \end{cases} \tag{5.2}$$

where v_c, v_r and v_s stands for the cut-in speed, the rated speed, and the cut-off speed respectively. Note P_m is the rated power capacity in a unit of either MW or KW depending on the size of the wind turbine.

The capacity factor of a WT, denoted as λ, is the ratio of the power generated by the WT when the wind speed is equal to ($v_c \le v \le v_r$) and the rated peak power P_m. It is a fraction between zero and one that can be estimated using below equation.

$$\lambda = \frac{p_m \left(\frac{v}{v_r}\right)^3}{p_m} \tag{5.3}$$

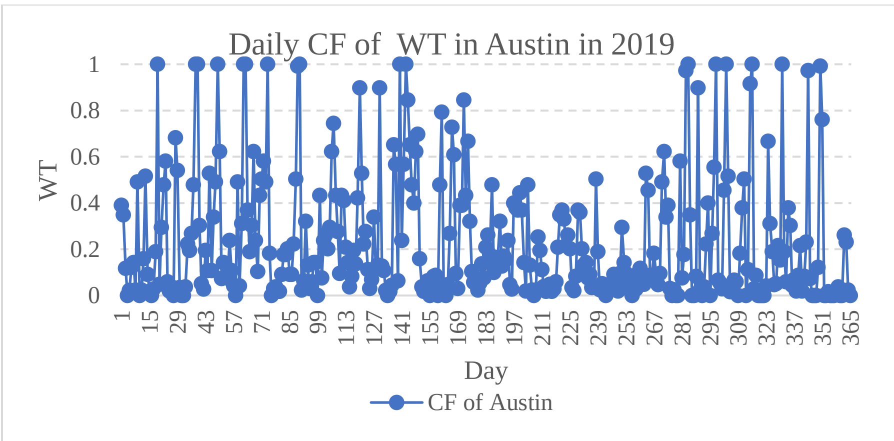

Figure 5.10 Daily Capacity Factor of WT in Austin in 2019

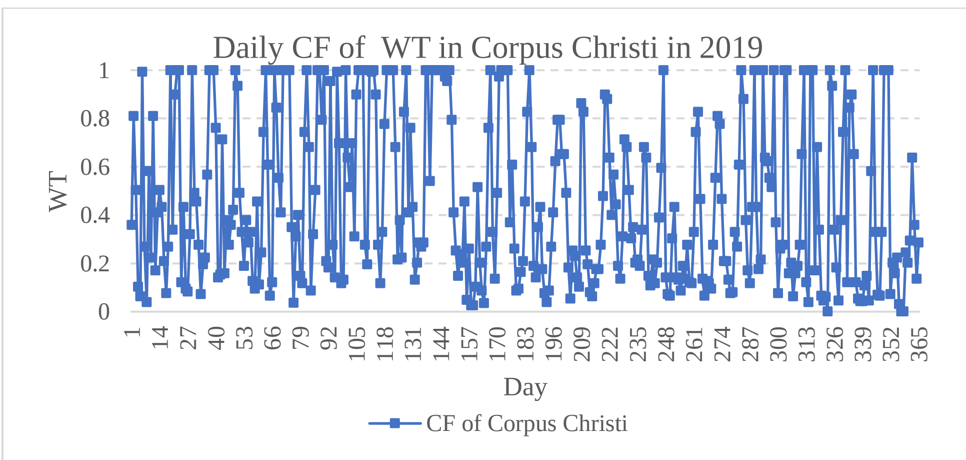

Figure 5.11 Daily CF of WT in Corpus Christi in 2019

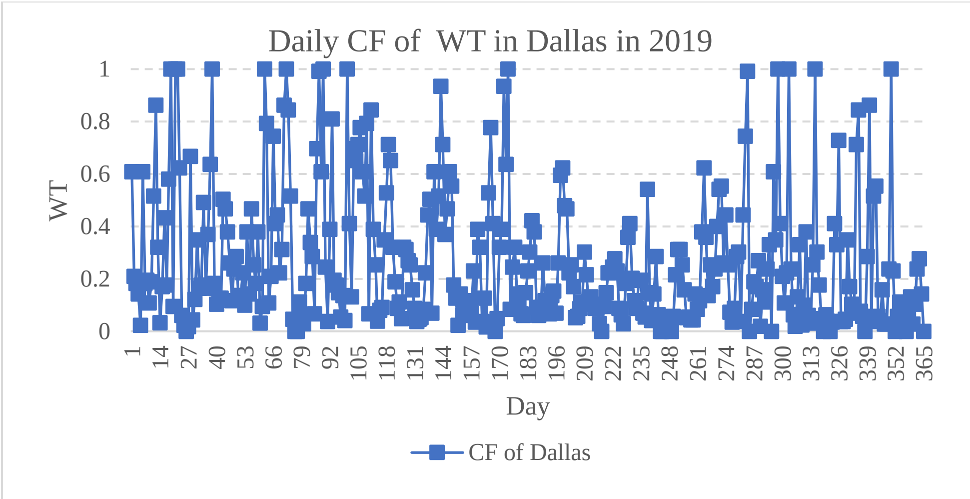

Figure 5.12 Daily CF of WT in Dallas in 2019

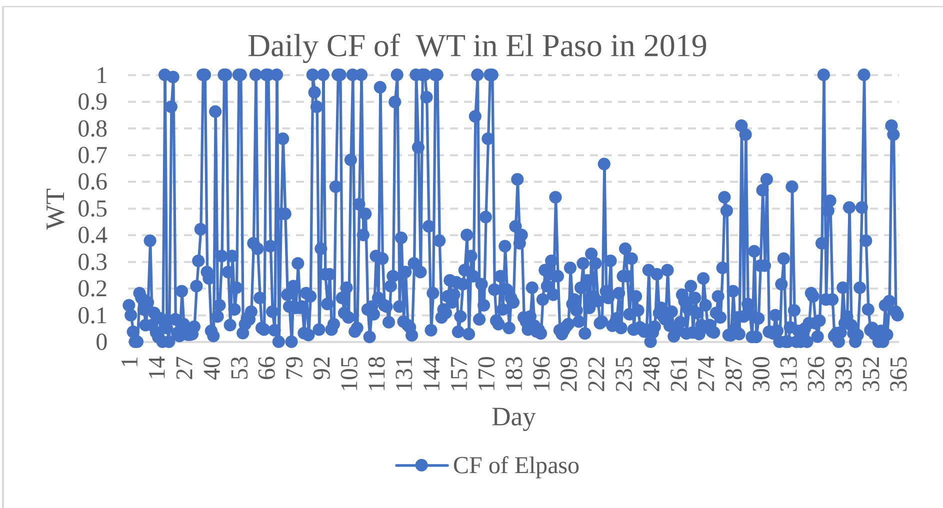

Figure 5.13 Daily CF of WT in El Paso in 2019

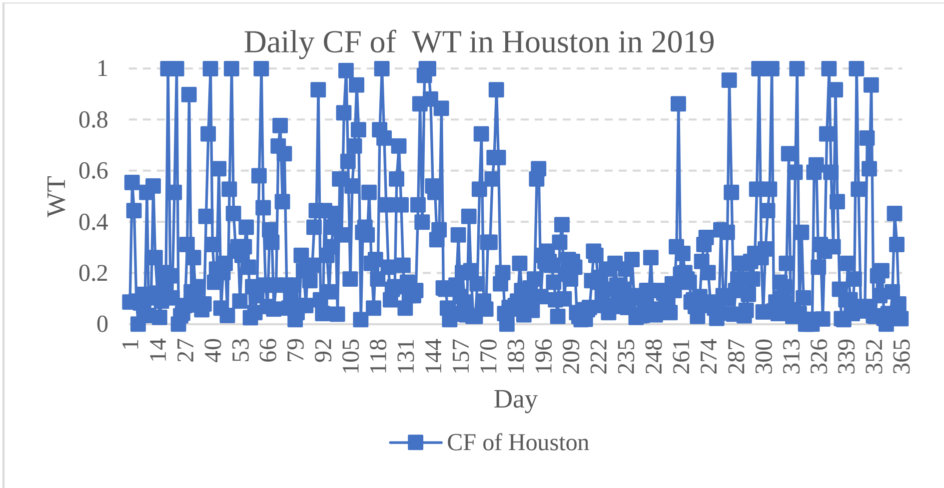

Figure 5.14 Daily CF of WT in Houston in 2019

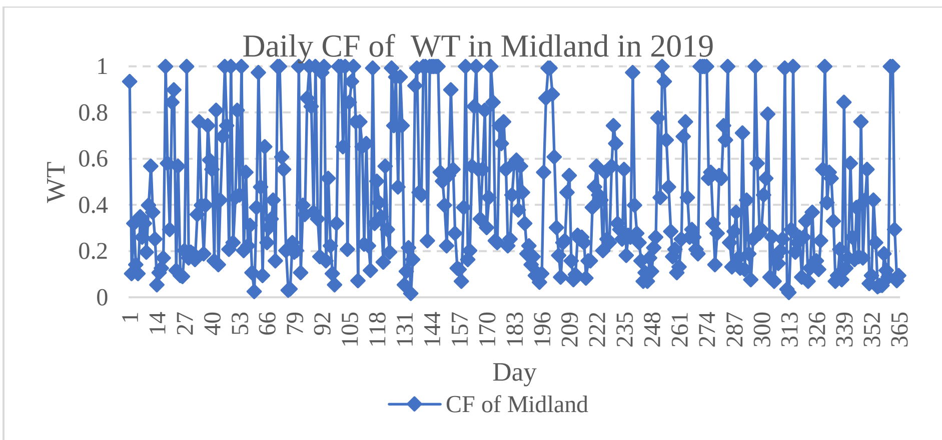

Figure 5.15 Daily CF of WT in Midland in 2019

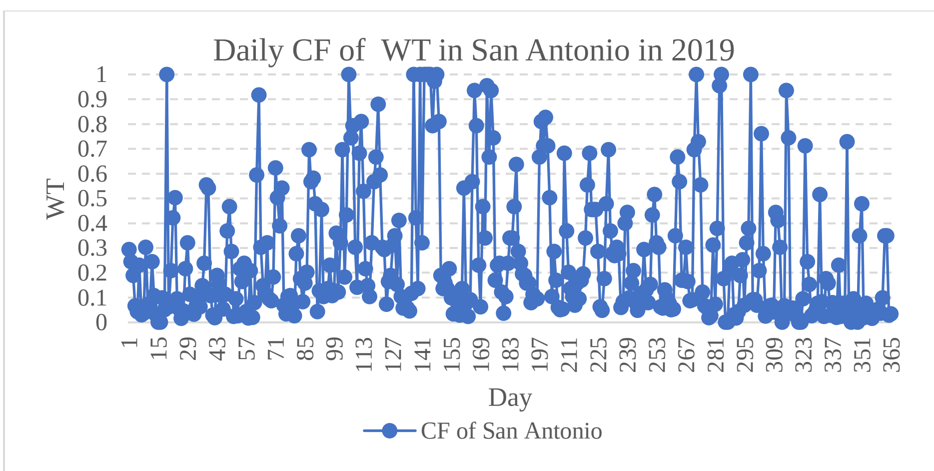

Figure 5.16 Daily CF of WT in San Antonio in 2019

5.3.3 Solar Data of Texas Cities

The below graph shows that in Austin, San Antonio, Dallas, Corpus Christi, Midland and Houston in August has the highest average temperature in 2019. In El Paso the highest average temperature takes place in July and August.

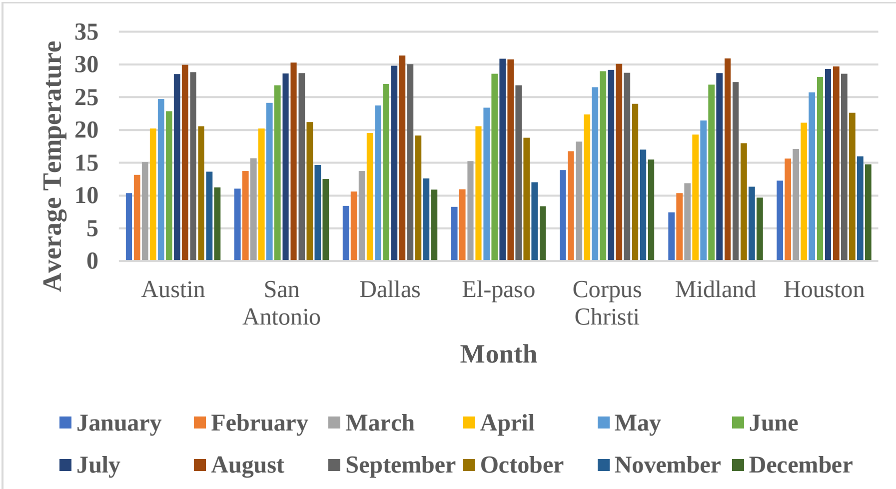

Figure 5.17 Average Monthly Temperature of Seven Cities of Texas

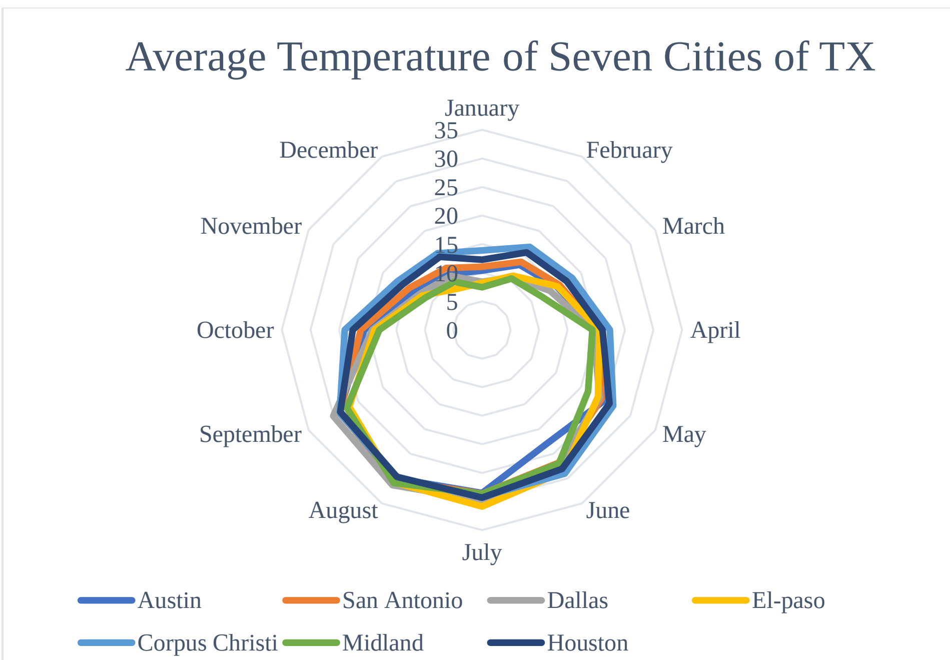

Figure 5.18 Radar Diagram of Average Monthly Temperature of Seven Cities of Texas

Table 5.6 Weather Condition of Texas Cities

Weather Condition	Austin	Corpus Christi	Dallas	El paso	Houston	Midland	San Antonio
Cloudy	124	132	119	50	94	80	134
Foggy	16	22	N/A	6	12	11	5
Mostly Cloudy	73	121	94	84	100	5	88
Mostly Sunny	82	47	118	157	63	260	83
Partly Cloudy	48	35	15	58	75	N/A	29
Scattered Showers	16	7	13	10	8	5	21
Thunderstorm	6	1	5	N/A	11	4	5
Rain	N/A	N/A	N/A	N/A	1	N/A	N/A
Scattered Thunderstorm	N/A	N/A	N/A	N/A	1	N/A	N/A
Rain Snow	N/A	N/A	1	N/A	N/A	N/A	N/A

5.3.4 Estimating Capacity Factor of Solar Photovoltaics (PV)

Originally from Pham et al. 2019, the output power of a PV system depends on multiple factors that are summarized in Table 5.6. Unless specified, the unit of all angles is radian (rad).

Table 5.7 Key Parameters in PV Power Generation.

Factor	Symbol	Explanation
weather coefficient	W_t	between 0 and 1
PV size (m^2)	A	PV surface area
PV efficiency	η	15–20% for commercial PV
calendar date	d	$d \in \{1, 2, \ldots, 365\}$
solar hour (rad)	ω	related to the local hour
PV temperature (^oC)	T_o	operating temperature
latitude (rad)	ϕ	depends on location
PV azimuth angle (rad)	α	if facing the south, $\alpha = 0$
PV tilt angle (rad)	β	between PV and the ground
Solar zenith angle (rad)	φ	between the zenith and Sun's ray
solar incident angle (rad)	θ	Between the norm to PV and Sun's ray
local hours	t	$t = 1, 2, \ldots, 24$

A 3-step procedure was presented to calculate the output power of a PV system based on the study of Cai et al. (2010). These steps are summarized as follows:

Step 1: For PV facing the south, the sunrise and sunset times in day $d \in \{1, 2, \ldots, 365\}$ are given by

$$\cos(-\omega_{rise}) = \cos(\omega_{set}) = -\tan(\phi - \beta)\tan\delta \qquad (5.4)$$

$$\delta = 0.40928\sin(\frac{2\pi(d+284)}{365}) \qquad (5.5)$$

where, ω_{rise} and ω_{set} are, respectively, the sunrise and the sunset angles in day d perceived by the PV panel, and δ is the declination angle. PV has no power output before sunrise and after sunset.

Step 2: Estimating the solar irradiance incident on the PV at time t on date d under clear sky condition,

$$I_t = 1370 * (0.7^{(\cos\phi)^{-0.678}})(1 + 0.034\cos(\frac{2\pi(d-4)}{365}))(\cos\theta + 0.1(1 - \frac{\beta}{\pi}) \qquad (5.6)$$

Where

$$\cos\phi = \cos\delta\cos\phi\cos\omega + \sin\delta\sin\phi \qquad (5.7)$$

$$\begin{aligned}\cos\theta = {} & \sin\delta\sin\phi\cos\beta - \sin\delta\cos\phi\sin\beta\cos\alpha + \cos\delta\cos\phi\cos\beta\cos\omega \\ & + \cos\delta\sin\phi\sin\beta\cos\omega\cos\alpha + \cos\delta\sin\beta\sin\omega\sin\alpha\end{aligned} \qquad (5.8)$$

In the above equation, the solar irradiance (W/m^2) is received by the panel at time t of day d. The solar zenith angle φ is estimated by equation (5.7). The solar hour angle ω is determined by the local time t. Starting from ω = -π/2 at 6am, It increases 15° every hour until reaching ω = π/2 at 6pm. In the northern hemisphere, to maximize the energy yield, the PV panel faces the South and its tilt angle shall equal the local latitude, namely if α = 0 and $\beta = \phi$, then equation (5.8) can be simplified as

$$\cos\theta = \cos\delta\cos\omega \qquad (5.9)$$

Step 3: The actual output of a PV system considering the weather uncertainty now can be estimated as:

$$p_t = W_t \eta A I_t \left[1 - 0.005(T_0 - 25)\right] \quad (5.10)$$

where P_t is the actual output power (in Watt) of the PV system and W_t is a weather coefficient that varies between 0 to 1 to mimic the nine states of the weather condition (Lave and Kleissl, 2011). The values of W_t are summarized in Table 5.8. The capacity factor of a PV system can be estimated by

$$\lambda_{PV} = \frac{1}{P_{PV}^{\max} * T} \sum_{t=1}^{T} P_t \quad (5.11)$$

where P_{PV}^{max} is the rated capacity of a PV system, and T is the number of generation hours. For PV in the southern hemisphere, simply set $\alpha = \pi$ and change ϕ into a native angle.

Table 5.8 Weather Coefficients under Different States

Weather State	Abbreviation	W_t
Mostly Sunny	MS	1
Partly Cloudy	PC	0.7
Cloudy	C	0.5
Mostly Cloudy	MC	0.3
Scattered Showers	SS	0.2
Scattered Thunderstorm	ST	0.2
Foggy	F	0.1
Thunderstorm	T	0.1
Rain	R	0.1
Rain Snow	RS	0.05

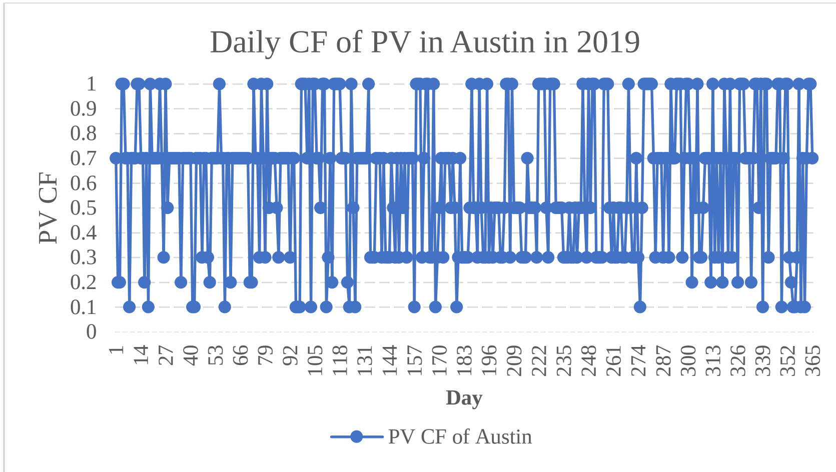

Figure 5.19 Daily CF of PV in Austin in 2019

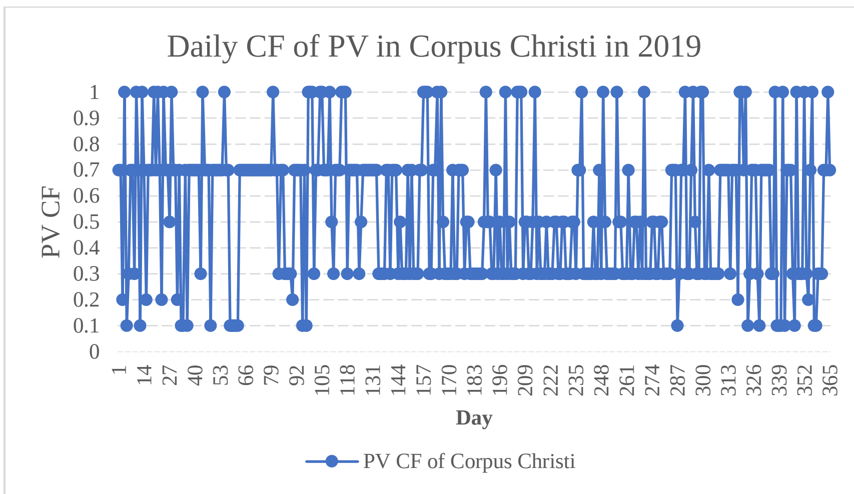

Figure 5.20 Daily CF of PV in Corpus Christi in 2019

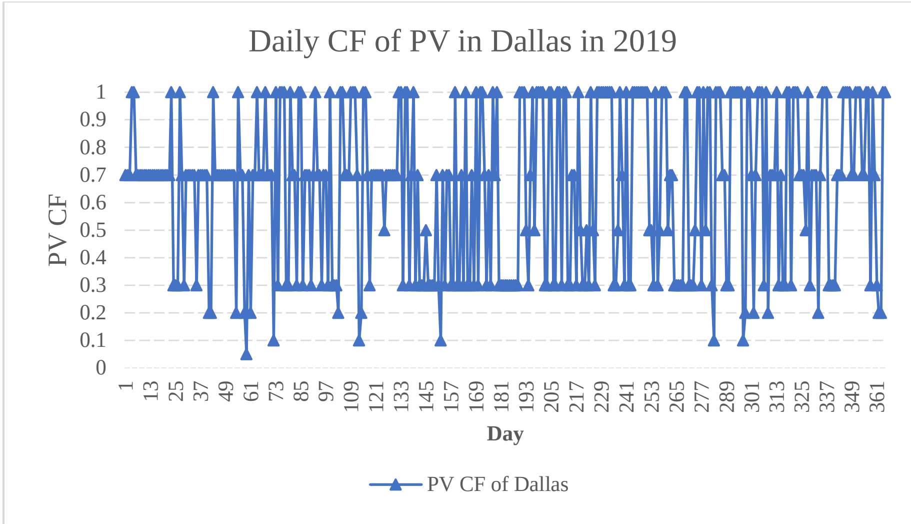

Figure 5.21 Daily CF of PV in Dallas in 2019

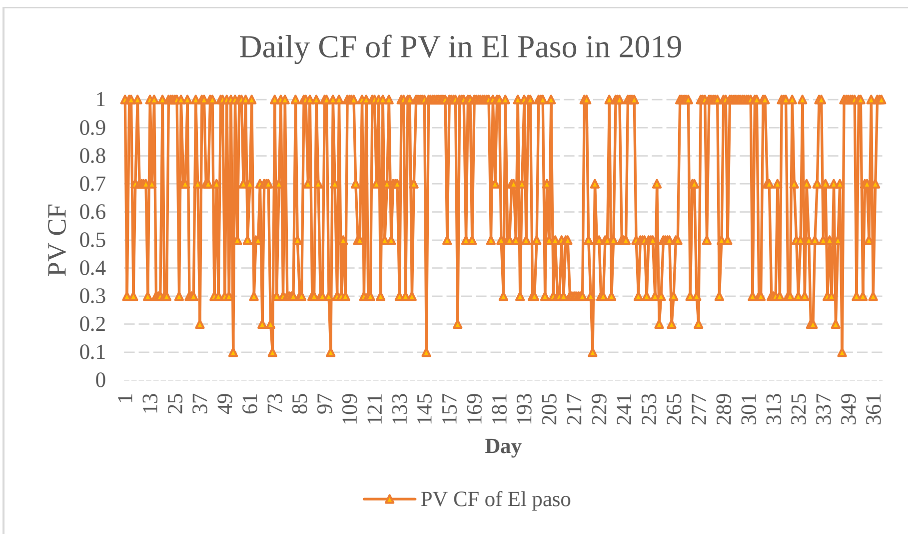

Figure 5.22 Daily CF of PV in El Paso in 2019

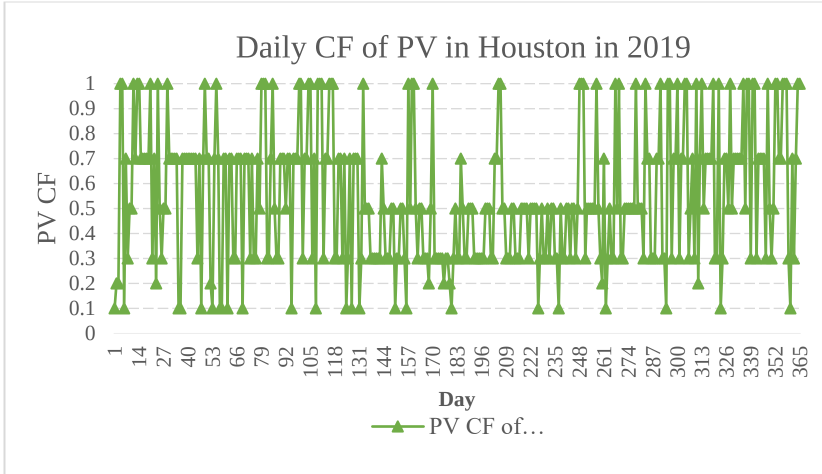

Figure 5.23 Daily CF of PV in Houston in 2019

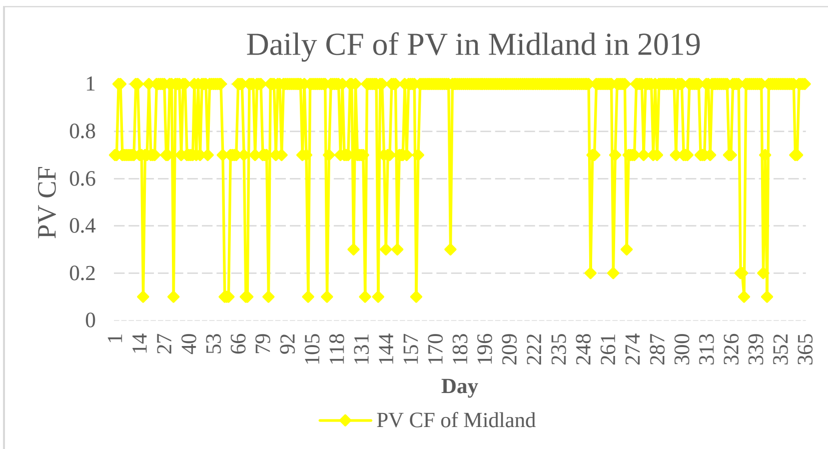

Figure 5.24 Daily CF of PV in Midland in 2019

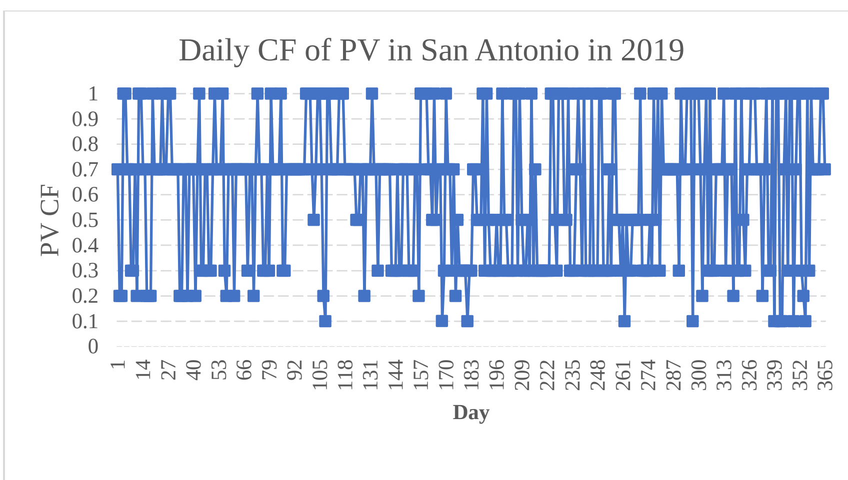

Figure 5.25 Daily CF of PV in San Antonio in 2019

5.4 Sizing Renewable Microgrid for VPP Operations

5.4.1 Model Formulation

This section aims to allocate the renewable portfolio and microgrid capacity in supercharging stations with following objectives:

1) Realizing two-way energy flow between microgrid and main grid.
2) Engaging transactive energy trading in prosumer energy market.
3) Minimizing annual operating cost of the supercharging infrastructure.
4) Attaining net-zero energy operation

The parameters and decision variables associated with the model is listed in Tables 5.9 and 5.10, respectively.

Table 5.9 Parameters for Model 5.1

Notation	Explanation
T	number of period in a year, and t=1, 2, …, T
J	number of supercharging stations for j=1, 2, …, J
G	number of renewable power generation type, for g=1, 2, …, G
a_g	capacity cost of generation g ($/MW)
b_g	operating and maintenance cost of generation g ($/MWh)
c_g	carbon credits or subsidies of generation g ($/MWh)
a_{ESS}	capacity cost of ESS unit ($/MWh)
b_{ESS}	operating and maintenance cost of ESS ($/MWh)
ϕ_g	capital recovery factor of generation g
ϕ_{ESS}	capital recovery factor of ESS unit
λ_{gjt}	capacity factor of generation g in station j at time t
$\lambda_{EV,jt}$	EV arrival rate of station j at time t
τ	time step size or duration of a period (unit: hour)
$P_{sc,j}$	power demand of a supercharger (MW)
$P_j^{station}$	maximum load of station j (MW)
ρ_{jt}^{buy}	electricity buying price ($/MWh)
ρ_{jt}^{sell}	electricity selling price ($/MWh)
B_{j0}	initial energy stored in ESS of station j

Table 5.10 Decision Variables for Model 5.1

Notation	Explanation
$P_{gj}{}^{c}$	installed capacity of generation *g* in station *j* (unit: MW)
$B_j{}^{c}{}_{ESS}$	installed capacity of ESS in station *j* (unit: MWh)
B_{jt}	energy stored in ESS unit in station *j* at time *t* (unit: MWh)
$E_{jt}{}^{buy}$	electricity purchased by station *j* from main grid at time *t* (unit: MWh)
$E_{jt}{}^{sell}$	electricity sold by station *j* to main grid at time *t* (unit: MWh)

The objective function consists of cost of investing station facility, superchargers, and microgrid system across the entire supercharging network. The microgrid consist of WT, PV, and ESS units. The following optimization model, denoted as Model 5.1, is formulated to minimize the annualized cost of the supercharging network.

The objective function:

Model 5.1

Minimize

$$f(P_{gj}^{c}, B_j^{c}, B_{jt}, E_{jt}^{buy}, E_{jt}^{sell}) = \sum_{j=1}^{J}\sum_{g=1}^{G}\phi_g a_g P_{gj}^{c} + \sum_{j=1}^{J}\sum_{t=1}^{T}\sum_{g=1}^{G} \tau(b_g - c_g)\lambda_{gjt}P_{gj}^{c} + \phi_{ESS}a_{ESS}\sum_{j=1}^{J}B_j^{c}$$
$$+\sum_{j=1}^{J}\sum_{t=1}^{T}b_{ESS}B_{jt} + \sum_{j=1}^{J}\sum_{t=1}^{T}(\rho_{jt}^{buy}E_{jt}^{buy} - \rho_{jt}^{sell}E_{jt}^{sell}) \tag{5.12}$$

The objective function is to minimize the annualized cost of the entire supercharging network comprised of *J* stations. The first and second terms represent the capacity cost, operating and maintenance cost and carbon credits of installing WT and PV in station *j*. The third and fourth terms are the capacity cost and operating and maintenance cost of ESS unit in station *j*. The last term is the purchase cost or revenue income in transactive energy trading.

Constraints of Model 5.1:

a) Energy balance equation in station j at time t

$$\tau\lambda_{EV,jt}P_{SC,j} + E_{jt}^{sell} + (B_{jt} - B_{j,t-1}) = \sum_{g=1}^{G}\tau\lambda_{gjt}P_{gj}^{c} + E_{jt}^{buy};$$

for t=1, 2, ..., T, and for j=1, 2, …, J. (5.13)

This constraint states that the amount of energy consumed including ESS storage at time t equals the sum of microgrid generation and the energy purchased from the main grid. If the planning is made hourly, then τ=1 hour, and T=8760 hours for one year.

b) Battery State at time t

$0 \le B_{jt} \le B_{j}^{c}$, for t=1, 2, ..., T, and for j=1, 2, …, J. (5.14)

The constraint simply states that the energy stored in the ESS should not be exceed its capacity.

c) Initial ESS energy is full

$B_{j0} = B_{j}^{c}$, for j=1, 2, …, J. (5.15)

This constraint states that the ESS unit is full at the initial time.

d) End time ESS energy state is also full

$B_{jT} = B_{j}^{c}$, for j=1, 2, …, J. (5.16)

This constraint states that the ESS unit is full at the last period of time.

e) The limitation of the selling energy

$0 \le E_{jt}^{sell} \le \tau P_{j}^{station}$, for t=1, 2, ..., T, and j=1, 2, …, J (5.17)

Where $P_j^{station}$ is the maximum power or load when all the superchargers in station j is in use. This constraint states that the maximum amount of energy sold to the main grid should not exceed the maximum supercharging station power. This constraint is in place to ensure that the traded energy to the main grid from station j is capped to ensure the grid stability.

f) Non-Negativity of Decision Variables

$$P_{gj}^{c}, B_{j}^{c}, B_{jt}, E_{jt}^{buy}, E_{jt}^{sell} \geq 0 \text{ , for } t=1, 2, ..., T, \text{ and } j=1, 2, \ldots, J, \text{ and } g=1, 2, ..., G. \quad (5.18)$$

These constraints simply defines the non-negativity condition of decison variables.

5.4.2 Values of Model Parameters

Parameters are the values (or data) which are known in the optimization model. These parameter values have chosen considering different facts with the best effort to use real life data. The capital recovery factor and supercharging rate are calculated based on actual data. The model parameters are summarized in Tables 5.11 and 5.12 respectively.

Table 5.11 Parameters for Model 5.1

Notation	Explanation	Value	Unit
T	number of period in a year, and t=1, 2, …, T	8760	hours
J	Number of supercharging stations for j=1, 2, …, J	Austin-5 San Antonio-6 El Paso-2 Dallas-17 Midland-4 Corpus Christi-4 Houston-8	N/A
G	Number of renewable power generation type, for g=1, 2, …, G	WT CF, PV CF (g=1, WT; g=2, PV)	N/A
a_g	capacity cost of generation g	1.5 (g=1 for WT), 2 (g=2 for PV)	\$M/MW
b_g	Operating and maintenance cost of generation g	8 (WT operating cost), 4 (PV operating cost)	\$/MWh
c_g	Carbon credits or subsidies of generation g	0 (WT carbon credit), 10 (PV carbon credit)	\$/MWh
a_{ESS}	capacity cost of ESS unit	0.4 (ES capacity cost)	\$M/MWh
b_{ESS}	Operating and maintenance cost of ESS	2 (ES operating cost)	\$/MWh
ϕ_g	capital recovery factor of generation g	ϕ_1 = 0.0944 (7% compound interest, 20 years), ϕ_2 = 0.0944 (7% compound interest, 20 years)	N/A
ϕ_{ESS}	capital recovery factor of ESS unit	0.1424 (7% compound interest, 10 years)	N/A
λ_{gjt}	capacity factor of generation g in station j at time t	See appendix	N/A
$\lambda_{EV,jt}$	EV arrival rate of station j at time t	5	cars/hour
τ	Time step size or duration of a period	1	hour
$P_{sc,j}$	Power demand of superchargers in station j	The total number of Superchargers in a particular station is multiplied by the power demand of a supercharger.	MW
$P_j^{station}$	Maximum load of station j when all superchargers are in use		MW
ρ_{jt}^{buy}	Electricity buying price	70 (electricity price of importing from main grid)	\$/MWh
ρ_{jt}^{sell}	Electricity selling price	35 (electricity sale price of exporting to main grid)	\$/MWh
B_{j0}	Initial energy in ESS of station j	full	

Table 5.12 Parameter Values of $P_{sc,j}$ and $P_j^{station}$

Station No	$P_{sc,j}$	$P_j^{station}$	Zone
1	1.8	2.16	
2	1.2	1.44	
3	1.296	1.5552	Austin
4	1.2	1.44	
5	1.2	1.44	
6	0.9	1.08	
7	1.2	1.44	Corpus Christi
8	1.2	1.44	
9	0.144	0.1728	
10	1.2	1.44	
11	1.152	1.3824	
12	1.5	1.8	
13	1.5	1.8	
14	1.65	1.98	
15	1.8	2.16	
16	0.9	1.08	
17	1.8	2.16	Dallas
18	1.2	1.44	
19	1.2	1.44	
20	0.9	1.08	
21	1.5	1.8	
22	1.5	1.8	
23	1.5	1.8	
24	1.2	1.44	
25	1.2	1.44	
26	1.2	1.44	
27	1.2	1.44	El Paso
28	1.2	1.44	
29	1.8	2.16	Houston
30	1.2	1.44	
31	0.9	1.08	
32	0.9	1.08	
33	1.2	1.44	
34	1.2	1.44	
35	1.2	1.44	
36	0.9	1.08	
37	1.2	1.44	
38	1.2	1.44	Midland
39	1.2	1.44	
40	1.2	1.44	
41	1.2	1.44	
42	0.9	1.08	
43	1.5	1.8	San Antonio
44	1.5	1.8	
45	1.2	1.44	
46	1.2	1.44	

5.4.3 Implementing in the Supercharging Network of Texas

Texas is divided into seven zones based on three considerations. The first consideration is weather conditions. The second consideration is where most of Tesla's supercharging stations are currently located in Texas. The third consideration is the largest cities of Texas. Based on these three considerations, the seven zones are Austin, San Antonio, Dallas, Houston, El Paso, Corpus Christi and Midland. According to Tesla website (Year 2020), Texas has 46 supercharging stations actively giving its service to the EV owners. Based on the distance to the next big city of any particular station, the zone of that particular supercharging station is assigned. For example, Tesla supercharging station at San Marcos, TX should be assigned to Zone Austin because the distance from San Marcos to the next big city, San Antonio is larger than to Austin. The 46 supercharging stations have classified in seven zones of Texas (See Table 5.4). According to Table 5.4, Austin has 5, Dallas has 17, Corpus Christi has 4, El Paso has 2, Midland has 4, San Antonio has 6 and Houston has 8 supercharging stations. All the supercharging stations in each zone follows the same weather condition so their WT and PV capacity factor are same (See Table 5.4). Model 5.1 is solved in two different ways. Firstly, the model has solved for each specific zones separately. Secondly, the model has solved at an aggregate network level consisting of all the zones together.

a) Solving the model for each specific zones separately:

Model 5.1 is solved in AMPL computational environment with the given parameters in Table 5.11 and 5.12. The model is implemented in seven different zones based on the hourly capacity factors of WT and PV of each Texas city. The optimal sizing of WT, PV and ESS units along with the associated annual cost are summarized in Table 5.13.

Table 5.13 Results of Objective Function and Decision Variables in Each Zone

Station Number	WT(MW)	PV(MW)	Annual Cost ($)	ESS Capacity (MWh)	Prosumer	Zone
1	0	0	20,529,936	0	Import	Austin
2	0	0				
3	0	0				
4	0	0				
5	0	0				
6	5.58	0	8,552,291	0	Import & Export	Corpus Christi
7	7.44	0				
8	7.44	0				
9	0.89	0				
10	6	0	69,402,772.28	0	Import	Dallas
11	5.76	0				
12	7.5	0				
13	7.5	0				
14	8.25	0				
15	9	0				
16	4.5	0				
17	9	0				
18	6	0				
19	6	0				
20	4.5	0				
21	7.5	0				
22	7.5	0				
23	7.5	0				
24	6	0				
25	6	0				
26	6	0				
27	0	0	7,358,400	0	Import	El Paso
28	0	0				
29	9	0	28,284,034	0	Import	Houston
30	6	0				
31	4.5	0				
32	4.5	0				
33	6	0				
34	6	0				
35	6	0				
36	4.5	0				
37	7.44	0	12,274,121.04	0	Import & Export	Midland
38	7.44	0				
39	7.44	0				
40	7.44	0				
41	6	0	22,879,621.80	0	Import	San Antonio
42	4.5	0				
43	7.5	0				
44	7.5	0				
45	6	0				
46	6	0				

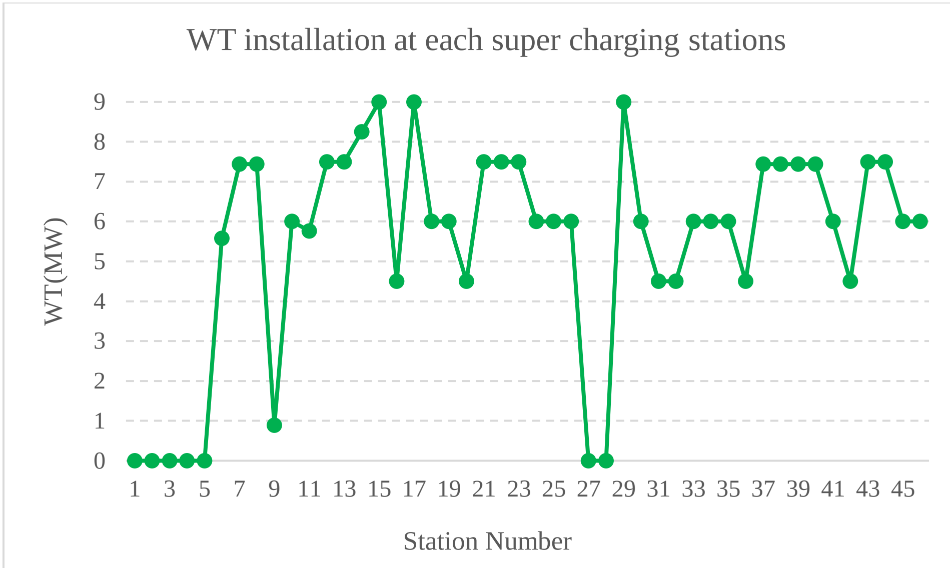

Figure 5.26 WT Installation at Each Supercharging Station

From Table 5.13, the four supercharging stations in Midland zone and the four super charging stations in Corpus Christi zone are installing WT as onsite generating units. Midland and Corpus Christi both are windy cities and the other cities near these cities also show similar weather condition, so it is obvious that in both cities the stations install WT instead of PV. The extra energy produced by the WT, sold to the main grid. When the generation of WT is not enough to fulfill the demand, the model chooses to buy electricity from the main grid. Because of this reason the model is fulfilling the prosumer function via importing and exporting energy between the station and the main grid. The model for Midland and Corpus Christi is not choosing ESS system to store the energy because it is more profitable to sell the energy to the main grid than storing it in ESS system.

From Table 5.13, the six supercharging stations in San Antonio zone, seventeen supercharging stations in Dallas zone and eight supercharging stations in Houston zone are installing WT as their power generating units. San Antonio, Dallas and Houston all the three cities are windy cities and the other cities near these cities also show similar weather condition, so it is obvious that the stations in or near these cities install WT instead of PV as onsite generating units. From Table 5.13, the model for San Antonio, Dallas and Houston are producing less electricity to fulfill the demand of supercharging stations in these three zones. Hence these supercharging stations are buying electricity from the main grid to fulfill their needs. All the supercharging stations from these three zones are not installing ESS system to store the energy or to sell the energy to the main grid because the power generating units are not producing surplus energy.

From Table 5.13, the five supercharging stations in Austin zone and the two supercharging stations in El Paso zone are not installing any WT and PV as onsite generation. Instead of installing WT and PV to fulfill the demand of their supercharging stations, Austin and El Paso supercharging stations are buying electricity from the main grid. The reason behind this activity is, it is more cost effective to buy the electricity from the main grid than to install power generating units to produce electricity.

b) A network planning model consisting of all the zones:

Now Model 5.1 is solved for sizing renewable microgrid for all the supercharging stations as an integrated network. The model is solved in AMPL computational environment with the given parameters in Tables 5.11 and 5.12. In this network model CF data of WT and PV are assigned to the supercharging stations based on their actual location (See Table 5.4). The optimal sizing of WT, PV and ESS units along with the associated annual cost and the results are summarized in Table 5.14.

Table 5.14 Results of Objective Function and Decision Variables in Network Model

Annual Cost ($)	**169,281,175.70**				
Station No.	**WT (MW)**	**PV (MW)**	**ESS Capacity (MWh)**	**Prosumer**	**Zone**
1	0	0	0	Import	Austin
2	0	0	0	Import	Austin
3	0	0	0	Import	Austin
4	0	0	0	Import	Austin
5	0	0	0	Import	Austin
6	5.58	0	0	Import & Export	Corpus Christi
7	7.44	0	0	Import & Export	Corpus Christi
8	7.44	0	0	Import & Export	Corpus Christi
9	0.89	0	0	Import & Export	Corpus Christi
10	6	0	0	Import	Dallas
11	5.76	0	0	Import	Dallas
12	7.5	0	0	Import	Dallas
13	7.5	0	0	Import	Dallas
14	8.25	0	0	Import	Dallas
15	9	0	0	Import	Dallas
16	4.5	0	0	Import	Dallas
17	9	0	0	Import	Dallas
18	6	0	0	Import	Dallas
19	6	0	0	Import	Dallas
20	4.5	0	0	Import	Dallas
21	7.5	0	0	Import	Dallas
22	7.5	0	0	Import	Dallas
23	7.5	0	0	Import	Dallas
24	6	0	0	Import	Dallas
25	6	0	0	Import	Dallas
26	6	0	0	Import	Dallas
27	0	0	0	Import	El paso
28	0	0	0	Import	El paso
29	9	0	0	Import	Houston
30	6	0	0	Import	Houston
31	4.5	0	0	Import	Houston
32	4.5	0	0	Import	Houston
33	6	0	0	Import	Houston
34	6	0	0	Import	Houston
35	6	0	0	Import	Houston
36	4.5	0	0	Import	Houston
37	7.44	0	0	Import &	Midland

				Export	
38	7.44	0	0	Import & Export	Midland
39	7.44	0	0	Import & Export	Midland
40	7.44	0	0	Import & Export	Midland
41	6	0	0	Import	San Antonio
42	4.5	0	0	Import	San Antonio
43	7.5	0	0	Import	San Antonio
44	7.5	0	0	Import	San Antonio
45	6	0	0	Import	San Antonio
46	6	0	0	Import	San Antonio

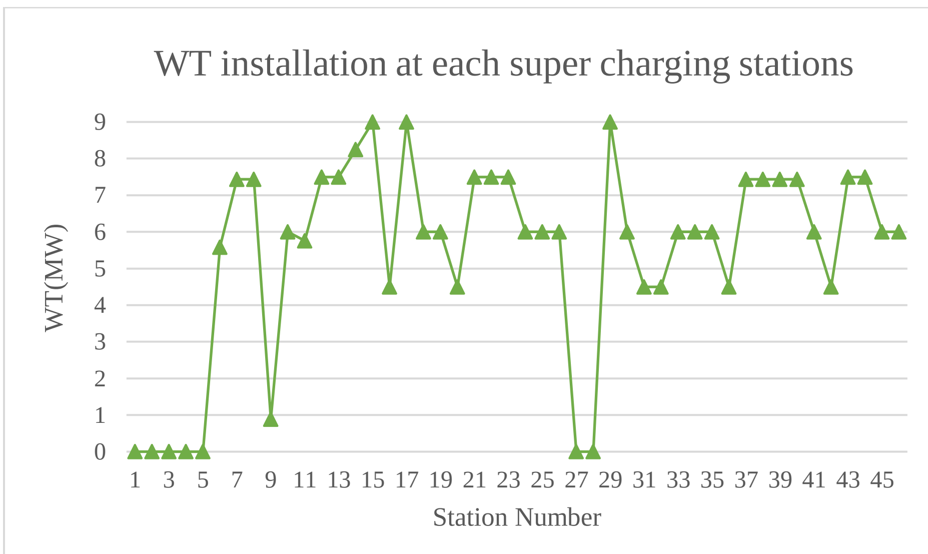

Figure 5.27 WT Installation at Each Supercharging Station

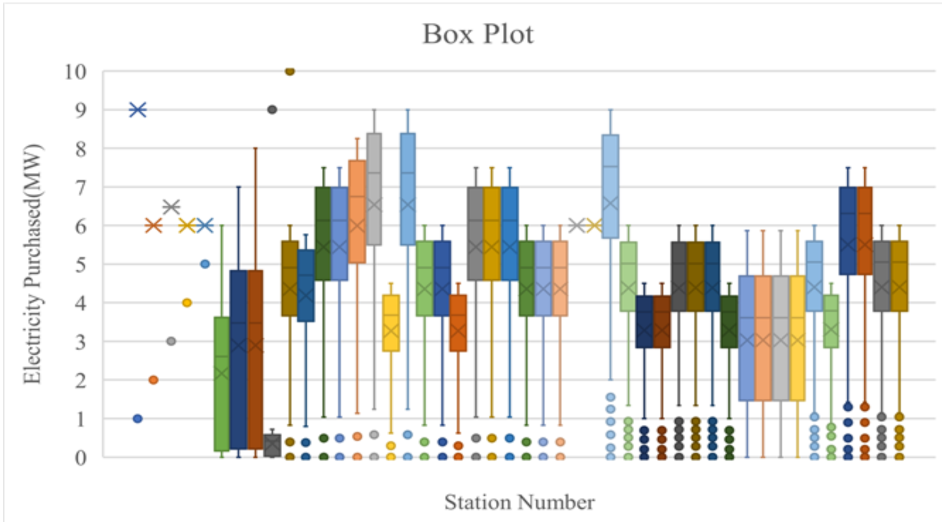

Figure 5.28 Amount of Electricity Purchased (MW)

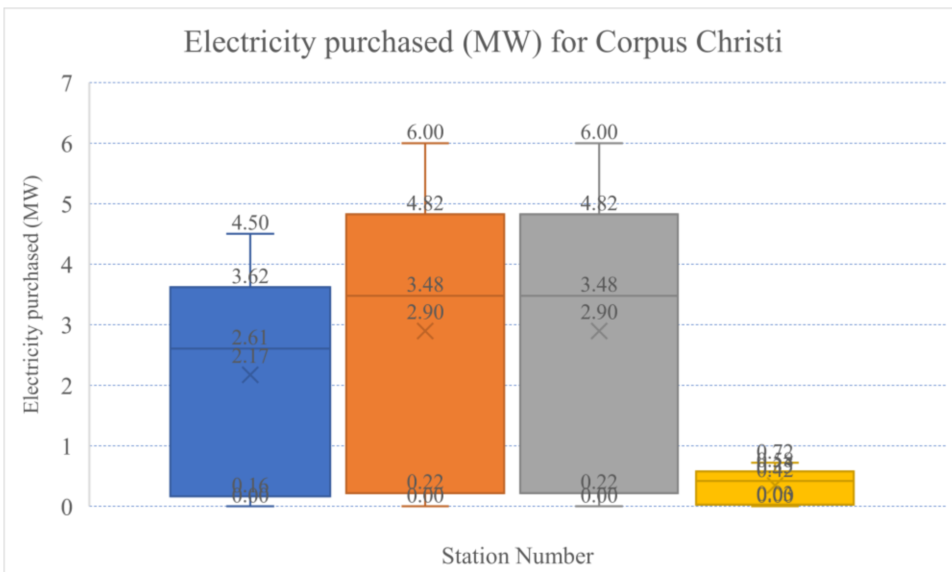

Figure 5.29 Electricity Purchased (MW) for Corpus Christi

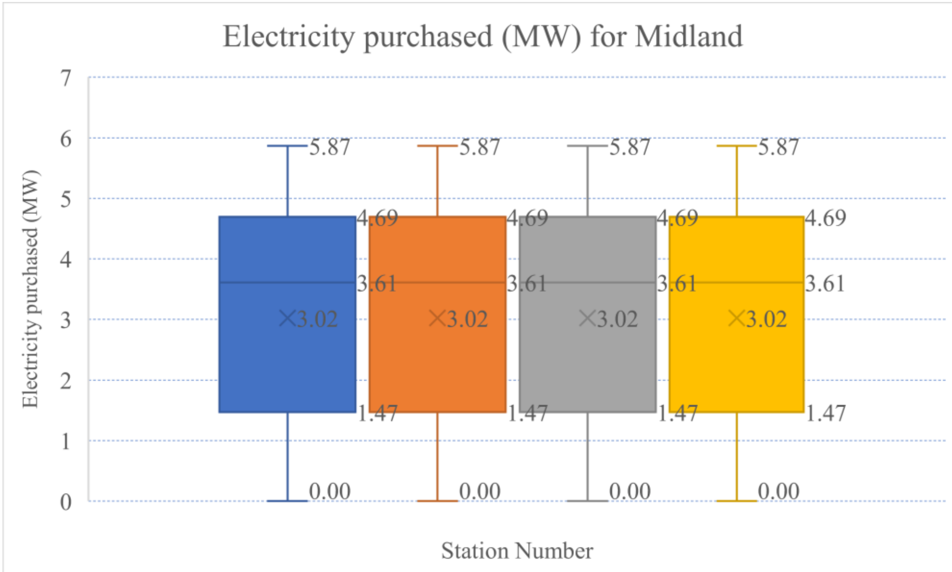

Figure 5.30 Electricity Purchased (MW) for Midland

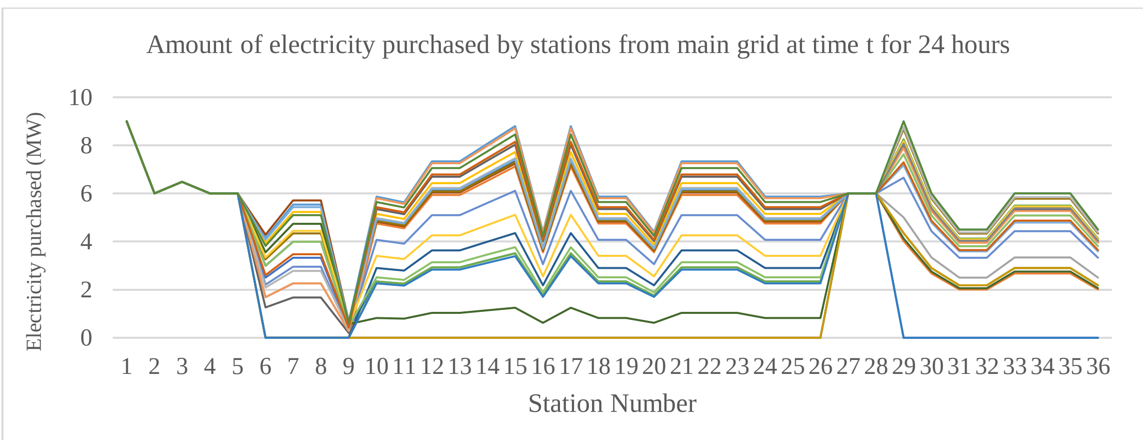

Figure 5.31 Amount of Electricity Purchased by Stations for 24 hours (MW)

Figure 5.32 Amount of Electricity Sold to Main Grid (MW)

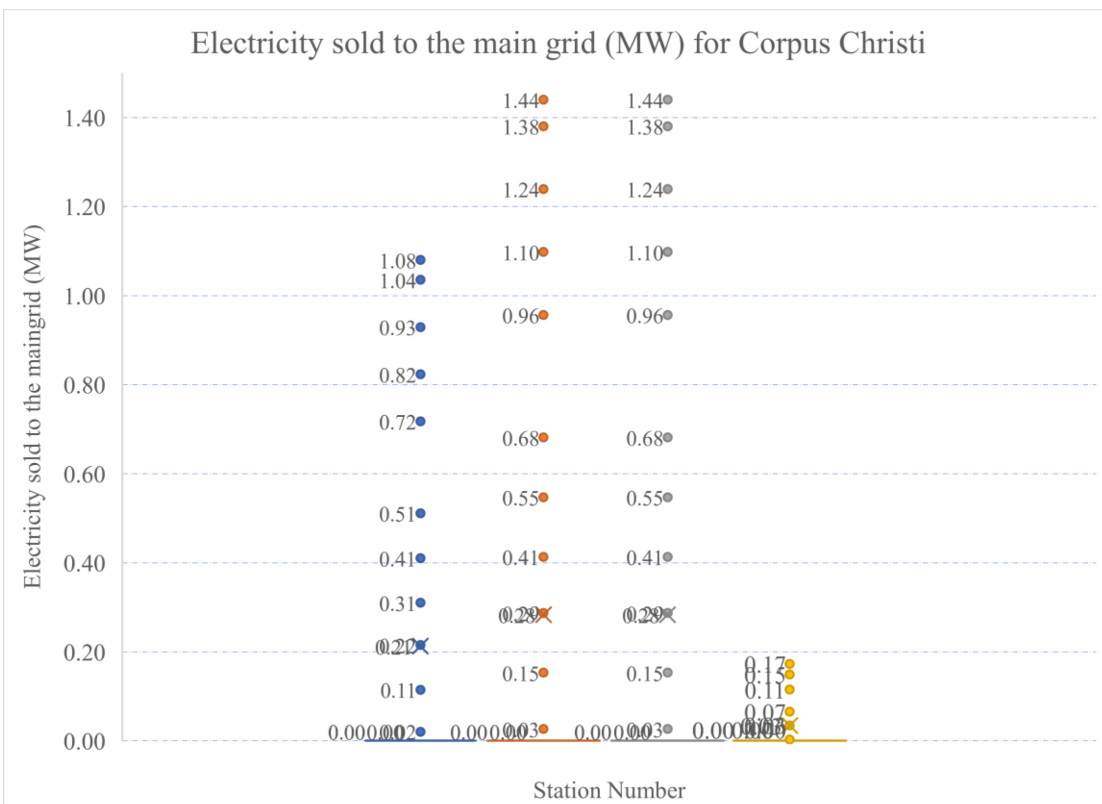

Figure 5.33 Amount of Electricity Sold to Main Grid for Corpus Christi

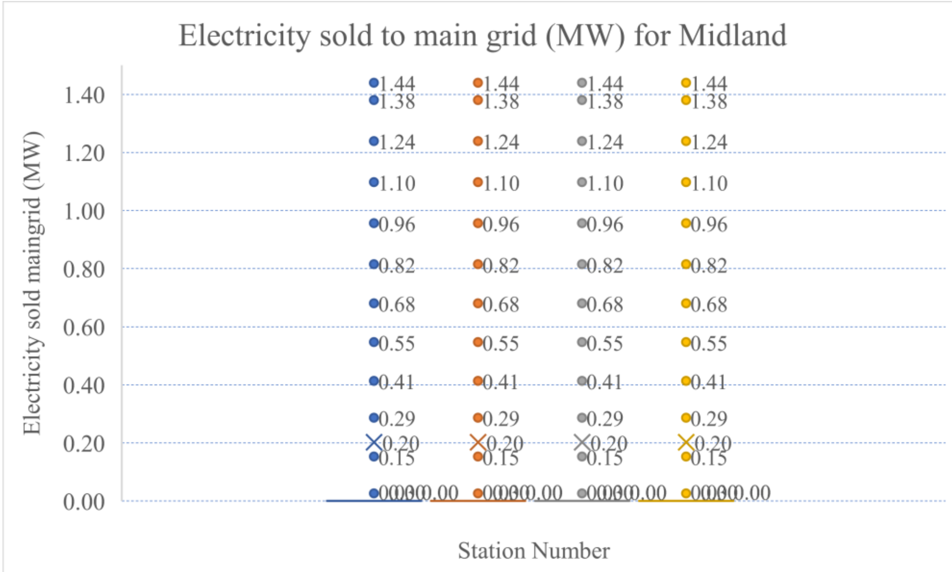

Figure 5.34 Amount of Electricity Sold to Main Grid (MW) for Midland

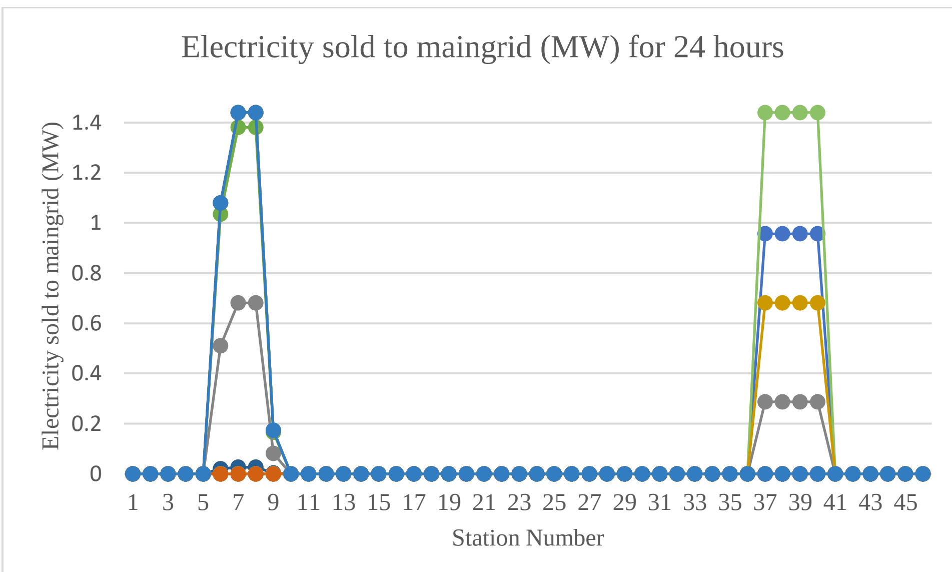

Figure 5.35 Amount of Electricity Sold to Main Grid (MW) for 24 hours

From Table 5.14, all the supercharging stations in Midland, Corpus Christi, San Antonio, Dallas and Houston zone are installing WT as their power generating units instead of PV because all these cities are windy. Another reason for choosing WT over PV is that PV only generates power in daytime hours, but WT can generate power for 24 hours.

From Table 5.14, the supercharging stations in Midland and Corpus Christi zones are producing extra energy after fulfilling their demand. All these supercharging stations are selling their extra energy to the main grid instead of storing the extra energy to the ESS system due to profitability. It is also found from Table 5.14 that all the supercharging stations at Midland and Corpus Christi zone are also buying electricity from the main grid in certain time periods when their onsite generation is lower than the demand.

From Table 5.14, supercharging stations in the zones of San Antonio, Dallas and Houston are installing WT as their power generating units. All the three cities are windy cities, so it is obvious that supercharging stations choose to install WT instead of PV. From Table 5.14, the network model is producing less electricity for San Antonio, Dallas and Houston zones to fulfill the demand of supercharging stations at these three zones, hence the supercharging stations are buying electricity from the main grid to fulfill their demand. All the supercharging stations from these three zones are not installing ESS system to store or sell the energy to the main grid because the power generating units are not producing extra energy.

From Table 5.14, supercharging stations in Austin and El Paso zones are not installing any WT and PV as their power generating units. Instead of installing WT and PV to fulfill the demand of their supercharging stations, the stations in both zones are buying electricity from the main grid. The reason behind this activity is, it is more cost effective to buy the electricity from the main grid than to install power generating units to self-produce electricity.

5.4.4 Sensitivity Analysis

The network problem of Model 5.1 is solved in AMPL computational environment with changing value of capacity cost of renewable microgrid generation PV from \$2M/MW to \$1.5M/MW, \$1M/MW and \$0.5M/MW. Other parameters and the hourly capacity factor of WT and PV of Texas in these cities stay the same. The sensitivity analysis parameters are chosen based on considering different facts and aspects. With the advancement of technology, the capacity cost of PV likely will continue to decline in near future. These scenarios have considered while choosing the sensitivity analysis value for Case 1, 2, and 3. The optimal sizing of WT installation for three cases including the benchmark case are summarized in Table 5.15.

Table 5.15 Comparison of WT Installation in Supercharging Stations in Different Cases

Station No.	Benchmark WT (MW)	Case 1 (MW)	Case 2 (MW)	Case 3 (MW)	Zone
1	0	0	0	0.00	Austin
2	0	0	0	0.00	Austin
3	0	0	0	0.00	Austin
4	0	0	0	0.00	Austin
5	0	0	0	0.00	Austin
6	5.58	5.58	5.58	1.90	Corpus Christi
7	7.44	7.44	7.44	2.54	Corpus Christi
8	7.44	7.44	7.44	2.54	Corpus Christi
9	0.89	0.8928	0.89	0.30	Corpus Christi
10	6	6	6	0.00	Dallas
11	5.76	5.76	5.76	0.00	Dallas
12	7.5	7.5	7.5	0.00	Dallas
13	7.5	7.5	7.5	0.00	Dallas
14	8.25	8.25	8.25	0.00	Dallas
15	9	9	9	0.00	Dallas
16	4.5	4.5	4.5	0.00	Dallas
17	9	9	9	0.00	Dallas
18	6	6	6	0.00	Dallas
19	6	6	6	0.00	Dallas
20	4.5	4.5	4.5	0.00	Dallas
21	7.5	7.5	7.5	0.00	Dallas
22	7.5	7.5	7.5	0.00	Dallas
23	7.5	7.5	7.5	0.00	Dallas
24	6	6	6	0.00	Dallas
25	6	6	6	0.00	Dallas
26	6	6	6	0.00	Dallas
27	0	0	0	0.00	El Paso
28	0	0	0	0.00	El Paso
29	9	9	9	0.00	Houston
30	6	6	6	0.00	Houston
31	4.5	4.5	4.5	0.00	Houston
32	4.5	4.5	4.5	0.00	Houston
33	6	6	6	0.00	Houston
34	6	6	6	0.00	Houston
35	6	6	6	0.00	Houston
36	4.5	4.5	4.5	0.00	Houston
37	7.44	7.44	2.56	0.00	Midland
38	7.44	7.44	2.56	0.00	Midland
39	7.44	7.44	2.56	0.00	Midland
40	7.44	7.44	2.56	0.00	Midland
41	6	6	6	0.00	San Antonio
42	4.5	4.5	4.5	0.00	San Antonio
43	7.5	7.5	7.5	0.00	San Antonio
44	7.5	7.5	7.5	0.00	San Antonio
45	6	6	6	0.00	San Antonio
46	6	6	6	0.00	San Antonio

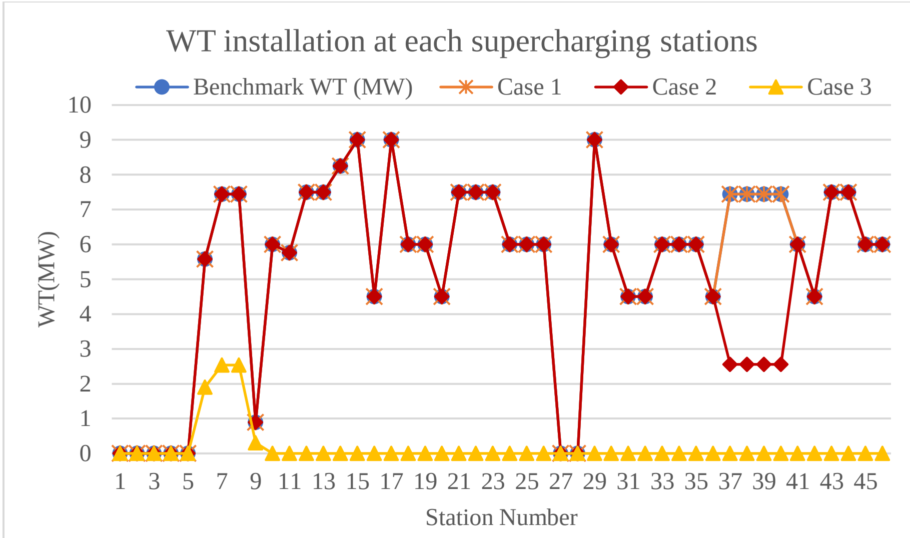

Figure 5.36 WT Installation at Each Supercharging Station (MW)

Comparison among benchmark case with three cases can be easily done using Table 5.15 and Fig 5.36. After comparing benchmark and case 1 from Fig 5.36, it is found out that after reducing the capacity cost of PV from \$2M/MW to \$1.5M/MW there is no significant difference in generation of WT. Secondly, after comparing benchmark with case 2 where the reduced capacity cost of PV from \$2M/MW to \$1M/MW, it can be seen from Fig 5.36 that in Midland's four supercharging stations the generation of WT is reduced from 7.44 MW to 2.56 MW because the generation of PV is increased in those stations because of reduced capacity cost of PV. Thirdly, from Fig 5.36, after comparing benchmark with case 3, it can be seen that the generation of WT is significantly reduced because of reducing capacity cost of PV from \$2M/MW to \$0.5M/MW. Because all those supercharging stations are installing more PV generation than WT because of reduced capacity cost of PV and it is profitable to install more PV.

Table 5.16 Comparison of PV Installation in Supercharging Stations in Different Cases

Station No.	**Benchmark PV (MW)**	**Case 1**	**Case 2**	**Case 3**	**Zone**
1	0	0	0	55.80	Austin
2	0	0	0	37.20	Austin
3	0	0	0	40.18	Austin
4	0	0	0	37.20	Austin
5	0	0	0	37.20	Austin
6	0	0	0	25.90	Corpus Christi
7	0	0	0	34.54	Corpus Christi
8	0	0	0	34.54	Corpus Christi
9	0	0	0	4.14	Corpus Christi
10	0	0	0	37.66	Dallas
11	0	0	0	36.15	Dallas
12	0	0	0	47.07	Dallas
13	0	0	0	47.07	Dallas
14	0	0	0	51.78	Dallas
15	0	0	0	56.48	Dallas
16	0	0	0	28.24	Dallas
17	0	0	0	56.48	Dallas
18	0	0	0	37.66	Dallas
19	0	0	0	37.66	Dallas
20	0	0	0	28.24	Dallas
21	0	0	0	47.07	Dallas
22	0	0	0	47.07	Dallas
23	0	0	0	47.07	Dallas
24	0	0	0	37.66	Dallas
25	0	0	0	37.66	Dallas
26	0	0	0	37.66	Dallas
27	0	0	0	37.20	El Paso
28	0	0	0	37.20	El Paso
29	0	0	0	37.20	Houston
30	0	0	0	24.80	Houston
31	0	0	0	18.60	Houston
32	0	0	0	18.60	Houston
33	0	0	0	24.80	Houston
34	0	0	0	24.80	Houston
35	0	0	0	24.80	Houston
36	0	0	0	18.60	Houston
37	0	0	24.62	37.20	Midland
38	0	0	24.62	37.20	Midland
39	0	0	24.62	37.20	Midland
40	0	0	24.62	37.20	Midland
41	0	0	0	39.60	San Antonio
42	0	0	0	29.70	San Antonio
43	0	0	0	49.50	San Antonio
44	0	0	0	49.50	San Antonio
45	0	0	0	39.60	San Antonio
46	0	0	0	39.60	San Antonio

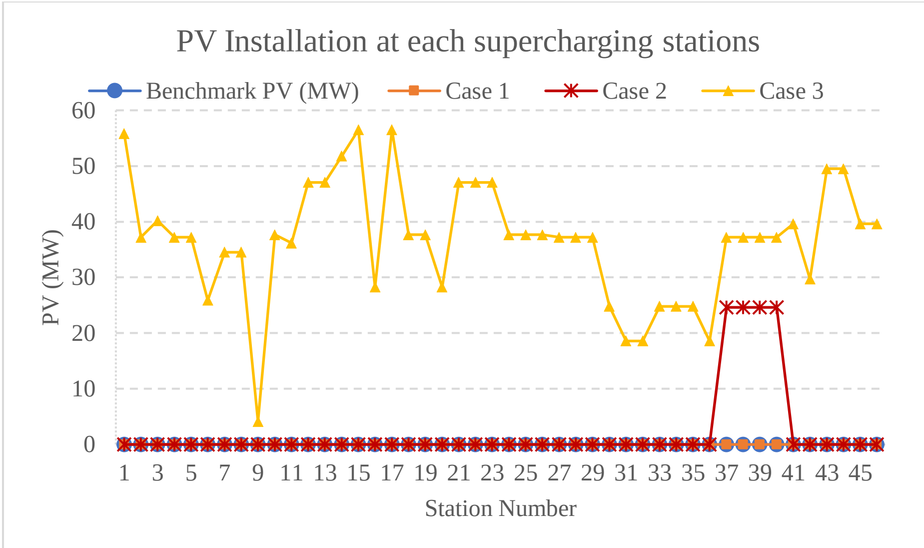

Figure 5.37 PV Installation at Each Supercharging Station (MW)

Comparison among benchmark case with other cases can be easily done using Table 5.16 and Fig 5.37. From Fig 5.37 it can be seen that by reducing the capacity cost of PV from \$2M/MW to \$1M/MW (case 2), the generation of PV at Midland's four supercharging stations has significantly increased from 0M to 24.62MW. It can be also seen from Fig 5.37, in case 3 where the reduced capacity cost of PV to \$0.5M/MW, the generation of PV has significantly increased for all supercharging stations in Texas.

Table 5.17 Comparison of ESS Storage of Supercharging Stations in Different Cases

Station No.	**Benchmark (MWh)**	**Case 1 (MWh)**	**Case 2 (MWh)**	**Case 3 (MWh)**	**Zone**
1	0	0	0	0.00	Austin
2	0	0	0	0.00	Austin
3	0	0	0	0.00	Austin
4	0	0	0	0.00	Austin
5	0	0	0	0.00	Austin
6	0	0	0	1.50	Corpus Christi
7	0	0	0	2.00	Corpus Christi
8	0	0	0	2.00	Corpus Christi
9	0	0	0	0.24	Corpus Christi
10	0	0	0	0.73	Dallas
11	0	0	0	0.70	Dallas
12	0	0	0	0.91	Dallas
13	0	0	0	0.91	Dallas
14	0	0	0	1.00	Dallas
15	0	0	0	1.09	Dallas
16	0	0	0	0.55	Dallas
17	0	0	0	1.09	Dallas
18	0	0	0	0.73	Dallas
19	0	0	0	0.73	Dallas
20	0	0	0	0.55	Dallas
21	0	0	0	0.91	Dallas
22	0	0	0	0.91	Dallas
23	0	0	0	0.91	Dallas
24	0	0	0	0.73	Dallas
25	0	0	0	0.73	Dallas
26	0	0	0	0.73	Dallas
27	0	0	0	0.00	El Paso
28	0	0	0	0.00	El Paso
29	0	0	0	0.00	Houston
30	0	0	0	0.00	Houston
31	0	0	0	0.00	Houston
32	0	0	0	0.00	Houston
33	0	0	0	0.00	Houston
34	0	0	0	0.00	Houston
35	0	0	0	0.00	Houston
36	0	0	0	0.00	Houston
37	0	0	0.04092	0.00	Midland
38	0	0	0.04	0.00	Midland
39	0	0	0.04	0.00	Midland
40	0	0	0.04	0.00	Midland
41	0	0	0.00	1.92	San Antonio
42	0	0	0	1.44	San Antonio
43	0	0	0	2.40	San Antonio
44	0	0	0	2.40	San Antonio
45	0	0	0	1.92	San Antonio
46	0	0	0	1.92	San Antonio

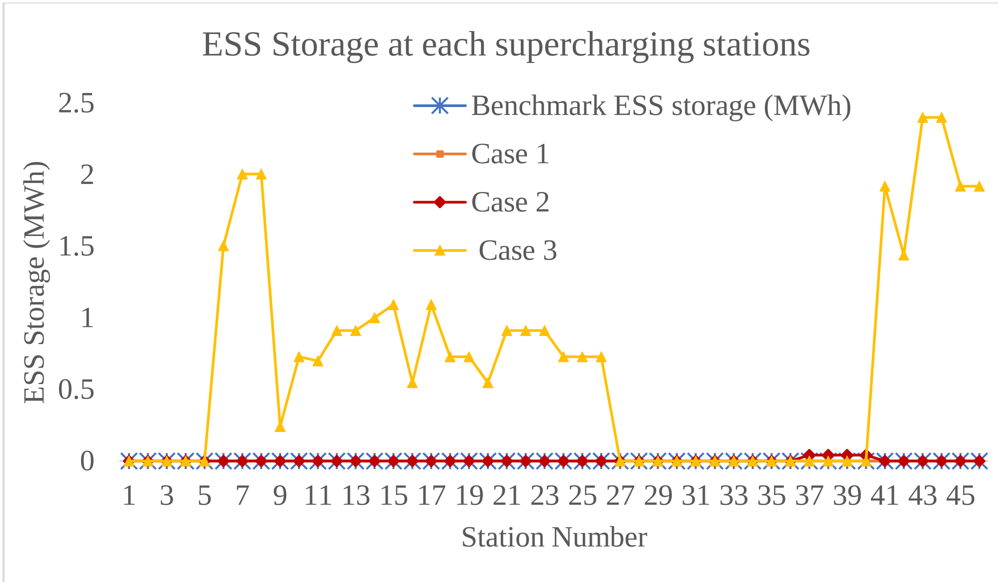

Figure 5.38 ESS Storage at Each Supercharging Station (MWh)

Using Table 5.17 and Fig 5.38, it can be seen that in case 3 where the capacity cost of PV is reduced from $2M/MW to $0.5M/MW, ESS storage system is used to store the extra generation from PV. It is profitable to do that because those extra energy can be used fulfilling the demand of supercharging stations at later time and also can be sold to the main grid when the selling price will be high to sale based on TOU rate. Note I&E stands for import and export.

Table 5.18 Comparison of Prosumer Activity of Supercharging Stations in Different Cases

Station No.	Benchmark Prosumer	Case 1	Case 2	Case 3	Zone
1	I	I	I	I & E	Austin
2	I	I	I	I & E	Austin
3	I	I	I	I & E	Austin
4	I	I	I	I & E	Austin
5	I	I	I	I & E	Austin
6	I & E	I & E	I & E	I & E	Corpus Christi
7	I & E	I & E	I & E	I & E	Corpus Christi
8	I & E	I & E	I & E	I & E	Corpus Christi
9	I & E	I & E	I & E	I & E	Corpus Christi
10	I	I	I	I & E	Dallas
11	I	I	I	I & E	Dallas
12	I	I	I	I & E	Dallas
13	I	I	I	I & E	Dallas
14	I	I	I	I & E	Dallas
15	I	I	I	I & E	Dallas
16	I	I	I	I & E	Dallas
17	I	I	I	I & E	Dallas
18	I	I	I	I & E	Dallas
19	I	I	I	I & E	Dallas
20	I	I	I	I & E	Dallas
21	I	I	I	I & E	Dallas
22	I	I	I	I & E	Dallas
23	I	I	I	I & E	Dallas
24	I	I	I	I & E	Dallas
25	I	I	I	I & E	Dallas
26	I	I	I	I & E	Dallas
27	I	I	I	I & E	El Paso
28	I	I	I	I & E	El Paso
29	I	I	I	I & E	Houston
30	I	I	I	I & E	Houston
31	I	I	I	I & E	Houston
32	I	I	I	I & E	Houston
33	I	I	I	I & E	Houston
34	I	I	I	I & E	Houston
35	I	I	I	I & E	Houston
36	I	I	I	I & E	Houston
37	I & E	I & E	I	I & E	Midland
38	I & E	I & E	I	I & E	Midland
39	I & E	I & E	I	I & E	Midland
40	I & E	I & E	I	I & E	Midland
41	I	I	I	I & E	San Antonio
42	I	I	I	I & E	San Antonio
43	I	I	I	I & E	San Antonio
44	I	I	I	I & E	San Antonio
45	I	I	I	I & E	San Antonio
46	I	I	I	I & E	San Antonio

From Table 5.18, it can be seen by reducing the capacity cost of PV from $2M/MW to

$0.5M/MW makes the system choosing more PV for generation which can be used to fulfill the demand of supercharging stations and also can be sold to the main-grid for making profit.

Table 5.19 Comparison of Annual Cost for Different Cases

Benchmark	Objective function	$169,281,175.70
Case 1	Objective function	$169,281,175.70
Case 2	Objective function	$168,833,353.20
Case 3	Objective function	$119,416,800.20

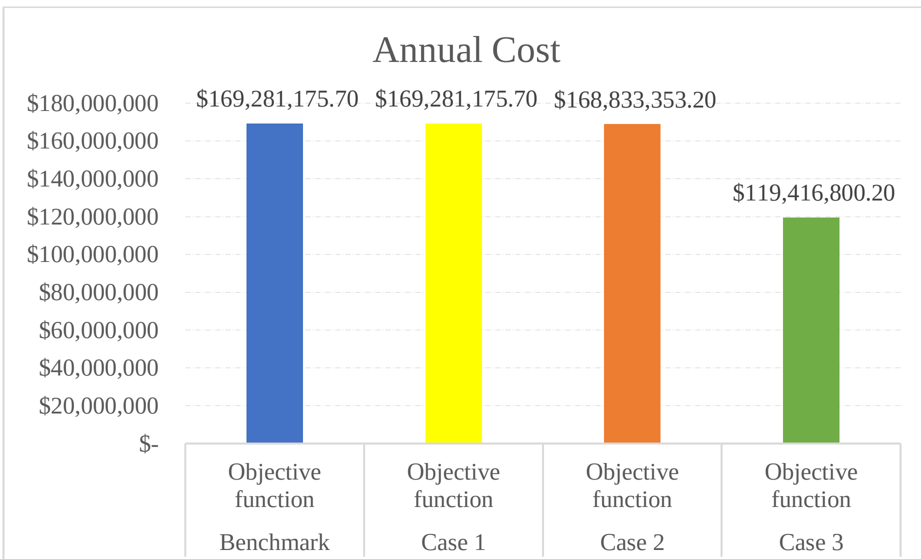

Figure 5.39 Annual Cost ($)

From Table 5.19 and Fig 5.39, it can be seen that by reducing the capacity cost of PV from $2M/MW to $1M/MW and $0.5M/MW significantly reduces the annual cost of the network system by selling the extra energy to the main-grid.

5.4.5 Comparison between results of Model 5.1 solved in two different ways

As it has mentioned earlier in Chapter 5 that Model 5.1 has solved in two different ways. In the first way, the model has solved for each specific zones separately and in the second way, the model has solved like a network planning model consisting of all the zones. After analyzing the results of Model 5.1, some interesting things have found which are described in Table 5.20.

Table 5.20 Comparison between Results of Model 5.1 Solved in Two Different Ways

Model for each specific zone separately					
Zone	**City**	**Total installed WT (MW)**	**Total installed PV (MW)**	**Total installed ESS (MWh)**	**Total Cost ($)**
1	Austin	0	0	0	20,529,936
2	Corpus Christi	21.35	0	0	8,552,291
3	Dallas	114.51	0	0	69,402,772
4	El Paso	0	0	0	7,358,400
5	Houston	46.5	0	0	28,284,034
6	Midland	29.76	0	0	12,274,121
7	San Antonio	37.5	0	0	22,879,622
Sum		249.62	0	0	169,281,176
Network model consisting of all zones					
Zone	**City**	**Total installed WT (MW)**	**Total installed PV (MW)**	**Total installed ESS (MWh)**	**Total Cost ($)**
1	Austin	0	0	0	
2	Corpus Christi	21.35	0	0	
3	Dallas	114.51	0	0	
4	El Paso	0	0	0	
5	Houston	46.5	0	0	
6	Midland	29.76	0	0	
7	San Antonio	37.5	0	0	
Sum		249.62	0	0	169,281,176

After comparing the results of Model 5.1 solved in two different ways in Table 5.20, it can be seen that the two results are identical. The findings of total installed WT, PV and

ESS are same both in the model for each specific zones separately and the network model consisting of all zones. It can be also seen from Table 5.20 that the total cost is also identical for the model solved for each specific zone separately and the network model consisting of all zones together. Based on the findings, the conclusion can be drawn that solving the problem in smaller section and combining it later, will give almost identical results if anyone solves the same problem creating a large network problem.

Providing validation for the conclusion sentence, model 5.1 is run again in AMPL computational environment by combining two zones into one (Austin and Corpus Christi zone), then three zones into one (El paso, Midland and San Antonio zone) and finally again two zones into one (Dallas and Houston zone). The findings are summarized in Table 5.21.

Table 5.21 Results of Model 5.1 Solved in Three Parts

Zone	Total installed WT (MW)	Total installed PV (MW)	Total installed ESS (MWh)	Total Cost ($)
Austin and Corpus Christi	21.35	0	0	29,082,227
El-Paso, Midland and San Antonio	67.26	0	0	42,512,143
Dallas and Houston	161.01	0	0	97,686,806
Sum	249.62	0	0	169,281,176

From Table 5.21, it can be seen that both Table 5.20 and Table 5.21 are showing identical results for total installed WT, PV and ESS and also for total cost. So, based on the current findings, the conclusion can be validated that solving the problem in smaller section and combining it later, will give almost identical results if anyone solves the same problem creating a large network problem.

6. CONCLUSION AND FUTURE WORK

6.1 Conclusion

This thesis addresses two research questions related to allocation of renewable microgrid in battery swapping and supercharging stations for electric vehicles: First, is it economically viable to integrate wind- and solar-based microgrid along with main grid to power the battery swap and supercharging facilities? Second, where and how should the battery swap and supercharging stations be located to minimize the facility operating cost?

An optimization framework was proposed for allocating renewable microgrid in battery swapping and supercharging stations with island and grid-tied microgrid mode, respectively. A microgrid is comprised of a wind turbine (WT), photovoltaics (PV) and energy storage systems (ESS). A network model is also proposed comprising of 46 supercharging stations to prove the viability of a real-world application of allocation of renewable microgrid for electric vehicle. The network model is tested using data from Tesla supercharging stations located in the state of Texas. A mixed integer linear programming model is developed to minimize the annualized cost of battery services considering facility setup, spare batteries, and superchargers. Those optimization models are tested on ten different cities in the US using hourly solar PV and WT capacity factor data across eleven years. For the network model, hourly solar PV and WT capacity factor data of Texas cities are used. The model is tested in real world Tesla supercharging stations using the data retrieved from Tesla website.

For island microgrid, it is shown that reducing the ESS cost does not stimulate the installation of ESS, PV and WT. This is because the energy generation largely depends on capacity factor of PV and WT. In grid-tied microgrid operation, reducing the PV capacity cost by 50% makes the system install more PV both in sunny and windy cities. This is because the station can sell the surplus renewable energy to the main grid and makes the overall system profitable. It is also shown that reducing the ESS cost by 75% from the current cost of $0.4M/MWh does not make the system choose ESS, instead the station opts to export energy to the main grid for both sunny and windy cities. For network model, it is shown that by reducing the PV capacity cost by 75% from the current cost of $2M/MW makes the system choose more PV for Texas cities and reduces the entire system annual cost by 29%. Moreover, the system opts to behave as "prosumer" acting as a consumer and producer at the same time.

There are three managerial implications from this study. Firstly, the integration of renewable microgrid in battery swap and supercharging stations makes the system prosumer and profitable. Secondly, this work shows that electric transportation is a cost-effective approach to reducing dependency on fossil fuel generation. Third, battery energy storage cost is the main driver behind the large scale installation of onsite wind and solar generation, rather demand responses and government policies plays the key roles.

6.2 Future Work

In this thesis, only Texas supercharging stations of Tesla have considered for building the network model. Future work can be expanded by enlarging the network model in state-wide, nation-wide, and globalized manner.

In this thesis, seven Texas cities weather data of 2019 have collected for calculating WT and PV hourly capacity factor. This work can be expanded by collecting weather data of Texas cities for multiple years for better forecasting of WT and PV hourly capacity factor or via considering different locations for the model.

In this thesis, passenger cars are considered for electric transportation. Future work can be expanded via considering e-trucks and other public transportation medium for electric transportation. By increasing the medium of electric transportation will give more power assurance via renewable energy.

The future work of this thesis can be expanded through using blockchain. Blockchain is a technology which helps storing real-time data with unalterable and transparent feature. Blockchain could be further incorporated in the decision making to facilitate the direct peer-to-peer trading. Blockchain gives the user opportunity to share data in a secure way.

APPENDIX SECTION

1. **MATLAB code of modeling battery swap with Erlang B: In this code, the notion theta=θ, lambdaB= λ_b, muB= μ_b.**

```
%ErlangB
clc
clear all
close all
K = input('the value of k');
lambdaB = input('arrival rate lambdaB');
muB = input('service rate muB');
theta=lambdaB./muB;
kk=1;
%pi will be using for performance analysis
for s=1:K
   num=power(theta,s)/factorial(s);
   den=0;
   for k=0:s
      den=den+power(theta,k)/factorial(k);
   end
   final(kk)=num/den;
   disp(final(kk));
   kk=kk+1;
end
```

2. **MATLAB code of modeling supercharging with Erlang C: In this code, the notion theta=θ, lambdaB= λ_b, muB= μ_b, B= *B(s)*, P= ρ_d, q=m* ρ_d.**

```
%ErlangC
clc
clear all
close all
K = input('the value of k');
lambdaB = input('arrival rate lambdaB');
muB = input('service rate muB');
B = input('probability of erlang b');
m = input('the number of super chargers');
theta=lambdaB./muB;
P=(lambdaB*B)./(m*muB);
q=m*P;
kk=1;
%pi will be using for performance analysis
for m=0:K
   num=power(q,m)/(factorial(m)*(1-P));
   den=0;
   for K=0:m
      den=(den+power(q,K)/factorial(K))+num;
   end
   final(kk)=num/den;
   F=1-final(kk);
   disp(F);
   kk=kk+1;
end
```

3. AMPL code of Model 3.1 Minimizing Cost of Battery Swap Station with Island Microgrid

Model File:

```
#Initial battery full hourly
set period;
set period0;
param fib >=0;
param ab >=0;
param s >=0;
param fiwt >=0;
param awt >=0;
param fipv >=0;
param apv >=0;
param fiess >=0;
param aess >=0;
param tauwt >=0;
param bwt >=0;
param cwt >=0;
param lambdawt{t in period} >=0;
param taupv >=0;
param bpv >=0;
param cpv >=0;
param lambdapv{t in period}>=0;
param bess >=0;
param cess>=0;
param lambdaev{t in period}>=0;
param tau >=0;
param pev >=0;

var pcwt>=0;
var pcpv>=0;
var bcess>=0;
var besst{t in period0}>=0;

minimize tot_cost:
(fib*ab*s)+
(fiwt*awt*pcwt)+
(fipv*apv*pcpv)+
(fiess*aess*bcess)+
(sum{t in period} tauwt*(bwt-cwt)*lambdawt[t]*pcwt)+
(sum{t in period} taupv*(bpv-cpv)*lambdapv[t]*pcpv)+
(sum {t in period} (bess-cess)*besst[t]);

subject to c1 {t in period}:(lambdaev[t]*tau*pev)+(besst[t]-
besst[t-1])<=(lambdawt[t]*tauwt*pcwt)+(lambdapv[t]*taupv*pcpv);
```

```
subject to c2 {t in period0}:0<=besst[t];
subject to c3 {t in period0}:besst[t]<=bcess;
subject to c4:besst[0]=bcess;
subject to c5:besst[8736]=bcess;
```

4. AMPL code of Model 3.2 Minimizing Battery Swap Station Cost with Grid-tied Microgrid.

Model File:

```
#Initial battery full
set GRID;
set BATTERY;
set PERIOD;
set PERIOD0;
param fig{g in GRID} >=0;
param ag{g in GRID} >=0;
param bg{g in GRID} >=0;
param cg{g in GRID} >=0;
param lambdagt{t in PERIOD,g in GRID} >=0;
param taug{g in GRID} >=0;
param fies >=0;
param des >=0;
param bes >=0;
param fib >=0;
param dbk{k in BATTERY} >=0;
param roimt{t in PERIOD} >=0;
param roext{t in PERIOD} >=0;
param lambdaev{t in PERIOD,k in BATTERY} >=0;
param pevk{k in BATTERY} >=0;
param tau >=0;

var pcg{g in GRID}>=0;
var sk{k in BATTERY} integer;
var bces>=0;
var best{t in PERIOD0} >=0;

var eimt{t in PERIOD} >=0;
var eext{t in PERIOD} >=0;

minimize tot_cost:
(sum{g in GRID} fig[g]*ag[g]*pcg[g])+
(sum{t in PERIOD,g in GRID} (bg[g]-
cg[g])*lambdagt[t,g]*pcg[g]*taug[g])+
(fies*des*bces)+
(sum{t in PERIOD} bes*best[t])+
(sum{k in BATTERY} fib*dbk[k]*sk[k])+
(sum{t in PERIOD} (roimt[t]*eimt[t]-roext[t]*eext[t]));

subject to c1{t in PERIOD}:(sum{k in BATTERY}
lambdaev[t,k]*tau*pevk[k])+best[t]-best[t-1]+eext[t]-
eimt[t]=(sum{g in GRID} lambdagt[t,g]*pcg[g]*taug[g]);
```

```
subject to c2{k in BATTERY,t in PERIOD}: lambdaev[t,k]*tau <=
sk[k];
subject to c3{t in PERIOD0}: 0 <= best[t];
subject to c4{t in PERIOD0}: best[t] <= bces;
subject to c5: best[0]=bces;
subject to c6: best[8736]=bces;
subject to c9{g in GRID}: pcg[g]<=20;
```

5. **AMPL code of Model 4.1 Microgrid Sizing for a Joint Battery Swap and Supercharging Station.**

Model File:

```
#Initial battery full
set GRID;
set BATTERY;
set SUPERCHARGER;
set PERIOD;
set PERIOD0;
param fig{g in GRID} >=0;
param ag{g in GRID} >=0;
param bg{g in GRID} >=0;
param cg{g in GRID} >=0;
param lambdagt{t in PERIOD,g in GRID} >=0;
param taug{g in GRID} >=0;
param fies >=0;
param des >=0;
param bes >=0;
param fib >=0;
param dbk{k in BATTERY} >=0;
param roimt{t in PERIOD} >=0;
param roext{t in PERIOD} >=0;
param lambdaev{t in PERIOD,k in BATTERY} >=0;
param bcvbk{k in BATTERY} >=0;
param tau >=0;
param fisc >=0;
param dsc >=0;
param pik >=0;
param pvbk{k in BATTERY} >=0;
param psc >=0;
param ak >=0;
param tauswap >=0;
param taumax >=0;

var pcg{g in GRID}>=0;
var sk{k in BATTERY} integer;
var bces>=0;
var best{t in PERIOD0} >=0;
var m{i in SUPERCHARGER} integer;
var eimt{t in PERIOD} >=0;
var eext{t in PERIOD} >=0;

minimize tot_cost{i in SUPERCHARGER}:
(sum{g in GRID} fig[g]*ag[g]*pcg[g])+
```

```
(sum{t in PERIOD,g in GRID} (bg[g]-
cg[g])*lambdagt[t,g]*pcg[g]*taug[g])+
(fies*des*bces)+
(sum{t in PERIOD} bes*best[t])+
(sum{k in BATTERY} fib*dbk[k]*sk[k])+
(fisc*dsc*m[i])+
(sum{t in PERIOD} (roimt[t]*eimt[t]-roext[t]*eext[t]));

subject to c1{t in PERIOD}:(sum{k in BATTERY}
lambdaev[t,k]*tau*bcvbk[k])+best[t]-best[t-1]+eext[t]-
eimt[t]=(sum{g in GRID} lambdagt[t,g]*pcg[g]*taug[g]);
subject to c2{k in BATTERY,t in PERIOD}:
lambdaev[t,k]*bcvbk[k]*(1-pik) <= sk[k]*pvbk[k];
subject to c3{i in SUPERCHARGER,t in PERIOD}: (sum{k in BATTERY}
pik*lambdaev[t,k]*bcvbk[k])+((1-pik)*tauswap*m[i]*psc) <=
taumax*m[i]*psc;
subject to c5{t in PERIOD0}: 0 <= best[t];
subject to c6{t in PERIOD0}: best[t] <= bces;
subject to c7: best[0]=bces;
subject to c8: best[8736]=bces;
```

6. **AMPL code of Model 5.1 Sizing Microgrid for VPP Operation at Tesla network.**

Model File:

```
#Initial battery full
#correct
set GRID;
set STATIONS;
set PERIOD;
set PERIOD0;

param fig{g in GRID} >=0;
param ag{g in GRID} >=0;
param bg{g in GRID} >=0;
param cg{g in GRID} >=0;
param lambdagjt{t in PERIOD,g in GRID,j in STATIONS} >=0;
param fiess >=0;
param aess >=0;
param bess >=0;
param robuyjt{t in PERIOD, j in STATIONS} >=0;
param roselljt{t in PERIOD, j in STATIONS} >=0;
param lambdaevjt{t in PERIOD, j in STATIONS} >=0;
param pscj{j in STATIONS} >=0;
param tau >=0;
param pstationj{j in STATIONS} >=0;

var pcgj{g in GRID, j in STATIONS}>=0;
var bcj{j in STATIONS} >=0;
var bjt{t in PERIOD0, j in STATIONS}>=0;
var ebuyjt{t in PERIOD, j in STATIONS} >=0;
var eselljt{t in PERIOD, j in STATIONS} >=0;

minimize tot_cost:
(sum{g in GRID, j in STATIONS} fig[g]*ag[g]*pcgj[g,j])+
(sum{t in PERIOD,g in GRID,j in STATIONS} (bg[g]-
cg[g])*lambdagjt[t,g,j]*pcgj[g,j]*tau)+
(fiess*aess*(sum{j in STATIONS}bcj[j]))+
(sum{t in PERIOD,j in STATIONS} bess*bjt[t,j])+
(sum{t in PERIOD,j in STATIONS} (robuyjt[t,j]*ebuyjt[t,j]-
roselljt[t,j]*eselljt[t,j]));

subject to c1{t in PERIOD,j in STATIONS}:
(lambdaevjt[t,j]*tau*pscj[j])+eselljt[t,j]+(bjt[t,j]-bjt[t-
1,j])=(sum{g in GRID}
lambdagjt[t,g,j]*pcgj[g,j]*tau)+ebuyjt[t,j];
subject to c2{t in PERIOD0, j in STATIONS}: 0 <= bjt[t,j];
subject to c3{t in PERIOD0,j in STATIONS}: bjt[t,j] <= bcj[j];
```

```
subject to c4{j in STATIONS}: bjt[0,j]=bcj[j];
subject to c5{j in STATIONS}: bjt[8760,j]=bcj[j];
subject to c6{t in PERIOD, j in STATIONS}: 0<=eselljt[t,j];
subject to c7{t in PERIOD, j in STATIONS}: eselljt[t,j]<=
tau*pstationj[j];
```

REFERENCES

1. Avci, B., Girotra, K., Netessine, S. (2015). Electric vehicles with a battery switching station: Adoption and environmental impact. Management Science, 61(4), 772-794.

2. Binding, C., Gantenbein, D., Jansen, B., Sundström, O., Andersen, P. B., Marra, F., Træholt, C. (2010). Electric vehicle fleet integration in the Danish EDISON project-a virtual power plant on the island of Bornholm. In IEEE PES general meeting, pp. 1-8.

3. Borba B, Szklo A, Schaeffer R. (2012). Plug-in hybrid electric vehicles as a way to maximize the integration of variable renewable energy in power systems: the case of wind generation in northeastern Brazil. Energy; 37(1), 469-481.

4. Built-in (2021). Retrieved from https://builtin.com/blockchain. (accessed on January 26, 2021).

5. Cohn, L. (2018). What is a virtual power plant? Microgrid Knowledge, Retried from https://microgridknowledge.com/virtual-power-plant-defined/. (accessed on Nov. 10, 2020).

6. Cowan, J. (2019). A virtual solar power plant for L.A.? It will happen. Retrieved from https://www.nytimes.com/2019/04/05/us/california-virtual-solar-power-sunrun.html. (accessed on Nov. 10, 2020).

7. Coren, M. (2016). New York wants to put a virtual power plant on 300 rooftops. Retrieved from https://qz.com/708228/new-york-wants-to-put-a-virtual-power-plant-on-300-rooftops/. (accessed on Nov. 10, 2020).

8. Cai, T., Duan, S., Chen, C. (2010). Forecasting power output for photovoltaic grid-connected power systems without using solar radiation measurement. In: Proceedings of Power Electronics for Distributed Generation Systems Symposium, pp. 773–777.

9. Calma, J. (2020). Virtual power plants are coming to California apartment buildings. Retrieved from https://www.theverge.com/2020/8/27/21403271/virtual-power-plants-california-apartment-buildings-solar-energy. (accessed on November 17, 2020).

10. Driscoll, W. (2019). Japan's ENERES developing virtual power plant with 10,000 assets. Retrieved from https://www.pv-magazine.com/2019/07/01/japans-eneres-developing-virtual-power-plant-with-10000-assets/. (accessed on November 17, 2020).

11. Enkhardt, S. (2020). Software for virtual power plants powered by residential solar-plus-storage. Retrieved from https://www.pv-magazine.com/2020/04/09/software-for-virtual-power-plants-powered-by-residential-solar-plus-storage/. (accessed on November 17, 2020).

12. Espe, E., Potdar, V., Chang, E. (2018). Prosumer communities and relationships in smart grids: a literature review, evolution and future directions. Energies, 11(10), 25-28. doi: 10.3390/en11102528.

13. Newsroom, E. (2020). Tesla launches UK-based virtual power plant project. Retrieved from https://www.edie.net/news/8/Tesla-launches-UK-based-virtual-power-plant-project/. (accessed on November 17, 2020).

14. Edelstein, S., (2020). EVs predicted to gain market share, despite 18% sales drop in 2020. Retrieved from https://www.greencarreports.com/news/1128234_evs-predicted-to-gain-market-share-despite-18-sales-drop-in-2020#:%7E:text=Electric%20cars%20are%20expected%20to,of%20the%20global%20car%20fleet. (accessed on November 17, 2020).

15. Field, K. (2020). Breaking! Tesla increases supercharging V2 speeds as S & X get on-route battery warmup. Retrieved from https://cleantechnica.com/2019/04/26/breaking-tesla-increases-supercharging-v2-speeds-as-s-x-get-on-route-battery-warmup/. (accessed on November 16, 2020).

16. Gao, Z., Ai, X., Zhang, H., Wang, Y. (2014). Access mode of EVs to grid based on VPP. In 2014 IEEE Conference and Expo Transportation Electrification Asia-Pacific (ITEC Asia-Pacific) pp. 1-5.

17. Hassan, A. S., Marmaras, C. E., Xydas, E. S., Cipcigan, L. M., Jenkins, N. (2013). Integration of wind power using V2G as a flexible storage. IET Conference on Power in Unity: a Whole System Approach, London, pp. 1-5, doi: 10.1049/ic.2013.0123.

18. Takagi, H., Walke, B. H. (Eds.). (2008). Spectrum requirement planning in wireless communications: Model and methodology for IMT-Advanced (Vol. 2). John Wiley & Sons, Chichester, West Sussex, U.K..

19. Heier, S. (2005). Grid integration of wind energy: onshore and offshore conversion systems-third edition. John Wiley & Sons, Chichester, UK.

20. Howland, E., (2020). Utilities advance virtual power plant projects. American Public Power Association. Retried from https://www.publicpower.org/periodical/article/utilities-advance-virtual-power-plant-projects. (accessed on November 17, 2020).

21. National Research Council (2010). Hidden Costs of Energy: Unpriced Consequences of Energy Production and Use. National Academies Press, Washington D.C., USA. Retrieved from https://www.nap.edu/read/12794/chapter/5. (accessed on November 17, 2020).

22. Ko, J., Shim, J. S. (2016). Locating battery exchange stations for electric taxis: A case study of Seoul, South Korea. International Journal of Sustainable Transportation, 10(2), 139-146.

23. Hara, K. (2019). Kyocera and LO3 ENERGY to demonstrate blockchain-managed virtual power plant. Nyheder. Retrieved from https://denmark.kyocera.com/news/2019/03/12225353.html. (accessed on November 17, 2020).

24. Kumagai, J. (2012). Virtual power plants, Real Power. IEEE Spectrum. Retrieved from https://spectrum.ieee.org/energy/the-smarter-grid/virtual-power-plants-real-power. (accessed on November 17, 2020).

25. Lambert, F. (2019). Tesla supercharger network reaches 15,000 chargers - still one of its best assets. Retrieved from https://electrek.co/2019/12/19/tesls-supercharger-reaches-15000-chargers-best-assets. (accessed on November 17, 2020).

26. Liu, X., Zhao, T., Yao, S., Boon Soh, C., Wang, P. (2019). Distributed operation management of battery swapping-charging systems. IEEE Transactions on Smart Grid, 10(5), 5320-5333. https://doi.org/10.1109/TSG.2018.2880449.

27. Lave, M., Kleissl, J. (2011). Optimum fixed orientations and benefits of tracking for capturing solar radiation. Energy, 36 (3), 1145–1152.

28. Lu, F., Hua, G. (2019). A location-sizing model for electric vehicle charging station deployment based on queuing theory. IEEE, pp. 1-5. Retried from https://ieeexplore.ieee.org/document/7369769/authors#authors.

29. Ma, J., Zhang, L. (2018). A Deploying Method for Predicting the Size and Optimizing the Location of an Electric Vehicle Charging Stations. Information, 9(7), 170-174.

30. Marcus, K. (2020). What's next for virtual power plants? Retrieved from https://energycentral.com/c/iu/what%E2%80%99s-next-virtual-power-plants. (accessed on October 30, 2020).

31. Minnesota Pollution Control Agency (2020, September 25). Electric vehicles. Retrieved from https://www.pca.state.mn.us/air/electric-vehicles#:%7E:text=Less%20harmful%20air%20pollution&text=Much%20like%20with%20greenhouse%20gases,operating%20and%20during%20power%20generation. (accessed on November 15, 2020).

32. Mahoor, M., Hosseini, Z., Khodaei, A. (2019). Least-cost operation of a battery swapping station with random customer requests. Energy, 172, 913-921.

33. Mandelbaum, A., Zeltyn, S. (2005). The palm/Erlang-A queue with applications to call centers. Retrieved from https://ie.technion.ac.il/~serveng/course2004/References/Erlang_A.pdf (accessed on Oct. 30, 2019).

34. Moon, J., Kim, Y. J., Cheong, T., Song, S. H. (2020). Locating Battery Swapping Stations for a Smart e-Bus System. Sustainability, 12(3), 1-21.

35. Mwasilu, F., Justo, J. J., Kim, E.K., Do, T. D., Jung, J.W. (2014). Electric vehicles and smart grid interaction: A review on vehicle to grid and renewable energy sources integration. Renewable and Sustainable Energy Reviews, 34, 501–516. https://doi.org/10.1016/j.rser.2014.03.031.

36. Musio, M., Damiano, A. (2012). A virtual power plant management model based on electric vehicle charging infrastructure distribution. In 2012 3rd IEEE PES Innovative Smart Grid Technologies Europe (ISGT Europe), pp. 1-7.

37. Kaltschmitt, M., Streicher, W., Wiese, A. (Eds.). (2007). Renewable energy: technology, economics and environment. Springer Science & Business Media, Berlin, Germany.

38. Ng, K. S., Moo, C. S., Chen, Y. P., Hsieh, Y. C. (2009). Enhanced coulomb counting method for estimating state-of-charge and state-of-health of lithium-ion batteries. Applied energy, 86(9), 1506-1511.

39. Nhede, N. (2018). Centrica develops Danish virtual system with 87,000 points. Retrieved from https://www.smart-energy.com/industry-sectors/distributed-generation/centrica-participates-danish-vpp-development-87000-points-grid-reliability/#:~:text=Centrica%20has%20won%20a%20contract,businesses%20into%20a%20single%20system. (accessed November 15, 2020).

40. Ibe, O., (2013). Markov processes for stochastic modeling-2nd Edition. Elsevier, Lowell, USA.

41. P. E. (2019). How fast is Tesla's supercharger V3- supercharger V2 vs V3. Retried from https://www.vehiclesuggest.com/how-fast-is-tesla-supercharger-v3/. (accessed on November 15, 2020).

42. Pashajavid, E., Golkar, M. (2013). Optimal placement and sizing of plug in electric vehicles charging stations within distribution networks with high penetration of photovoltaic panels. Journal of Renewable and Sustainable Energy, 5(5), 53-126.

43. Pham, A., Jin, T., Novoa, C., Qin, J. (2019). A multi-site production and microgrid planning model for net-zero energy operations. International Journal of Production Economics, 218, 260-274.

44. Rahman, K., Ghani, N. A., Kamil, A. A., Mustafa, A., Chowdhury, M. A. K. (2013). Modelling pedestrian travel time and the design of facilities: a queuing approach. PloS one, 8(5), 1-5.

45. Raz, N. (2017). National solar installation numbers down after Tesla purchase. Retrieved from https://www.reviewjournal.com/business/energy/national-solar-installation-numbers-down-after-tesla-purchase/. (accessed on October 31, 2020).

46. Reisz, W. (2020). Edge to cloud: building the Tesla virtual power plant. Retrieved from https://www.infoq.com/news/2020/03/tesla-vpp/.(accessed on October 31, 2020).

47. One Energy (2019). Retrieved from http://oneenergywind.com/. (accessed on November 30, 2019).

48. Tesla website (2020). Retrieved from https://www.tesla.com/. (accessed on November 30, 2020).

49. Statkraft website (2020). Retrieved from www.statkraft.com. (accessed on November 30, 2020).

50. Centrica website (2020). Retrieved from https://www.centrica.com/. (accessed on November 30, 2020).

51. Energy.gov (2020). Retrieved from https://www.energy.gov/eere/articles/consumer-vs-prosumer-whats-difference. (accessed on November 30, 2020).

52. Richardson, D. B. (2013). Electric vehicles and the electric grid: A review of modeling approaches, impacts, and renewable energy integration. Renewable and Sustainable Energy Reviews, 19, 247–254. https://doi.org/10.1016/j.rser.2012.11.042.

53. Berry, R. (2006). Queuing theory. Senior Project Archive, 1-14.

54. Short W., Denholm P.A. (2006). Preliminary assessment of plug-in hybrid electric vehicles on wind energy markets. National Renewable Energy Laboratory, Golden, CO, USA.

55. Sousa, T., Morais, H., Vale, Z., Faria, P., Soares, J. (2011). Intelligent energy resource management considering vehicle-to-grid: A simulated annealing approach. IEEE Transactions on Smart Grid, 3(1), 535-542.

56. Tan, X., Sun, B., Tsang, D. (2014). Queueing network models for electric vehicle charging station with battery swapping. In: 2014 IEEE International Conference on Smart Grid Communications (Smart Grid Comm). Retrieved from https://ieeexplore.ieee.org/document/7007613. (accessed 30 Oct. 2019).

57. Tan, Z., Yang, P., Nehorai, A. (2014). An optimal and distributed demand response strategy with electric vehicles in the smart grid. IEEE Transactions on Smart Grid, 5(2), 861-869.

58. Turton H., Moura F. (2008). Vehicle-to-grid systems for sustainable development: an integrated energy analysis. Technological Forecasting & Social Change; 75(10), 91–108.

59. Thiringer, T., Linders, J. (1993). Control by variable rotor speed of a fixed pitch wind turbine operating in a wide speed range. IEEE Trans. Energy Convers. 8 (3), 520–526.

60. Trabish, H. K. (2015) "Rooftop solar is now cheaper than the grid in 42 American cities." Utility Dive. Retrieved from www.utilitydive.com/news/rooftop-solar-is-now-cheaper-than-the-grid-in-42-american-cities/352799/. (accessed on November 20, 2020).

61. EIA (2017). Independent statistics and analysis. Retrieved from https://www.eia.gov/outlooks/ieo/index.php. (accessed on November 30, 2020).

62. Winston, W. (2009). Operations research. Belmont, Calif: Brooks/Cole, Cengage Learning, USA.

63. WU (Weather Underground), (2020). Retrieved from http://www.wunderground.com/. (accessed on June 2, 2020).

64. Wu, S., Xu, Q., Li, Q., Yuan, X., Chen, B. (2017). An optimal charging strategy for PV-based battery swapping stations in a DC distribution system. International Journal of Photoenergy, 1-5.

65. Xu, X., Yao, L., Zeng, P., Liu, Y., Cai, T. (2015). Architecture and performance analysis of a smart battery charging and swapping operation service network for electric vehicles in China. Journal of Modern Power Systems and Clean Energy, 3(2), 259-268.

66. Yan, J., Menghwar, M., Asghar, E., Kumar Panjwani, M., Liu, Y. (2019). Real-time energy management for a smart-community microgrid with battery swapping and renewables. Applied Energy, 238, 180-194.

67. Yang, S., Yao, J., Kang, T., Zhu, X. (2014). Dynamic operation model of the battery swapping station for EV (electric vehicle) in electricity market. Energy, 65, 544-549.

68. Yang, Z., Li, K., Foley, A., Zhang, C. (2014). Optimal scheduling methods to integrate plug-in electric vehicles with the power system: a review. IFAC Proceedings. 47(3), 8594–8603. https://doi.org/10.3182/20140824-6-ZA-1003.01804.

69. Yao, L., Damiran, Z., Lim, W. (2017). Optimal charging and discharging scheduling for electric vehicles in a parking station with photovoltaic system and energy storage system. Energies, 10(4), 550-555.

70. Yang, J., Dong, J., Hu, L. (2017). A data-driven optimization-based approach for siting and sizing of electric taxi charging stations. Transportation Research Part C: Emerging Technologies, 77, 462-477.

71. Zhang, X., Wang, G. (2016). Optimal dispatch of electric vehicle batteries between battery swapping stations and charging stations. Presented at the 2016 IEEE Power and Energy Society General Meeting (PESGM), 1-5. https://doi.org/10.1109/PESGM.2016.7741893.

72. Zhang, Y., Qi, D., Jiang, W., Lei, S. (2016). Optimal allocation of changing station for electric vehicle based on queuing theory. Promet-Traffic & Transportation, 28(5), 497-505.

73. Zhang, Y., Qi, D., Jiang, W., Lei, S. (2016). Optimal allocation of changing station for electric vehicle based on queuing theory. PROMET – Traffic & Transportation, 28(5), 497-505.

74. Zheng, D., Wen, F., Huang, J. (2012). Optimal planning of battery swap stations. Presented at the International Conference on Sustainable Power Generation and Supply (SUPERGEN 2012), Hangzhou, China, 153-154. Retrieved from https://doi.org/10.1049/cp.2012.1846.

75. Zheng, Y., Dong, Z., Xu, Y., Meng, K., Zhao, J., Qiu, J. (2014). Electric vehicle battery charging/swap stations in distribution systems: comparison study and optimal planning. IEEE Transactions on Power Systems, 29(1), pp. 221-229.

76. Zhang, C., Wu, J., Zhou, Y., Cheng, M., & Long, C. (2018). Peer-to-Peer energy trading in a Microgrid. Applied Energy, 220, 1-12.

77. Zhang, J., Bai, L., Jin, T. (2021), Joint planning for battery swap and supercharging networks with priority service queues. International Journal of Production Economics, 233, https://doi.org/10.1016/j.ijpe.2020.108009.